National University of Lesotho

Cascading wind and solar pumping systems to recirculate water for pumped hydropower storage system at Lets'a-la-Letsie dam

Marasi Monyau (202104004)

A dissertation submitted in partial fulfilment of
the requirements for the degree of

Master of Science in Sustainable Energy

Offered by the

Energy Research Centre
Faculty of Science & Technology

May 2024

Abstract

This dissertation investigates the use of cascading wind and solar power pumping systems for recirculating water for pumped hydropower generation at Lets'a-la-Letsie in the Quthing district, Lesotho. The study's main goals are to identify optimal wind and solar resources for positioning wind turbines and solar panels; to design a solar/wind pumping system for recirculating water for pumped hydropower storage; and to design a hybrid system that considers the LCOE (least cost of energy) and system performance.

The digital elevation, solar energy and wind energy potential maps, in conjunction with QGIS, were used to analyse the heads of the study regions, and TURBNPRO was used to estimate the power outputs and specifications of the selected Pelton turbine. The net head for Lets'a-la-Letsie was 157 metres. The design flow rate for Lets'a-la-Letsie was 0.06 m^3/s. To provide water to the top reservoir, 19 similar pumps are required. Each pump has a power control of 37 kW (kilowatts). The top reservoir volume was calculated to be 2700 m^3.

This study uses the HOMER Pro simulation software to illustrate the performance of the Lets'a-LaLetsie hybrid renewable energy system. The system's total load includes the school load, clinic load, residential load, pumping load, and commercial load. The proposed hybrid system design consists of a 5379 kW solar PV array, a 1500 kW wind turbine, a 1985 kW converter, and a battery model for a pumped storage with a maximum capacity of 4331 Ampere hours (Ah). The optimal system has an LCOE of $0.417/kWh (Maluti 7.61/kWh) . The average solar irradiation and wind speed are determined to be 5.26 kWh/m^2/day and 4.77 m/s, respectively. The project would require an initial capital commitment of about $27.9 million (509 million Maluti), with a total NPC (Net present Value) of $39.6 million (720 million Maluti).

The findings show that Lets'a-La-Letsie has enough sun resources as well as the topography for the construction of pumped hydropower storage facilities. However, the country lacks a legislative and commercial framework to support the development of pumped-storage power facilities.

Acknowledgements

First and foremost, I would like to express my sincere gratitude to my supervisors Dr Khaba and Dr Makhele, for their invaluable guidance, unwavering support, and insightful feedback throughout the entire process. Their expertise and encouragement have been instrumental in shaping this work.

Secondly, my sincere thanks go to my family for their endless love, encouragement, and understanding during this challenging journey. Their unwavering belief in me has been my greatest motivation.

Thirdly, I extend my heartfelt appreciation to my friends and colleagues for their togetherness, support and team spirit in ensuring the completion of this thesis.

Lastly, thank you to everyone who has played a part, no matter how big or small, in bringing this thesis to fruition.

List of Figures

List of tables

Contents

CHAPTER 1: Introduction

1.1 Background

Climate change, limited application of thermal power plants, potential dangers of nuclear power plants, as well as the depletion of oil, gas, and coal resources play a role in the new global energy policy [1]. In addition, the negative effects of using fossil fuels and their escalating costs have made it evident that renewable energy sources are required [2]. Moreover, the adverse effects of fossil fuel consumption for energy production result in environmental deterioration (carbon dioxide emissions). This calls for the use of renewable energy resources to help reduce fossil fuel consumption and the chances of the greenhouse effect [3]. Furthermore, energy is a major concern in sustainable development. However, renewable energy is being developed as an energy supply solution for the 21st century, assuring a stable and secure energy supply in such communities. It is also important to mention that grid expansion is difficult on islands and in isolated villages, and fuel transportation and logistics are complex and expensive [4]. As a result, the shift to using renewable sources such as solar and wind for power generation has begun in several European nations as they phase out nuclear and coal generation [5]. The need to use renewable energy sources is also enshrined in the Sustainable Development Goal (SDG) 7 whose main objective is to ensure that everyone has access to modern, sustainable, and cheap energy. It aims to achieve the following goals: ensuring that everyone has access to energy services, improving renewable energy penetration in the energy mix, and enhancing energy efficiency [6].

More than 1 billion people who do not have access to electricity might have their need for power reduced by small-scale alternative energy technologies [7]. African renewable energy markets must expand quickly but sustainably given that more than 600 million people lack access to electricity while more than 730 million rely on risky, inefficient methods of cooking [8]. Although renewable energy sources continue to gain ground globally, progress has been uneven across sectors and regions. In many developing countries, particularly in sub-Saharan Africa, energy access rates remain low, recent estimates show that almost 580 million people in Sub-Saharan Africa lack access to electricity, while more than 900 million cook on inefficient and polluting stoves [9], [10]. In contrast, Africa has the chance to take the lead as the world's energy systems move towards a net-zero future. The geographic variety of the continent gives it a huge opportunity for the production of solar and wind energy, and many of the minerals and rare earths required for renewable energy technology may be found in the soils [11].

The biggest challenges to utilizing renewable energy in Africa are political instability, lack of technical knowledge, policy uncertainty, poor infrastructure, fragile financial circumstances, and minimal access to international funding. Lesotho faces challenges such lack of implementation of the national energy policy objectives, which hinders the promotion of sustainable energy technologies and the implementation of new regulatory instruments such as IPPs and PPAs. This poses a threat to the security

of electricity supply options. Additionally, there is a lack of appropriate human resource development and institutional capacity to effectively implement and manage these issues [12].

However, off-grid hybrid systems have enabled the supply of reliable, sustainable, and environmentally friendly energy to rural areas, particularly for populations living in remote areas where grid extension is expensive [13]. Modern energy is essential to human progress since it helped spark the Industrial Revolution more than 200 years ago and has played a role in the nearly uninterrupted global economic expansion [6].

As a result of the extensive deployment of variable solar and wind-producing capacities, the requirement for storage in electrical networks is growing. Solar and wind power constitute approximately two-thirds of the net yearly additions to the world's power capacity [14]. The rated power of solar panels, wind turbines, and other renewable energy systems is increasing worldwide [15]. To maintain a stable and effective electrical system, electricity conversion and storage during periods of lower consumption, as well as electricity generation from the stored energy during periods of higher consumption or decreased production, are essential. This requirement has shown importance owing to the expansion of the integration of new wind and solar plants [1].

1.2 Problem Statement

According to the Lesotho Electricity and Water Authority (2018) report, the country's electrification rate reached 41% for all households. This indicates that additional efforts should be made to electrify the remaining 59% of households, the majority of which are located in the rural areas of the country. Currently, only 10% of rural households are connected to the grid compared to 80% of urban households [16]. Figure 1 depicts the electricity load forecast for Lesotho from 2016 to 2035 [17]. The results show that the peak demand is predicted to increase from 170 Mega Watt (MW) in 2021 to approximately 240 MW in 2035.

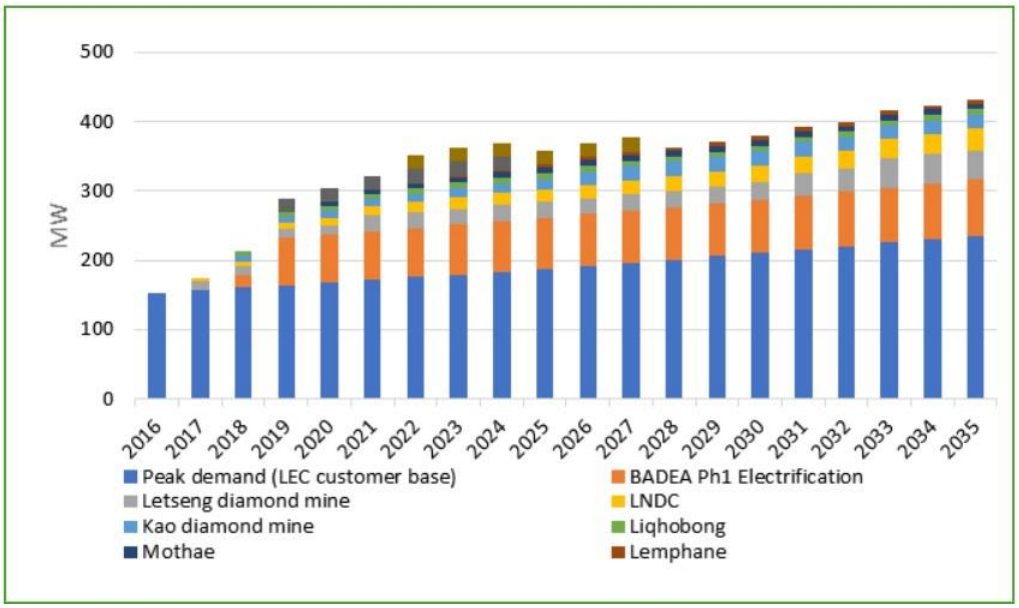

Figure 1: Lesotho Load Forecast, 2016-2035 (MW) [17].

The increasing energy demand results in a significant supply gap for the nation since generation has remained stagnant at approximately 74 MW. Consequently, a strong supply and demand balance is important and necessary.

Figure 2 below shows Lesotho's national transmission and distribution grid. It demonstrates that the national grid is mostly accessible in the lowlands. For instance, the access rate in Quthing is only 12%.

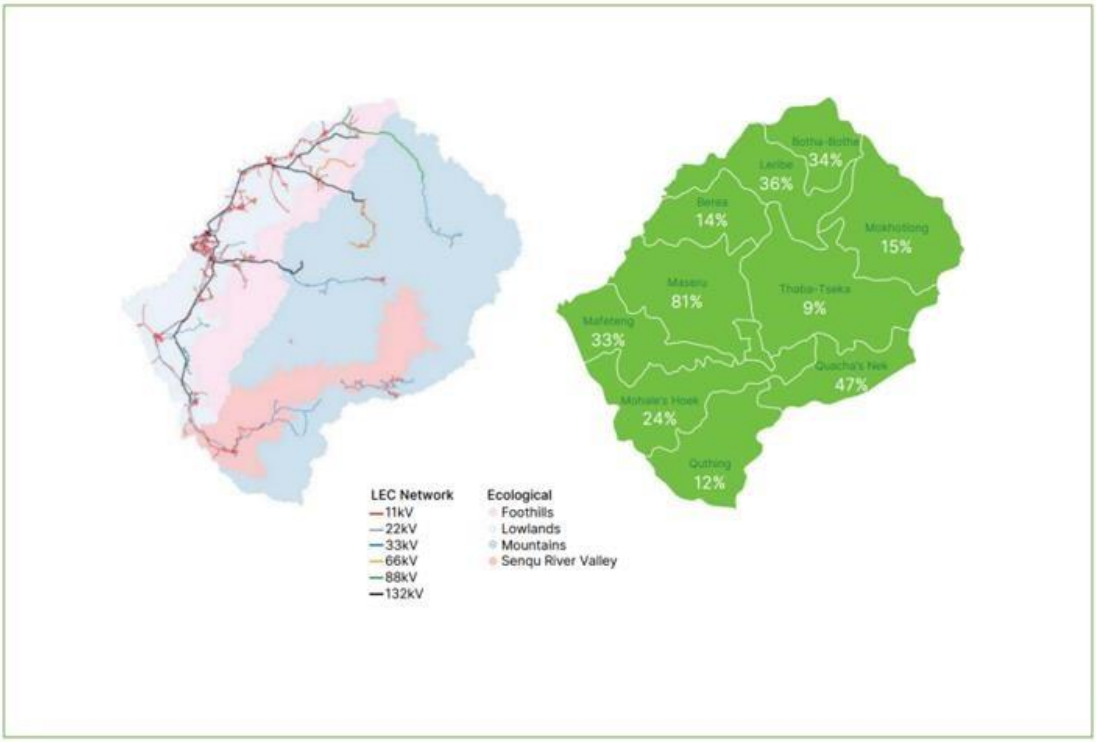

Figure 2: Lesotho national transmission and distribution grid [16]

Taele et al [18] indicated that one option for producing electricity near potential users and avoiding high reticulation costs in rural regions with wide distribution is using hydropower. Lesotho has a large commercially feasible hydropower potential, which is projected to be 450 MW for traditional hydropower systems and more than 3000 MW for pumped storage projects [18].

Figure 3 shows the Lets'a-La-Letsie lake as extracted from Google Earth Pro. The area lies between 30º 17′ 02′′ S and 30º 21′ 53′′ S; 28º 08′ 53′′ E and 28º 15′ 30′′ E.

Figure 3: Lets'a-la Letsie as obtained from Google earth

Renewable energy sources are increasingly the greatest alternative for electrification, owing to the steadily rising demand for power, especially in distant areas, and to satisfy relatively small loads [18]. Because of its flexibility in generation and storage potential, hydropower already facilitates the integration of wind and solar energy into the supply system [19]. Pumped hydro-energy storage (PHES) is the most widespread and mature utility-scale storage technology currently available, and it is likely to remain a competitive solution for modern energy systems based on the high penetration of solar PV and wind energy. Storage solutions are essential for addressing the issues of intermittent generation, supply and demand mismatches, generation shortages, and surplus supply to allow the integration of variable RE [5].

Lesotho has some of the highest quantities of solar radiation on the planet. The daily average solar radiation fluctuated between 5 and 7 kWh/m^2, with December and January having the highest radiation levels, while June and July had the lowest. The majority of the country receives radiation in certain areas in the southwest, receiving over 7 kWh/m^2/day on average [20]. The estimates further showed that Lesotho has significant potential for the development of solar energy, with an average of more than 10 hours of light per day and more than 300 days of sunshine annually.

Against this background, immediate action is required to improve clean energy production in Lesotho. Therefore, the country must conduct studies to analyze its electrical power resources to overcome the threat of power security, environmental pollution, and economic deterioration [21]. In this study, the possibility of utilizing wind and solar power pumping systems for recirculating water to sustain hydropower generation at Lets'a-la-Letsie in Quthing Lesotho is investigated.

1.3 Objectives

In this project, a hybrid energy conversion technology based on wind and solar energy with a hydrobased energy storage system is proposed. This study investigates how pumped hydropower storage (PHPS), solar, and wind energy production can be coupled for maximum flexibility, dependability, and sustainability in energy storage. Based on this context, this study explores the potential of coupling pumped hydro-power storage, solar, and wind to generate stable and sustainable energy for villages near Lets'a-La-Letsie in the Quthing district of Lesotho. The objectives of this research are:

- Evaluating the potential for hydropower, wind and solar at the Lets'a-La-Letsie.
- Assessing the feasibility of coupling these renewable energy resources, including possible use of wind and solar to recirculate water for pumped hydropower storage at Lets'a-La-Letsie.

1.4 Research questions

- Investigate the available wind and solar resources for designing wind and/or solar pumping systems for recirculating water for pumped hydropower storage systems at Lets'a-La-Letsie.
- Determine the potential locations and capacities of pumped hydropower storage system upper and lower reservoirs.
- Design and optimize a solar, wind, and pumped hydropower storage hybrid system.

1.5 Significance of the study

The intention of this study is to add to the scientific knowledge of hydropower storage using wind and solar energy to recirculate water at Lets'a-La-Letsie in Quthing, Lesotho. As highlighted earlier, storage solutions are essential for addressing the issues of intermittent generation from solar and wind, supply and demand mismatches, generation shortages, and surplus supply to allow the integration of variable renewable energy (RE). The findings of this research are intended to benefit Lesotho's energy sector

and the country as a whole. This research is also planned to raise awareness of the urgency of reducing greenhouse gas emissions by using renewable energy. Moreover, the study is also in line with SDG 7 which advocates for access to affordable, reliable, sustainable, and modern energy. SDG7 is underpinned by three targets: ensuring universal access to energy services, increasing the share of renewables in the energy mix, and improving energy efficiency [6]. The rationale behind this research is to develop an affordable, reliable, and sustainable energy generation solution for the Quthing District. Potentially, the implementation of the findings of this study can help the country to save money on energy purchases and reduce the amount of imported energy. This study also supports the Lesotho Energy Policy 2015-2025 and the National Strategic Development Plan 2012-2017 which both advocate for sustainable development, power supply security, economic growth and non-discriminate access to the electricity ([12], [22]).

1.6 Outline of the study

This study is organized into five chapters: introduction, literature review, methodology, results, discussion, and finally, the conclusion and recommendations. Chapter 1 provides the background of the study, problem statement, objectives, and research questions, significance of the study, and research scope. Chapter 2 details the evaluation of previous studies on wind, solar, and pumped hydro-power storage hybrid systems. Chapter 3 describes the methodology followed to design and optimize the hybrid system. Chapter 4 discusses the results, and Chapter 5 provides the conclusions of the study and recommendations for further research.

CHAPTER 2: Literature review

2.1 Solar Energy

Solar energy, which is readily available in many regions of the world, is regarded as one of the best natural renewable energy sources [2]. Solar energy is converted into electricity by photovoltaic (PV) effects, using sunlight captured by solar panels. This energy can then be used to power electrical equipment or stored to provide power in emergencies.

The factors that affect PV output are as follows:

- The sun intensity: Increasing solar radiation incident on the module increases the output power.
- Tilt angle: When the sun's rays are perpendicular to the surface of the PV, it generates its maximum output power. The PV array has to be oriented to maximize the amount of radiation it gets from the sun if tracking is not used to follow the sun. The PV system in the northern hemisphere should, as a general rule, face south, slanted by an angle equal to the location's latitude. Similarly, the PV

system in the southern hemisphere should face north, inclined by an angle equal to the location's latitude.

- Partial shading: Partial shading of the PV module affects the open voltage and short circuit current of the PV cell. The shaded PV cell in a long line of connected PV cells maintains string current even if its photovoltaic potential is lost. Since the shaded cell is now acting as a load on the string and is no longer providing power, the I-V characteristics of the string are impacted. A location with minimal shading must be chosen before installing the PV system.
- Cell temperature: The short circuit current and open voltage of the PV cell drop with the increasing cell temperature, which also results in a decrease in the cell's power production.

The output energy of the solar module is estimated from Equation 1:

$$\boldsymbol{Q_e = \eta_{pv} A I_{array}} \qquad \text{Equation 1}$$

Where $\boldsymbol{\eta_{pv}}$ is the efficiency of the solar cell, A is the area of the module in m^2, and $\boldsymbol{I_{array}}$ is the irradiation incident of the module per unit area.

The array efficiency is estimated from Equation 2:

$$\boldsymbol{\eta_{pv} = \eta_{STC}(1 - \beta(T_c - T_{c,STC})} \qquad \text{Equation 2}$$

where $\boldsymbol{\eta_{STC}}$ is the PV efficiency at standard test conditions (STC), $\boldsymbol{T_c}$ is the cell temperature, and $\boldsymbol{T_{c,STC}}$ is the cell temperature at STC.

The incident irradiation $\boldsymbol{I_{array}}$ is determined from Equation 3:

$$\boldsymbol{I_{array} = I_{bn} cos\theta + \frac{1}{C} I_d} \qquad \text{Equation 3}$$

where $\boldsymbol{I_{bn}}$ is the direct irradiance at normal incidence, $\boldsymbol{\theta}$ is the angle of incidence of the beam radiation on the collector surface, $\boldsymbol{I_d}$ is the diffuse irradiance, $\boldsymbol{C}$ is the concentration factor for flat plates.

Figure 4 shows an I-V curve. The plot indicates the open circuit voltage (VOC) and short circuit current (ISC). These are the maximum currents and voltages that a solar cell can achieve; if the cell is shortcircuited, ISC will happen, and if it is open-circuited, VOC will happen [23].

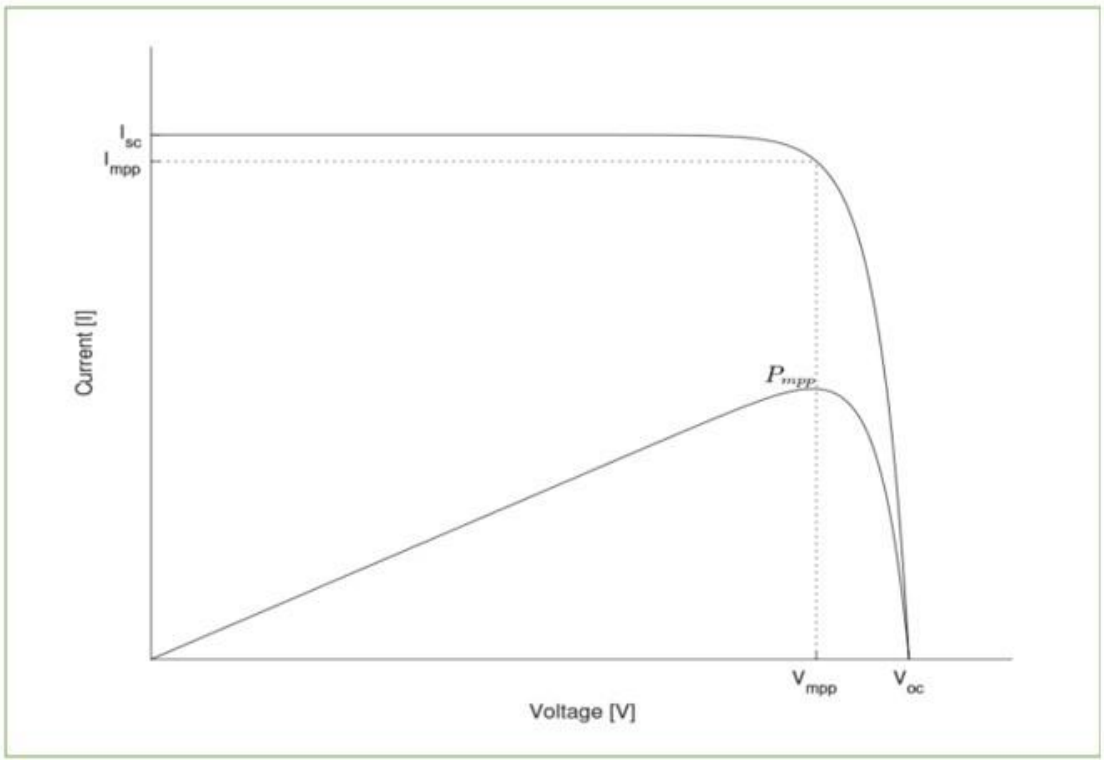

Figure 4: Typical I-V curve of a solar cell [28]

For decades, PV systems have been successfully installed worldwide in a range of different applications, such as grid-scale power plants, household installations, community micro grids, and electricity for remote weather stations and telecommunications towers. Previous studies have indicated that a successful PV system can deliver electricity for almost 20 years without maintenance [24]. Figure 5 shows an increase in the PV installations in SSA (Sub Saharan Africa) from 2017 to 2022. The results show that the PV capacity additions in SSA are forecasted to increase from 1.1 Gigawatts (GW) in 2021 to above 2.5 GW in 2023-2025 [25].

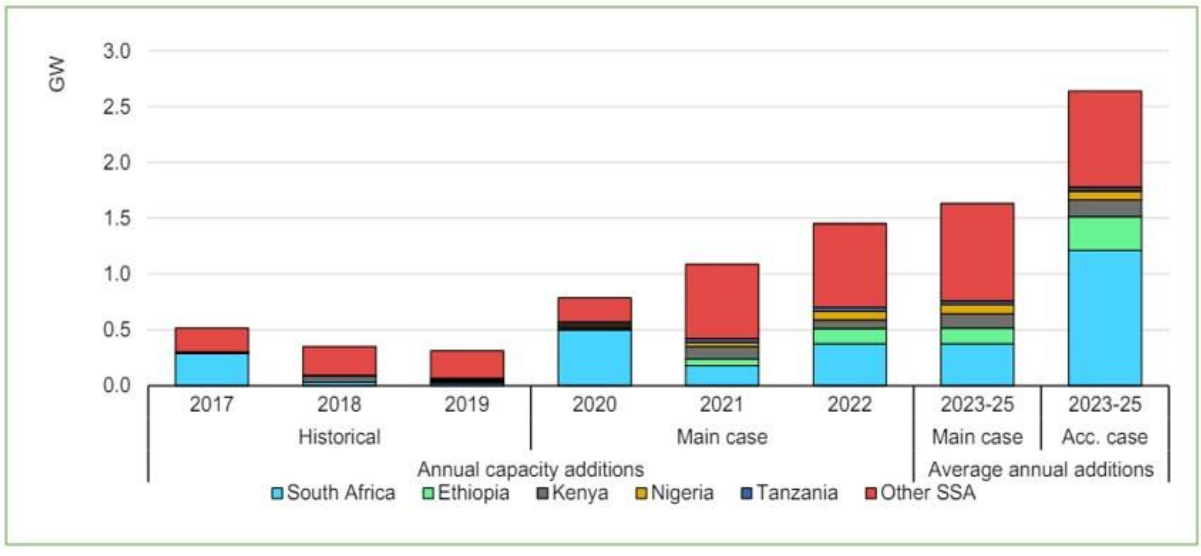

Figure 5: Sub-Saharan Africa solar PV capacity additions and average annual additions [25].

Figure 6 shows the generated solar power, PV power, and CSP power. The solar energy has been increasing slowly thus far. This could be because its technology is relatively expensive for African countries, and it is not a well-known technology [26].

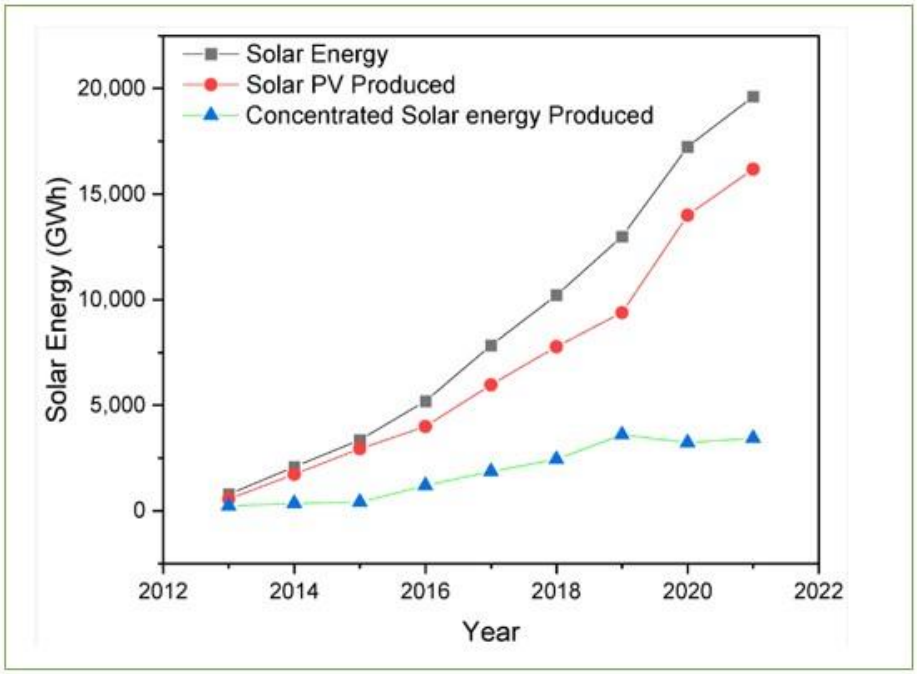

Figure 6: The produced solar power, PV power, and the CSP power in Africa [26].

Numerous models have been developed to estimate global solar radiation based on various meteorological and geographic factors, including sunshine duration, mean ambient temperature, maximum and minimum ambient temperatures, relative humidity, cloud cover, precipitation, latitude, longitude, altitude, and extraterrestrial radiation [2]. Several technologies are available to estimate solar resources, but they may be broadly divided into two groups: ground-based measurements and data acquired from satellites. In addition, several commercial companies offer data on solar radiation, and they all make use of satellite-derived information that is then put into their algorithms to produce time series for numerous variables with varying levels of uncertainty.

Figure 7 shows the distribution of solar energy over Lesotho as provided by the Global Solar Atlas website. The first Global Atlas was launched at a time when many countries were looking to enhance their renewable energy deployment and wanted to know how much wind and solar resources were available in their country. By providing a high-resolution resource map using a consistent manner all over the world, the Global Solar Atlas and Global Wind Atlas have been able to provide a single starting point for answering that question, avoiding the requirement for each country to conduct its own wind and solar atlas at an early stage of investigation [27]. On the other hand, ground-based sensors such as pyranometers allow for the acquisition of high-quality solar radiation data with a lot less uncertainty

than data received from satellites. However, ground-based measurement projects may be challenging to perform because of their high cost, security, and cleaning requirements.

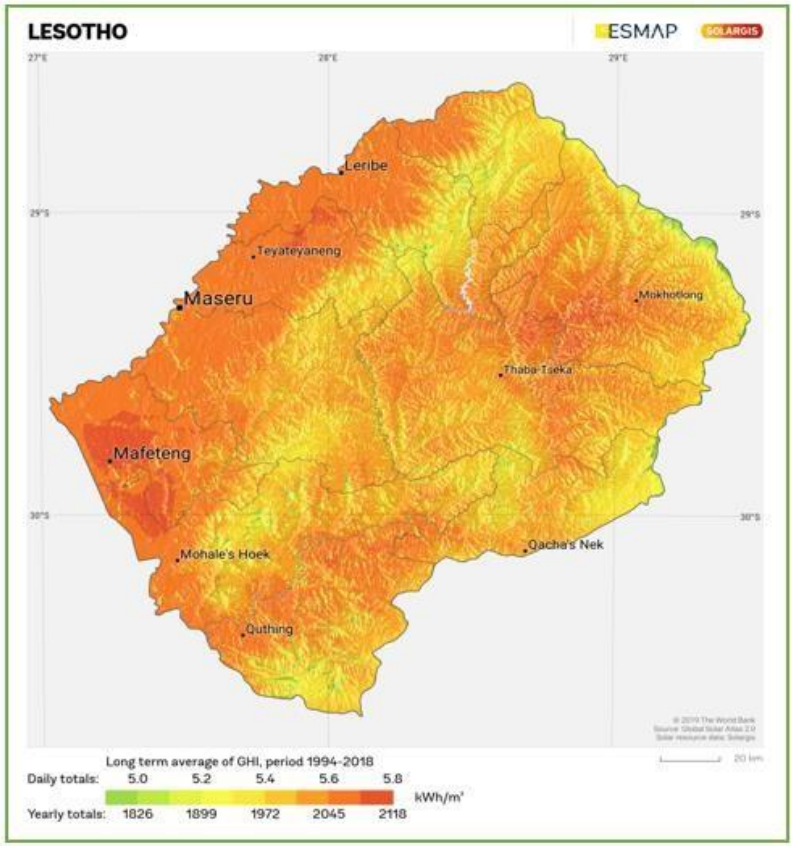

Figure 7: Global horizontal irradiation Map for Lesotho as extracted from Global Solar Atlas.

2.2 Wind Energy

Globally, the amount of power produced from wind energy is significantly increasing. Many nations do not have large amounts of installed wind power, but they are seeing significant development. This is largely because of the extensive research and national energy policies that provide incentives to the industry [28]. Wind energy has great potential to provide significant amounts of electricity in Lesotho. However, grid connection to the sparsely populated mountainous rural areas which form the majority of the population in Lesotho is undoubtedly a huge challenge. This is one of the major factors that have resulted in the current grid connection of less than 15% of the population. Moreover, the cost for the national grid connection of all turbines that would be erected on hills with high wind resources would be enormous [28].

An electrical device, known as a wind turbine, can efficiently convert wind energy into electricity. The wind initially strikes the turbine blades, turning them to generate mechanical energy on the rotor which is then converted to electricity by a generator [29]. Vertical-axis wind turbines (VAWT) and horizontalaxis wind turbines (HAWT) are the most common types of wind turbines. Turbine size and

design are extremely important. Two of the main goals of wind turbine research are to maximize wind collection and reduce costs [30]. The typical components of a wind turbine include blades, rotor, tower, gearbox, and generator, as shown in Figure 8.

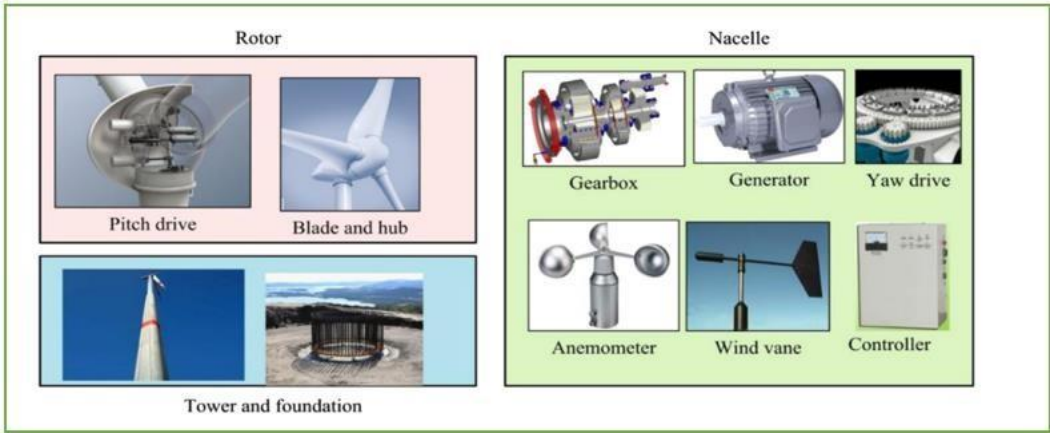

Figure 8: Main components of the wind turbine [30].

The rotor consists of large blades mounted on the hub. The nacelle is positioned on top of the turbine tower and contains the main technical parts such as the rotor shaft and gearbox. The gearbox converts the low rotor speeds to higher speeds to make the generator functional. The generator converts the mechanical energy of the rotor into electrical energy. A tower is used to place the rotor at high altitudes to capture more wind energy [30].

As shown in Figure 9, wind power capacity is gradually increasing in Africa. Global wind power development is largely dependent on robust government regulations. Nonetheless, this is slowing down the expansion of wind energy in Sub-Saharan Africa, where policies for renewable energy are lax. SSA is still in the early phases of renewable energy technology development [26].

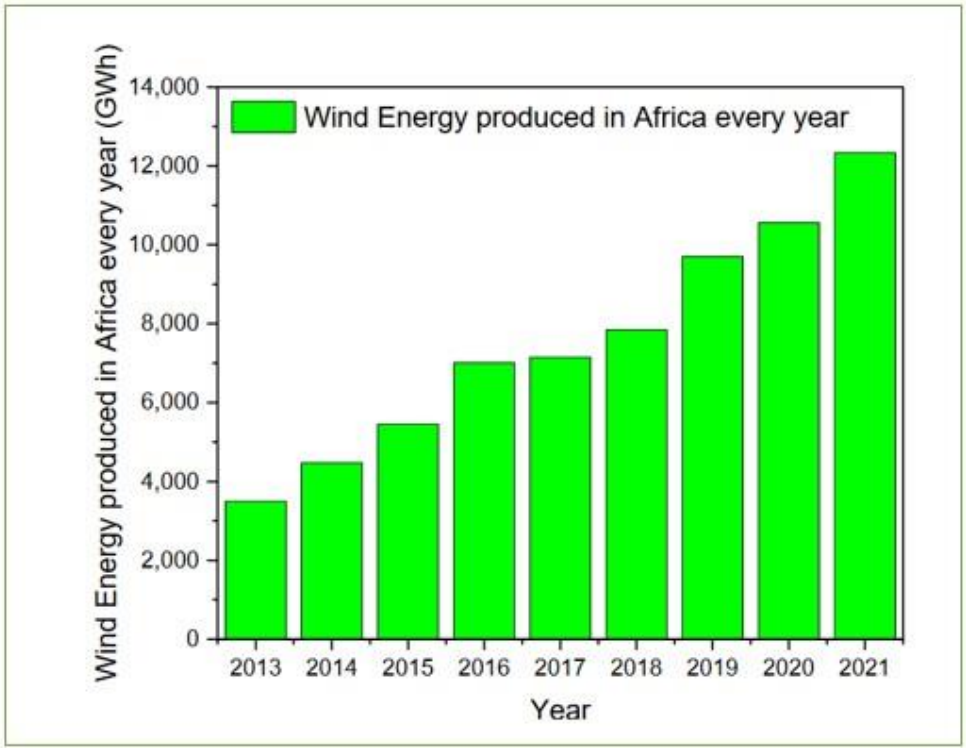

Figure 9: Installed wind energy in Africa [26]

Wind resource assessment is the process of determining the wind power potential at one or more locations or across a region. The mean wind speed or power density variation across a region is often displayed on a wind resource map at a certain height above ground level [31]. Even though there is a growing need for wind energy, its unpredictable nature makes wind energy assessment the most challenging and important aspect of wind energy development.

Regarding the significance of determining wind potential, it was acknowledged that measured data is the best option for evaluation. However, satellite wind data might be utilized as an alternative in areas where year-long time series data are not available [32]. A detailed map of wind resources provides a powerful instrument for the positive exploitation of wind energy, and it is appreciated by a wide range of users [33]. Additionally, estimating the quantity of potential power to be produced by wind at suggested locations requires an accurate analysis of wind data [28]. Wind speed, power density, and their directional distribution are all crucial factors in determining the wind energy potential [34].

As previously indicated, wind energy has great potential to provide significant amounts of electricity in Lesotho. Mountainous and sparsely inhabited sites help maximize the amount of power generated by the wind because they allow the turbines to be positioned to benefit from wind hill effects. Over and above this, there is enough room in the mountains away from habitations to build many turbines [28].

Wind speed is the first factor to be considered when examining a suitable location for the installation of wind turbines to generate power. It is crucial to understand the total quantity of energy that may be

generated over a specific time, as well as the periodic fluctuations caused by the wind's unpredictability. It is worth noting that the power density (PD), which is the strength of the wind on the site per unit area, is another crucial factor to evaluate because it directly correlates to the quantity of power that may be generated on the site [28]. It is also crucial to determine the direction that provides the most energy as wind energy is directly proportional to the amount of electricity that will be generated [34].

The terrain's form and altitude above the ground also affect wind speed. This is because the wind moves slower on uneven terrain. After all, there is more friction between the air and the surface, whereas wind is freer to move across flat surfaces [23].

The kinetic energy of the stream of air with mass *m* and velocity *V* is calculated by Equation 4:

$$E = \frac{1}{2} mV^2 \quad \text{Equation 4}$$

Then, the power from the wind turbine P_{wt} can be given by Equation 5:

$$P_{wt} = \frac{1}{2} \rho A C_p \eta V^3 \quad \text{Equation 5}$$

Where, A is the area swept by the rotor blades, C_p is the rotor power coefficient, and η is the drive train efficiency.

2.3 Solar/Wind and pumped hydropower storage hybrid systems

Photovoltaic production depends on the varying solar radiation, thus the use of energy storage systems is required to minimize reliance on the fluctuating output [43]. First, photovoltaic cells convert solar energy into electrical energy. Then, a mechanical interface consisting of a step-up gear and an appropriate coupling transmits the energy to an electrical generator which also consists of a reciprocating pump for pumping water to the upper reservoir [29]. In other words, solar energy is harvested and stored in the form of potential energy which can be used during peak hours. Figure 10 illustrates a typical and simplified scheme of a photovoltaic (PV)-pumped hydropower energy storage system.

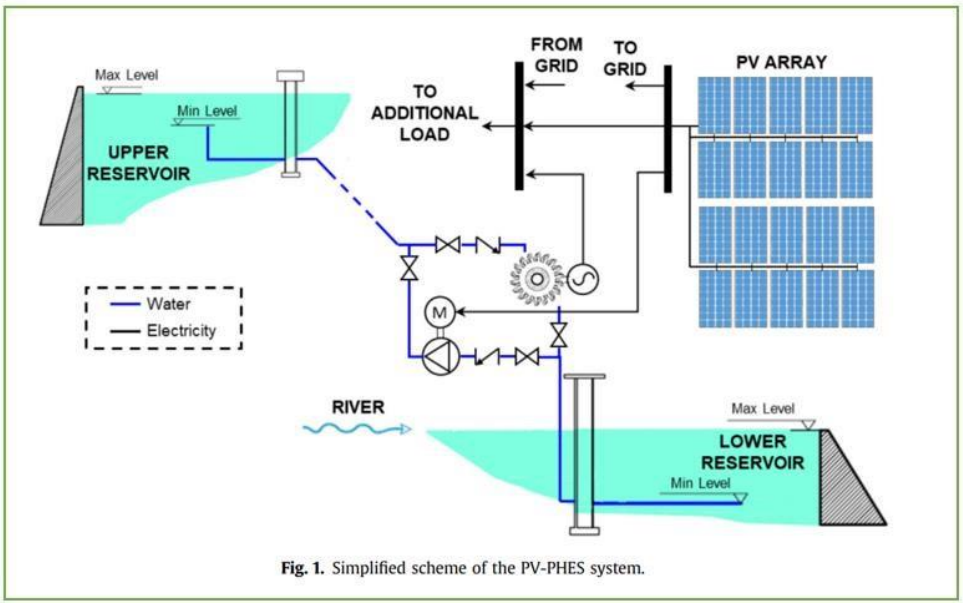

Figure 10: Simplified scheme of the PV-PHES system [43]

Secondly, in recent years, the scientific community has begun to focus on the combined use of wind and storage capacity. Forecasting methods for wind energy have already been significantly developed, and such methods are important for identifying the best practices to be used when operating the system. [46]. The pumped-storage approach appears to be the most promising option for utilizing available wind resources at a high penetration degree for isolated locations with minimal installed electricity [47].

Figure 11 shows the main components of the wind and hydropower hybrid storage systems. A typical wind-powered pumping station consists of several similar pumps that raise water from the lower to the upper reservoir while operating simultaneously [47]. Wind energy is stored by pumping water from the lower to the upper reservoir. Electricity is then generated by conveying water from the upper reservoir to the lower reservoir through the turbine and returning it to the upper reservoir through tunnels or pipes.

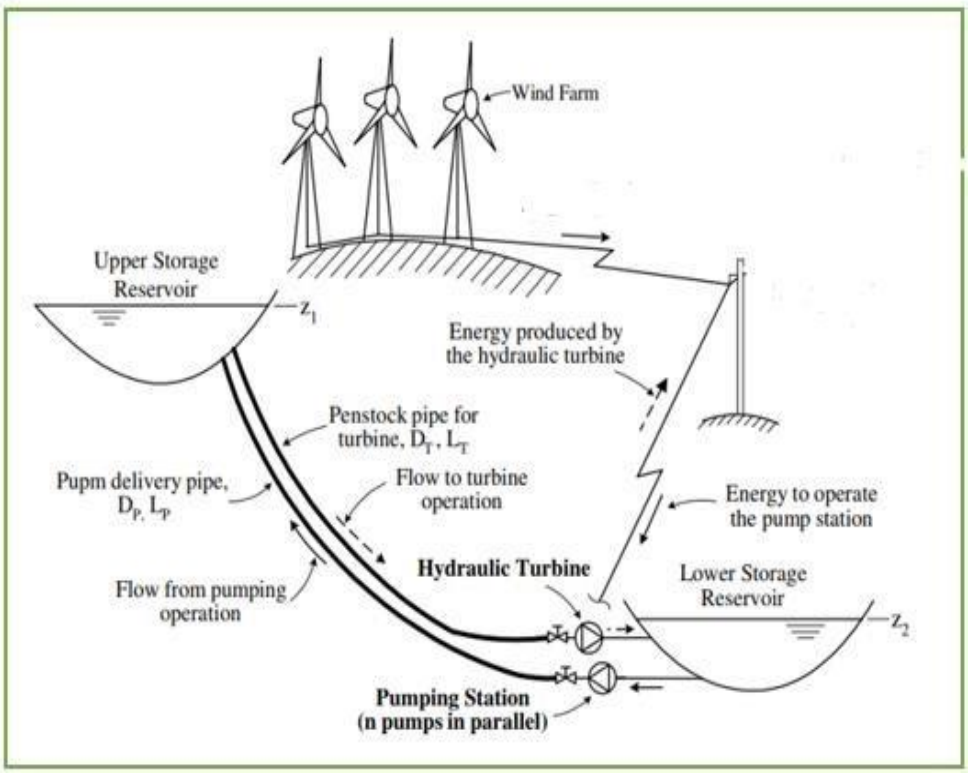

Figure 11: Main components of the hybrid (wind and hydropower storage) plant [47].

A hybrid system that combines various renewable energy sources in a complimentary manner is crucial - the best method to address energy deficiencies is to combine renewable energy sources, which not only increases storage capacity and creates more dependable power networks, but also lessens the consequences of climate change [19]. Also, since HRESs generate electricity from multiple energy sources and can transition between them when one is inadequate, effectively managing the inherent variability of renewables. [48]. Thus, the rapid advancement of renewable energy hybrid systems and their associated technologies has required their integration with energy storage to balance supply and demand.

2.4 Pumped Hydropower Energy Storage systems

Most nations have access to large water supplies via rivers and canals. Hence electricity can be generated from renewable resources without harming the environment. This suggests the need to estimate the future potential of hydropower to balance the increasing need for electricity [35]. There are currently 161 GW of PS plants around the globe and by 2030, there should be another 78 GW [36]. Figure 12 illustrates the historical and projected global rise in pumped hydropower storage developments; it is clear that there is slow traction in the annual pumped storage capacity additions in the sub-Saharan region.

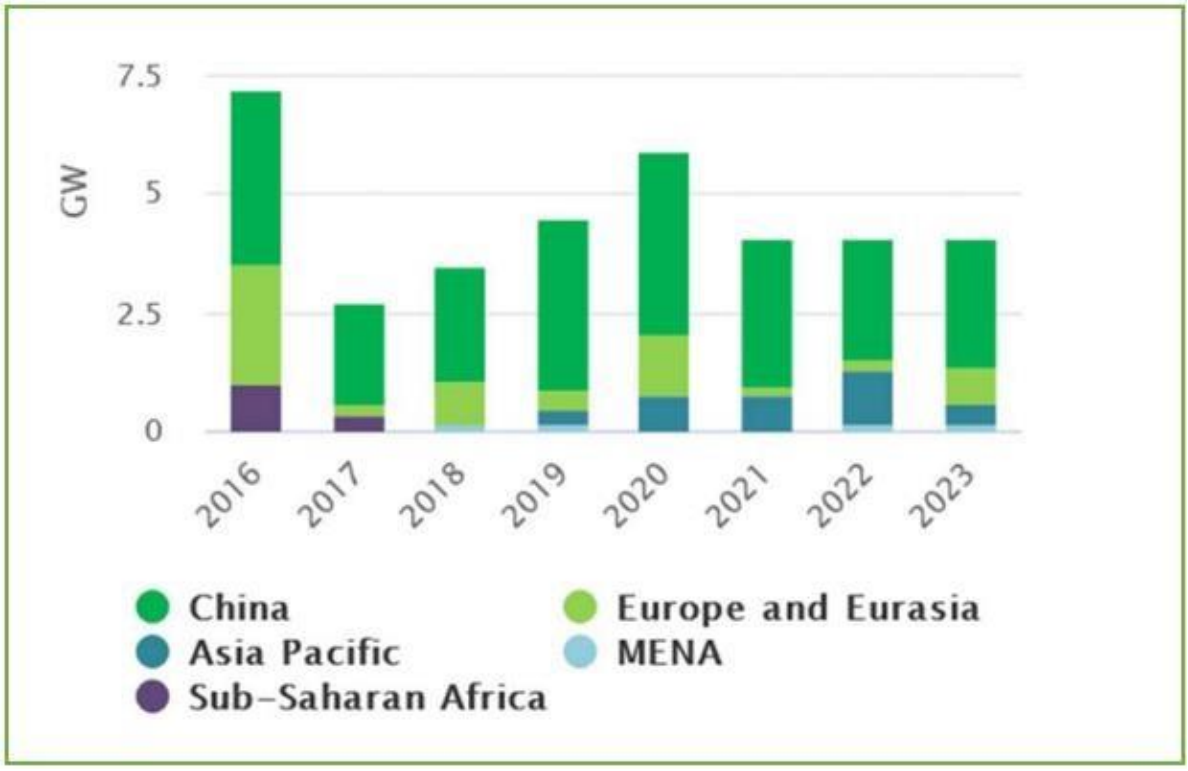

Figure 12: Annual PS capacity additions by region [36].

To ensure the continuous availability and effective use of the energy produced, it is necessary to address the natural unpredictability of various renewable energy sources as their role in the power supply increases. A balanced supply technology portfolio, geographical supply distribution, improved forecasting techniques, demand-side management, and suitable storage options are just a few examples of effective methods for handling this fluctuation [4]. Currently, the most widely used and developed utility-scale storage technology is pumped hydro energy storage (PHES), which is anticipated to continue to be a competitive option for contemporary energy systems with the significant penetration of solar PV and wind energy [5]. In the past, PPS employed two engines or electric motors: one to pump water to the top tank and the other to power the hydro plant and produce energy. Reversible turbines are a single pump that can perform both tasks. These reversible turbines result in lower installation and upkeep expenses [37].

One of the most effective storage technologies that can balance the use of highly variable renewable energy sources such as wind and solar is the pumped-storage power plant (PSPP). This is a mature, large-scale, quick-response technology. When used in an energy system, hydroelectricity is advantageous because it can quickly adapt to changing loads by altering water flow through the turbine [14]. By far the most tested of the power storage technologies, PSPP was estimated to account for 99% of the 127 GW of the total global storage capacity in 2010 [38]. Autonomous power networks with substantial renewable output must take the necessary precautions to overcome the unpredictable and intermittent nature of most of these energy sources to maintain the balance between energy supply and

demand. It is essential to maintain this balance to regulate grid voltage and frequency and preserve the quality of the energy supply. Combining energy storage and dispatchable technology is a common strategy for achieving this balance [39]. However, it must be noted that one major challenge with PHS systems is their capital investment which has the potential to escalate the initial cost estimations to cater for unforeseen delays and unexpected site-specific factors; this can also result in extended lead times for these projects [40].

As illustrated in Figure 13, a typical PHES system transfers the water flow between two reservoirs at various heights to store and produce energy. Pumping water from the lower reservoir to the upper reservoir can store energy in the form of hydraulic potential energy when the price of electricity is low owing to an excess energy supply. By releasing the water held in the higher reservoir to the lower reservoir, energy may be produced when the price of power is high owing to an increase in energy demand [41]. According to their operational architecture, PHES systems may be split into two broad categories: closed-loop systems and open-loop systems. In closed-loop systems, the PHES facility is completely cut off from any naturally flowing water sources [42]. Closed-loop systems have a lower environmental impact than open-loop systems because they conserve water and avoid damaging natural water bodies. Moreover, their placement may be in regions where restricted water resources make openloop systems impractical [40].

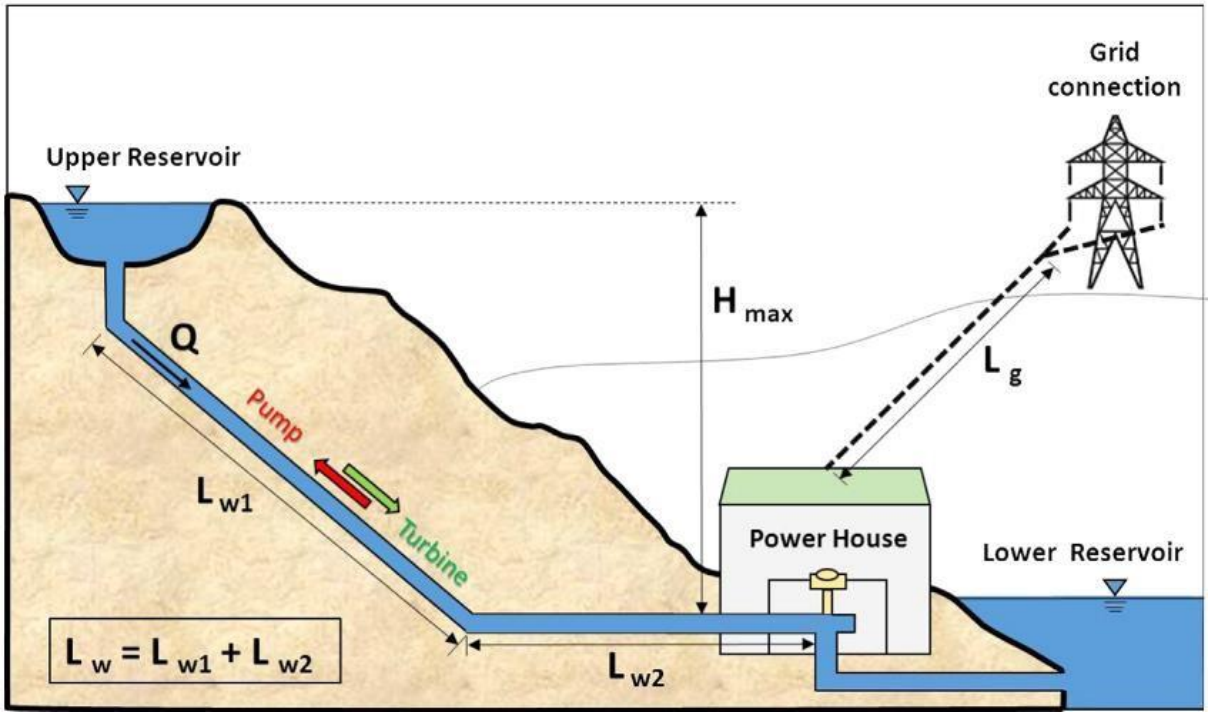

Figure 13: Schematic drawing of a pumped-storage power plant [38]

The storage capacity of pumped hydro storage (PHS) plants can also be used to distinguish them as it directly affects their run times (performance). Systems for daily pumped hydro storage (DPHS) are

often appropriate for controlling the daily variations in the power demand (day-night energy arbitrage) [40].

The cascade system makes use of hydropower as a flexible energy source to offset the fluctuation of wind and solar output, resulting in a steadier and more dependable electricity supply. Solar and wind are variable energy sources and are difficult to align with the demand; hence there is a need to introduce hydropower storage [19]. This system consists of a photovoltaic array, wind turbine, pumped-hydro energy storage system, and control station. Based on the deciding variables such as capital costs, appropriate terrain, and climate change issues, this is currently the most economical method of storing huge volumes of renewable energy [19]. A pumped hydro storage (PHS) plant typically pumps water uphill into a reservoir while using power during times of low demand and low electricity costs, and then permits water to flow downhill through turbines while producing electricity during times of high demand and high electricity prices .

The operating ranges and efficiency values depend on the pressure losses, pump/turbine characteristics, electric losses, and gross-head-dependent plant losses [43]. The hydro turbines transform the mechanical shaft power of the water pressure into electrical generator-driveable power. The relationship between the available power, head, and discharge is shown by Equation 6.

$$\boldsymbol{P = \eta \rho g Q h} \qquad \text{Equation 6}$$

Where η is the hydraulic efficiency of the turbine, $\boldsymbol{\rho}$ is the density of water (kg/m^3), **g** is the acceleration due to gravity (m/s^2), **Q** is the discharge (m^3/s), and **h** is the head of water acting on the turbine (m).

A hydrograph is used to demonstrate flow rate fluctuations and a flow duration curve is used to show the times of the year when a specific flow is attained or surpassed [14]. To estimate the rated power of a hydropower plant, a design flow is estimated to be between $\mathbf{Q_{50}}$ and $\mathbf{Q_{60}}$.

In a typical modest hydropower system, water is retrieved from the river by redirecting it via an intake weir. Before reaching the turbine, the water travels through a desilting tank which is sufficiently slow to allow suspended particles to settle. In systems with medium or high heads, the canal transports water to the forebay. Water often enters the turbine straight from the weir in low-head systems. It is transported from the forebay to the turbine through a penstock and pressure pipe [35]. The vertical distance which the water travels as it transforms its potential energy into kinetic energy known as the head is another crucial quantity to consider in addition to flow rates. The net head is estimated from Equation 7;

$$\boldsymbol{H_n = H_g - H_f} \qquad \text{Equation 7}$$

Where $\mathbf{H_g}$ is the gross head, $\mathbf{H_f}$ is the total head losses, and $\mathbf{H_n}$ is the net head.

The total head losses that arise in the pipeline can be longitudinal ($\mathbf{h_f}$) and local losses ($\mathbf{h_{loc}}$) which is expressed by Equation 8:

$$H_f = h_f + h_{loc} \quad \text{Equation 8}$$

Where $\mathbf{h_f}$ are longitudinal losses (m) and $\mathbf{h_{loc}}$ are local losses (m).

The total friction losses, $\mathbf{H_f}$ is a function of the length, **L**(m), diameter, **D**(m), and friction factor **f** of the penstock and can be calculated using the Darcy-Weisbach from Equation 9:

$$H_f = f.\ \frac{L}{D}\ \frac{V^2(t)}{2g}. \quad \text{Equation 9}$$

Where **v** is water velocity (m/s), and **g** is gravity (m/s^2).

For maximum power production, $\mathbf{H_f}$ is determined from Equation 10:

$$H_f = \frac{1}{3} H_g \quad \text{Equation 10}$$

Capacity factor is the ratio of the actual annual energy produced by the power plant to the rated annual energy is determined from Equation 11:

$$C_p = \frac{actual\ annual\ energy}{rated\ annual\ energy} \quad \text{Equation 11}$$

Reynold's number ($\mathbf{R_e}$) is estimated to determine the type of flow, and it is determined from Equation 12. It is described as the dimensionless ratio that defines the relationship between inertial forces and viscous forces of a fluid.

$$R_e = \frac{\rho V D}{\mu} \quad \text{Equation 12}$$

Where **ρ** is water density (Kg/m^3), **V** is the average fluid velocity (m/s), **D** is the diameter of a penstock (m), **μ** is the dynamic viscosity of fluid (Kg/m-s), and **v** is the kinematic viscosity of a fluid in (m^2/s). The estimated Reynold's number is used to determine the type of flow as well as the friction factor. For non-uniform roughness, estimates of the friction factor **f** can be made as functions of the Reynold's number $\mathbf{R_e}$ and relative roughness (**ε /D**) as show by Equation 13.

$$Relative\ Roughness = \frac{\varepsilon}{D}$$ Equation 13

Hydroelectric power can be produced without hazardous waste and has far lower greenhouse gas emissions than fossil fuel energy plants. It is relatively affordable, dependable, sustainable, and renewable [44]. Resources for hydropower rely on discharge and gross head. Hydropower plants receive their fuel from the river networks' discharge [45].

2.5 Stream flow measurement methods

River flow can be measured using various traditional and advanced methods. Traditional techniques are simple to employ to determine the flow rate of a possible hydropower site. However, they measure only the modest flow rates and have poor accuracy. An advanced technique was utilized for highly accurate measurements of high flow rates. The flow characteristics of a river or stream are analyzed by the use of the flow duration curve [45].

Table 1 shows the methods used to measure the flow rate of the stream:

Table 1: Methods used to measure stream flow rates ([45], [49]).

Discharge Measurement	
Method	Description
Bucket method	The procedure involves the bucket of choice and collects the water for the time taken to fill it as presented
Float method	This technique involves lowering a floating device to a specific depth to assess the velocity and flow rate in a river. The surface velocity of the stream is determined by the amount of time it takes a floating item to reach a specific distance.
Dilution method	The dilution approach involves injecting a tracer into a river and having it travel a certain distance to completely mix with water. Utilizing radioactive, fluorescent, or chemical substances as a tracer is common.
Velocity-area method	The vertical flow velocity and water depth are measured using the velocity distribution method at various locations between the riverbed and the water's surface. The depth increments vary from 0.1 to 0.9. The area under the curve divided by the water depth yields the mean velocity.
Advanced measurement methods	Common instruments: Current Meters, Hydraulic Structure, Slope-area Manning, Electromagnetic flow meter, and Ultrasonic device.
Indirect flow rate measurement	The ungauged catchment uses the indirect flow rate measurement. The catchment area ratio, stage-discharge relationship, regression, and spatial interpolation methods are used to calculate the flow rate in the ungauged catchments.

To manage water resources, understanding the behaviour of a river's flow is crucial. Nevertheless, only a small percentage of rivers worldwide have streamflow monitoring, and the majority of catchments are still entirely ungauged. Also, since many river basins are in isolated, mountainous areas and have complicated environments, measuring flow from these basins is extremely difficult and not economically viable. As a result, mountainous river basins that are ungauged do not regularly monitor their river discharge [50]. However, several methods in modern-day hydrology could be used to calculate hydrological characteristics at ungauged sites [51]. Methods that can be used for ungauged basins include extrapolating data from gauged basins, utilizing satellite remote sensing for information gathering, employing process-based hydrological models with specified or measured climate inputs, and using integrated meteorological-hydrological models that don't require specific precipitation inputs. [52]. The choice of a model is determined by the purpose of the model and the availability of data [53].

Hydrological analysis [54] indicated that it is important for any hydropower plant to consider the available average water supply in terms of flow rates ((Q_d = design flow (m^3/s)). This is estimated from available historical data from the past. Since the data has some uncertainty due to varying rainfalls, the mean stream flow rate values are used to estimate the amount of energy to be produced by a power plant. A hydrograph is used to show variations in stream flow rates; it shows the actual flow rates concerning time. The flow duration curve is used to present data in a manner that a certain flowrate is reached or exceeded.

Goodarzi et al [55] applied the geostatistical approach to estimate the flow duration curve parameters in ungauged basins for Dez river in the west and southwest of Iran. The geostatistical method is used to forecast flow duration curves at non-measured stations. This approach applies the maximum likelihood (ML), inverse distance weighting (IDW), and probability kriging methods to forecast the flow duration curve over extended periods in a basin with ungauged areas. Prieto et al. [56] also studied the prediction in ungauged catchment problems by exploiting advances in flow index selection and regionalization in the Bayesian inference, and developing new statistical tests of model performance in ungauged catchments.

Lee et al. [57] investigated the application of a QGIS-Based Model to estimate the monthly stream flow by applying a Long-Term Hydrologic Impact Analysis (L-THIA) simulation. The L-THIA model is a useful analytical tool because it establishes curve numbers based on the hydrological soil type and land use before determining the direct runoff based on rainfall totals [57].

Osei et al. [58] carried out a complementary hydro-climatic study of the Owabi watershed using the Soil-Water-Assessment-Tool (SWAT) to simulate the stream flow and water balance of the watershed and predict its future state using the QGIS interface. Abate et al. [59] also used the same approach to model the hydrology of the Kobo-Golina catchment in Ethiopia.

Saka et al. [60] explored the drainage area ratio (DAR) to estimate discharge values at ungauged sites. In this case, three basins with similar hydrologic characteristics were chosen for this purpose. The DAR method mainly depended on a regression analysis between the project site and the other basins/subbasins that have long-term data [60]. Emerson et al. [61] also applied the DAR method in their study to estimate stream flow for sites where no stream flow data were collected. The technique is simple to apply, needs minimal data, does not require development, and is frequently the only one accessible since precipitation-runoff models or regional statistics have not been created [61]. The drainage area ratio (DAR) just needs the stream flows at an index site and the drainage areas of the index and ungauged sites [60].

$$\frac{Qy}{Ay} = \frac{Qx}{Ax} \qquad \text{Equation 14}$$

Where **Q** is the stream flow, **A** is the drainage area, **X** is the gauged site, and **Y** is the ungauged site. Saka et al. further indicated that more often than not, the logarithms of the stream flow are better behaved than the flows in real space, thus;

$$\frac{\ln(Qy)}{\ln(Ay)} = \frac{\ln(Qx)}{\ln(Ax)} \qquad \text{Equation 15}$$

Kim et al. [62] adopted a lumped conceptual model to generate stream flow values at small, ungauged watersheds using the spatial propagation concept. To guarantee that the error rates on the simulated stream flow data were similar to those for observed data; event-based beginning conditions were optimized while parameters of physical attributes were fixed throughout the spatial propagation phase. Kim et al. [62] concluded that by employing the suggested method, stream flow data for tiny, ungauged watersheds upstream may be produced by a single gauged downstream stream flow without the need for a significant quantity of gauged stream flow data from other sites. Applying the aforementioned approach requires that the runoff conditions at the planned dam site and the gauging station be identical, including the terrain, soil, vegetation, land use, and meteorology (rainfall). A location close to the dam site for the gauging station is ideal.

2.6 Gross head measuring tools

The gross head is the vertical height along the river between the intake point upstream and downstream at the hydropower plant. Sometimes the gross head is referred to as an elevation difference. The gross head can be caused by high slopes that are either natural or artificially created from the intake point to the hydropower house [45].

Natural raised gradient: As shown in Figure 14, water is diverted from the river's main channel upstream through a network of penstock pipes to reach the hydropower plant's turbine before returning to the river [45].

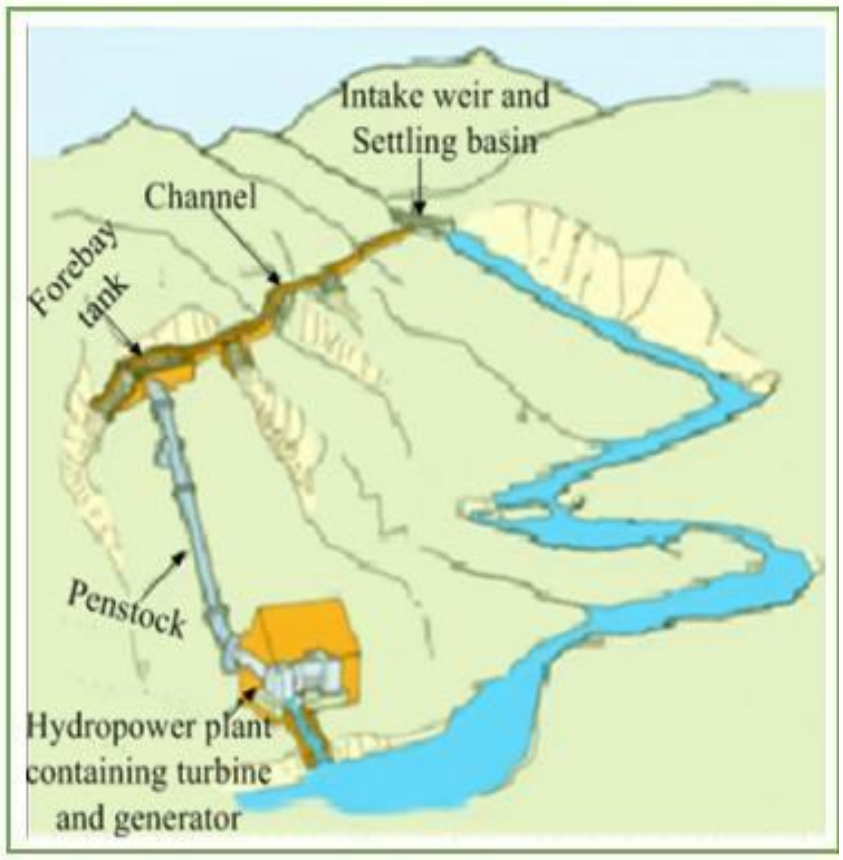

Figure 14: Hydropower plant on the natural elevated gradient [45].

Artificially elevated gradient: A barrage or dam is used to create a reservoir with an artificially high gradient. To get to the turbine intake, the barrage or tunnel was linked to a penstock as indicated in Figure 15 [45].

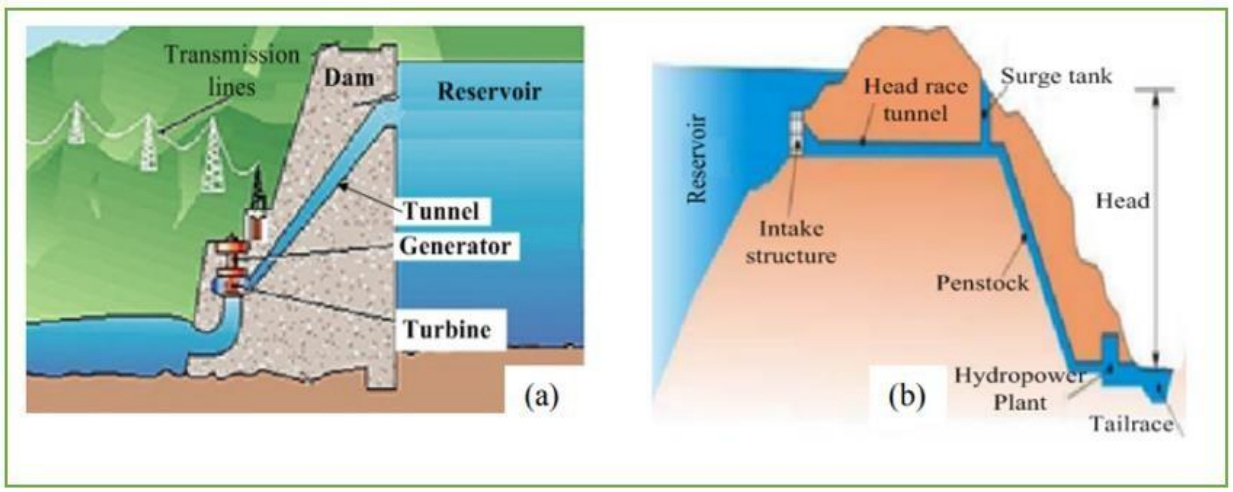

Figure 15: Artificially elevated gradient for hydropower house [45]

The topographic map, DEM map, hose level and pressure gauge, sight and spirit levels, altimeter, hypsometer, clinometer, theodolites, and total stations are some of the tools used in gross head measurement [45]. Table 2 below shows the gross head measurement methods.\ Table 2: Gross Head measuring tools [45]

Gross Head Measurement	
Method	Description
Topographic map	The topographic map is used to give an idea of the vertical drop along the river. The gross head is calculated by taking the difference of the contour lines between two points.
DEM map	A DEM raster map is analyzed using GIS software to calculate the gross head from the intake to the hydropower plant. The technique follows similar steps to how a topographic map is utilized and is primarily employed during desk-based investigations
Hose level	The water-filled hose has two ends—one at the uphill and one at the downward. When both hose ends are in balance, the height difference is measured. To get to the intake or hydropower house, use the same procedures going uphill or downhill.
Hose with pressure gauge	One end of the hose is filled with water and placed uphill while the other end is linked to a pressure gauge and placed downstream to calculate the elevation difference. The gross head is then calculated from the pressure gauge difference.
Sight level	A shooter at a level angles a signal towards a graded ruler downward to determine the gross head. To obtain the gross head, repeat to log each step between the intake and the hydropower house.
The advanced methods	Altimeter, Hypsometer, Clinometer/ Inclinometer, Theodolites and Total Stations.

2.7 Turbine types

There are two basic types of hydropower turbines, namely; impulse and reaction turbines. In reaction turbines, the water pressure exerts a force on the face of the runner blades, but in impulse turbines, the water pressure is converted into kinetic energy before entering the runner. While reaction turbines work better at low head and high flow rates, impulse turbines perform better at high and medium heads [63]. The two most common types of impulse turbines are the Turgo and the Pelton [49]. The Francis and Kaplan turbines, which are part of the reaction turbine family, use the force of the moving water to rotate a runner inside the turbine. Despite having very high specific speeds, reaction turbines perform poorly at low flows [44]. Figure 16 below depicts different types of water turbines.

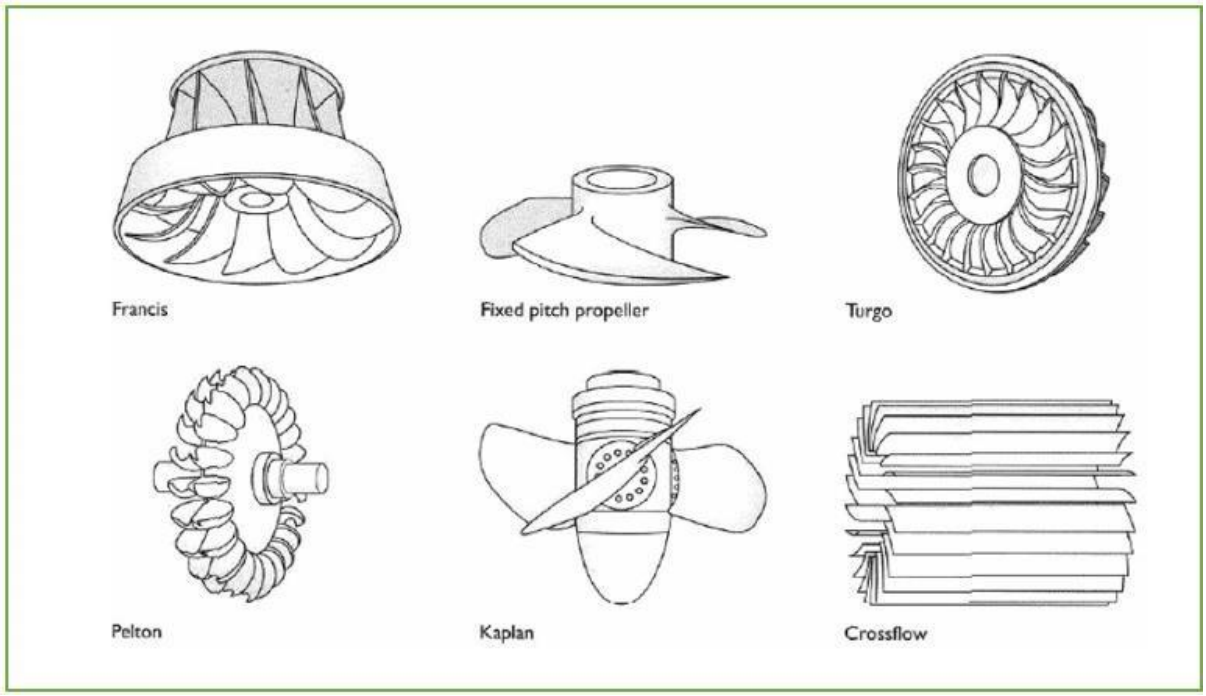

Figure 16: Different types of water turbines [63].

Reservoirs gather water during rainy seasons. This aids in flood management, and in turn, reserves water to be delivered consistently to the turbines all year. The wall of the dam is the most crucial component because it must be able to resist the pressure exerted by the water inside it. Local populations may also utilize this water for cultivation purposes. Gravity, buttress, and arch dams are among the several types of dams. The water flowing in the channel must be regulated during high and low river flow conditions. A weir can be used to raise the water level and ensure a constant intake supply. A hydro-system must extract water from the river in a reliable and controllable manner.

Water is transported from the intake to the power house using penstocks (pipes). Depending on the type of ground, penstock materials, surrounding temperature, and environmental requirements, the penstocks can be erected above or below the ground surface [64].

After determining the type and size of the turbine, the next step is to choose a suitable generator. Synchronous and asynchronous generators can be utilized for small-scale hydro applications. The cost of the generator, the amount of power available, and the type of electrical output (such as AC/DC, frequency, and voltage) all play a role in generator selection [63]. Synchronous generators (SG) are often outfitted with a voltage regulator and a DC electric or permanent-magnet excitation system to regulate the output voltage. Induction Generators operate at a speed directly correlated to the system frequency, and voltage control is not possible in these generators. They obtain their excitation current from the grid and utilize their magnetic field to collect reactive energy. Permanent Magnet Synchronous Generators (PMSGs) create the magnetic field of the rotor. An excitation circuit is not required. The

key benefits of PMSGs are their high energy and efficiency, which means that excitation requires no extra power source [63].

For power transmitted over a long distance, step-up transformers are used to convert lower voltage into higher-voltage electricity to reduce technical losses. At the transmission end, a step-down transformer can be used to decrease the voltage required for distribution. Transmission lines carry electricity from a power plant to customers; their diameters vary depending on the voltage that has to be conveyed; examples are 11 kV, 32 kV, and 132 kV lines. A tailrace directs the water that is released from the power plant after the turbines have spun back into the river downstream. Proper design of the tailrace is important to prevent cavitation and damage to the turbine blades.

Pumping stations often include several parallel pumps connected to pump water up to the higher reservoir. A PHES system's pumping station enables the use of the pumps even for "charging" the higher reservoir with a certain volume of water that will later be discharged [43].

Even for seasoned hydro engineers, finding suitable sites for PHES is challenging. Finding locations where reservoirs can be built that hold a large amount of water relative to the amount of rock and other materials needed to build the reservoir walls is the first criterion. The second condition is to choose pairs of locations that are close to one another and have a significant variation in height. The first condition is necessary because the pipelines and tunnels that connect the two reservoirs are costly, and the second condition is necessary because increasing the head doubles the volume and power of the storage system without increasing the overall system cost [14].

Significant effects on the river environment result from changes in the hydrological regime caused by reservoir operation, particularly when diversion-type hydropower plants which significantly reduce the water content of a portion of the natural river channel are used. The best strategy to repair harm is to maintain the ecological flow [65].

2.8 System performance evaluation

The most popular methods for assessing the performance of the hybrid renewable energy systems are simulation programs [66]. Simulation is the most effective way to evaluate the performance of hybrid renewable energy systems (HRES). Simulation software tools can increase dependability by analysing operational efficiency, unit size, power supply losses, and energy production costs for various hybrid system configurations [67]. Among the software tools available for HRES optimisation are HOMER, HYBRID2, HOGA, TRANSYS, RET Screen, GAMS, ORIENTE, Opt Quest, LINDO, WDILOG2, DIRECT, DOIRES, SimPhoSys, GSPEIS, and GRHYSO [67].

The National Renewable Energy Laboratory (NREL)'s HOMER program sizes a hybrid system based on renewable energy sources from an economic and technological standpoint [68]. HOMER is a popular program used for simulating small hybrid systems that may be used for both design and study [69]. The "Micropower Optimisation Model" or HOMER software analyses energy and computes costs for a hybrid system that is put together using pre-existing internal models. Systems including hydro power plants, solar modules, wind turbines, batteries, diesel generator sets, and other common micro and small hybrid system components may be simulated [39], [70]. Additionally, a pumped hydropower plant can be represented in HOMER by creating an equivalent battery [70].

HOMER software's primary features are [71];

Simulation: It makes an effort to construct a workable setup for every combination you would like to evaluate.

Optimization: HOMER is a fuel-efficient optimization model that enables fuel consumption reduction. It is possible to specify the requirements to view the optimal matches. These criteria are also used to classify analog systems. Figure 17 illustrates a typical schematic diagram of the solar, wind and pumped hydropower storage hybrid system.

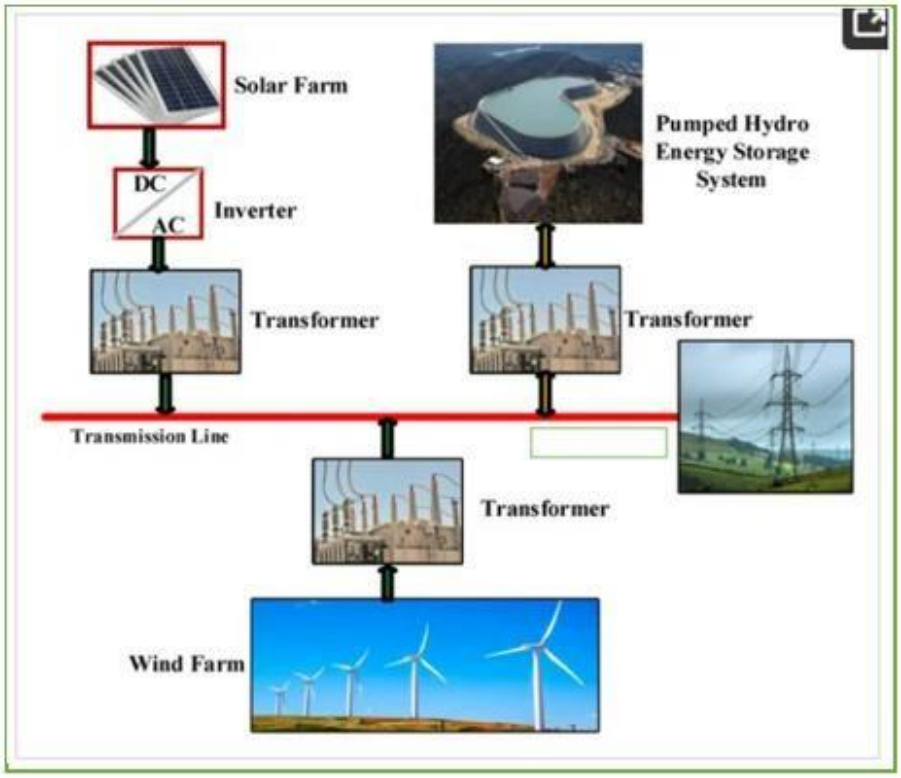

Figure 17: Schematic diagram of the solar PV/Wind/PHES system [72]

HOMER can also be used to perform the techno-economic analysis of renewable energy hybrid systems. To compute the techno-economic analysis of an engineering system, the following economic data are

required: project lifetime, nominal discount rate, predicted inflation rates, and currency [73]. Different economic measurements apply to different conditions, and it is generally a good idea to utilize many when analyzing an investment. The economic measurements presented in this section can be used to compare various investments or projects. The most often used economic indicators are the LCOE, NPC, internal rate of return (IRR), modified internal rate of return, and simple payback time. However, the analyst should be mindful that when comparing alternatives, different measurements may not necessarily produce the same results. Simple payback requirements, for example, reject an alternative with a longer payback period but higher long-term returns [74].

HOMER uses the total net present cost (NPC) to represent a system's life-cycle cost. The NPC aggregates all costs and revenues over the project's lifetime into a single sum of money, discounting future cash flows to the present using a specified discount rate. NPC accounts for initial construction costs, component replacements, maintenance, fuel, power purchases from the grid, and miscellaneous costs like emissions penalties - In NPC calculations, costs are positive, and revenues are negative [75]. The LCOE is defined as the cost of 1 kWh of electricity production [76]. HOMER calculates the cost of generating electricity annually by dividing the yearly total cost (minus the cost of supplying the load) by the total usable electric energy output [73]. Simple payback is the number of years required for the cumulative cash flow difference between the optimized and reference case systems to turn from negative to positive. The payback period is the duration needed to recoup the investment cost difference between the optimized and reference case systems [73]. The internal rate of return (IRR) is the discount rate at which the net present costs of the reference case and the optimized system are equal [73]. Cost of Energy (COE) and Net Present Cost (NPC) are crucial metrics for assessing hybrid energy systems. By performing optimization calculations and analysis with HOMER Pro software, the hybrid system with the lowest COE and NPC is identified, confirming the performance of the optimal RHES arrangement [77].

CHAPTER 3: Research Methodology

3.1 Study area description

The Mohlakeng River, a tributary of the Quthing River, originates in the Lets'a-la-Letsie wetland in the Quthing district [78]. Lets'a-la Letsie is a 0.38 km^2 lake in Lesotho's Maloti Mountains. It is located on the boundary between Lesotho and the Eastern Cape Province of South Africa, some 200 km southeast of Maseru. The steep terrain and elevation differences at Lets'a-La-Letsie are of utmost importance in hydropower generation; the minimum elevation above sea level is approximately 2400 m, while the maximum elevation above sea level is 2820 m. Figure 18 depicts Lets'a-La-Letsie river network.

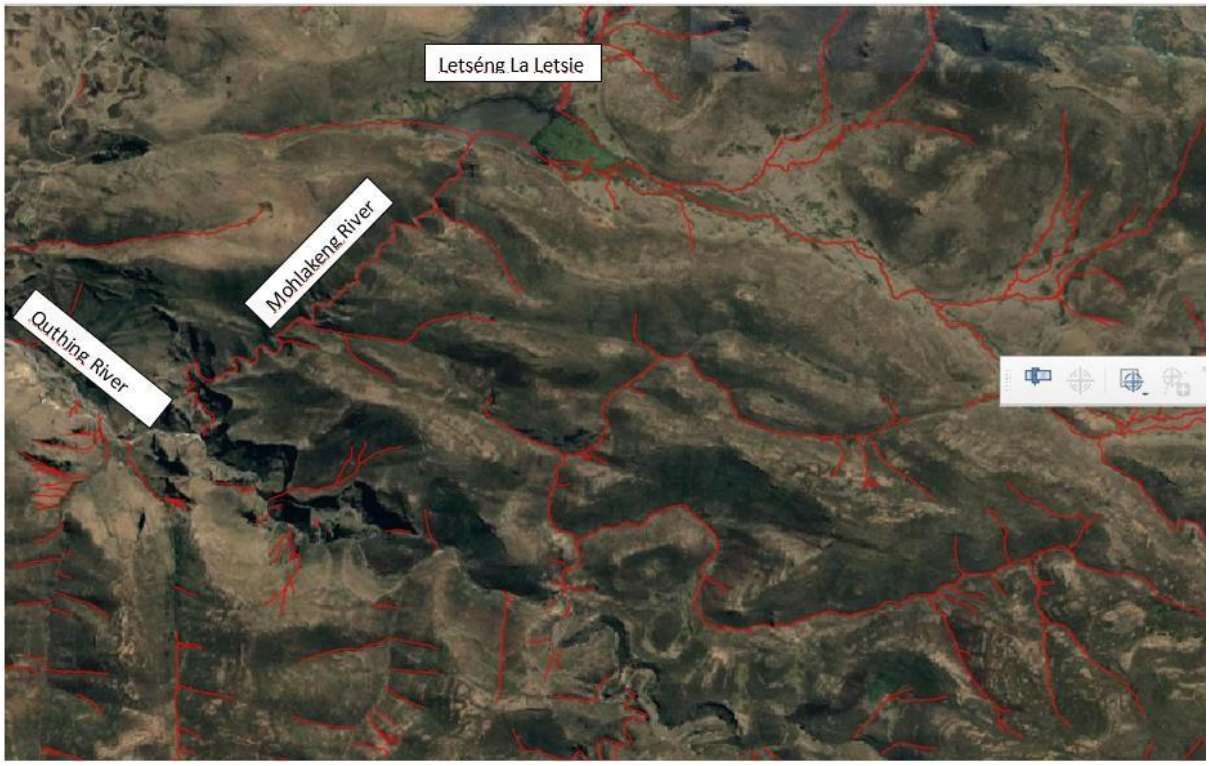

Figure 18: Lets'a-la-Letsie river network

In 2001, the Prime Minister of Lesotho and the Principal Chief of the region jointly proclaimed the 413.9 km^2 watershed region as the Letšeng-la Letsie Protected Area. The lake's greatest recorded depth is 1.4 meters, with a mean depth of around 1 meter [79]. There are recent alluvial deposits on the valley floor including the lake, and the dominating geology is basaltic with dolerite intrusions. The predominant plant species in the Lets'a-La-Letsie area include woody shrubs, sedges, and grasses [79]. Temperatures go as low as -5º C in winter. Snowfall is common in winter, which is in June and July. Maximum temperatures of 26ºC are reported in January. The region also gets around 800 mm of rain a year on average. The mountain tops record the most annual rainfall reaching up to 1000 mm. From October through March, the warmer months get more than 80% of the total rainfall. The main

hydrological value of the wetland is as a source of the Quthing River, one of the major tributaries of the Senqu (Orange) River. The Quthing River contributes about 3% of the Senqu River in Lesotho [80]. In 1984, it was estimated that the mean flow at Lets'a-La-Letsie is approximately 0.5 m^3/s which means a specific runoff of 11,6 1/s/km.

There is a stream-gauging station at Hoko, in the lower part of the Quthing river. This was proposed to be rebuilt as a recording station. The construction work was carried out during the dry season in 1989 and the station has since been in operation [81].

Figure 19 shows the potential sites for hydropower generation around the Lets'a-La-Letsie region.

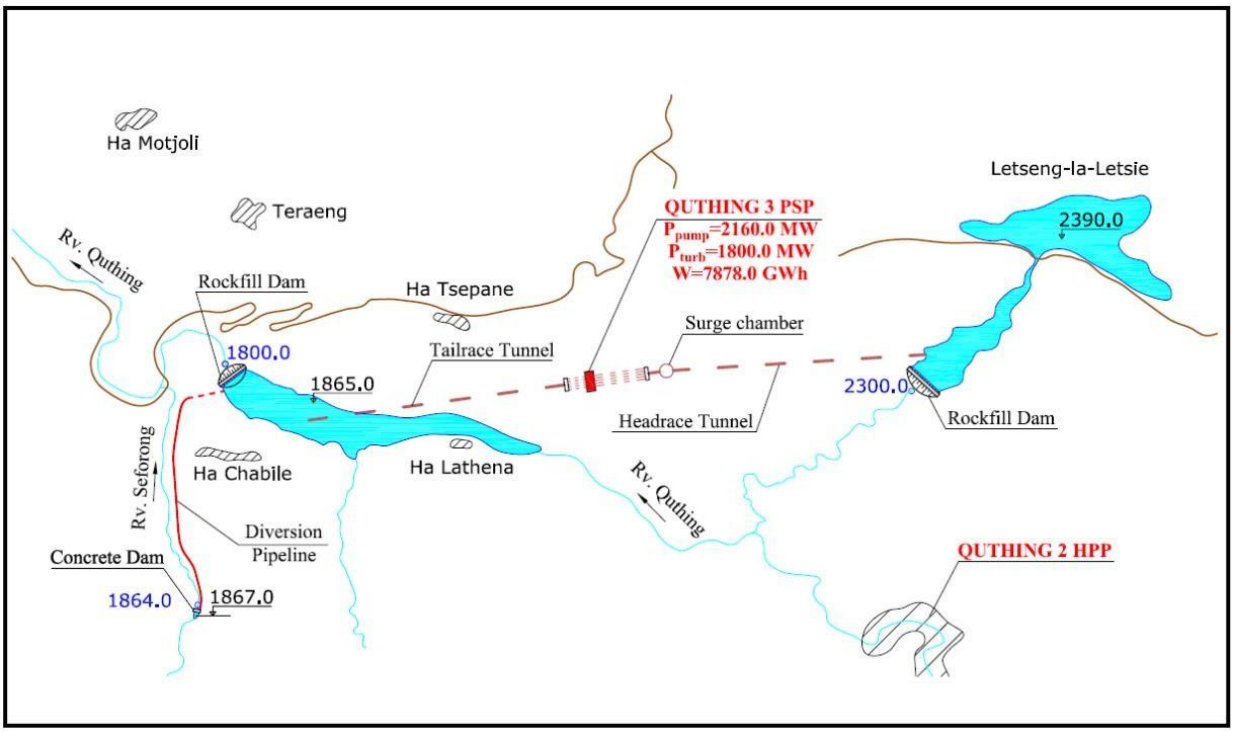

Figure 19: Hydropower potential sites along Quthing river [82].

The electrical demand that the power system must supply at a given time is known as the primary load. Primary load is the term used to describe the electrical demand that is connected to lights, radios, TVs, computers, domestic appliances, and industrial activities. A light that a consumer turns on requires an immediate electricity supply from the power system; the load cannot be delayed [75].

3.2 Research design

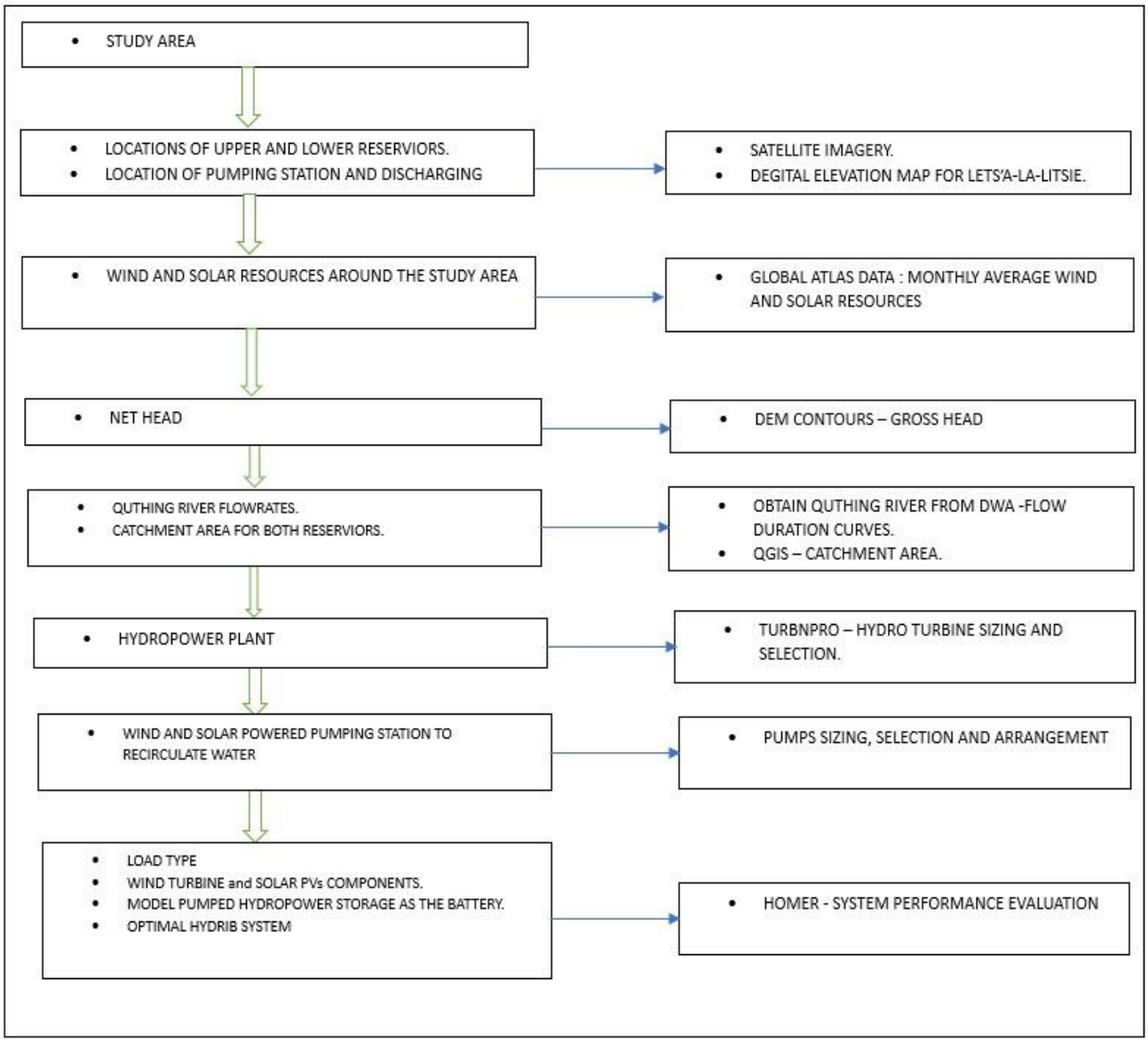

3.3 Wind and solar energy resources assessment

High-resolution datasets and maps of the wind resource are available for all land locations within 200 kilometres on the Global Wind Atlas (GWA) to help the energy experts, decision-makers, and planners use the GWA to identify and comprehend the global, national, regional, and local potential for wind energy [27]. Furthermore, before local measurements are available, wind atlases are a very helpful tool for gaining an initial understanding of the wind resource at a particular place. The degree of certainty in the wind resource and the associated risk of funding a new wind project decreases with the increasing accuracy of the wind atlas [83]. The optimal wind and solar resources location around Lets'a-La-Letsie

were estimated using a web-based global wind/solar atlas tool as shown in Figure 20 and Figure 21. The coordinates with the highest wind and solar resources were identified as the location for positioning the wind turbines and solar panels. Solar and wind energy resources were then determined from HOMER using the coordinates obtained from both the wind and solar global atlas maps.

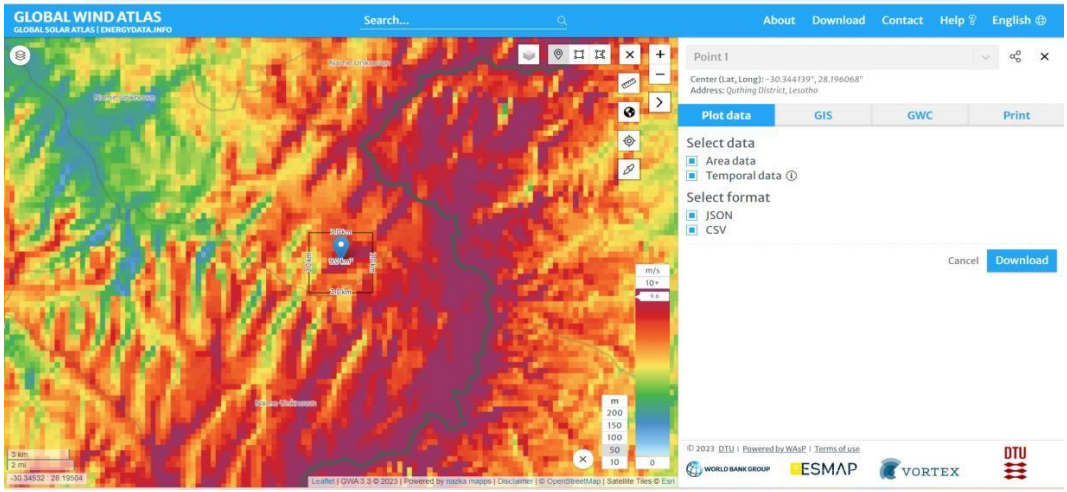

Figure 20: Wind map at Lets'a- la-Letsie as extracted from Global Wind Atlas

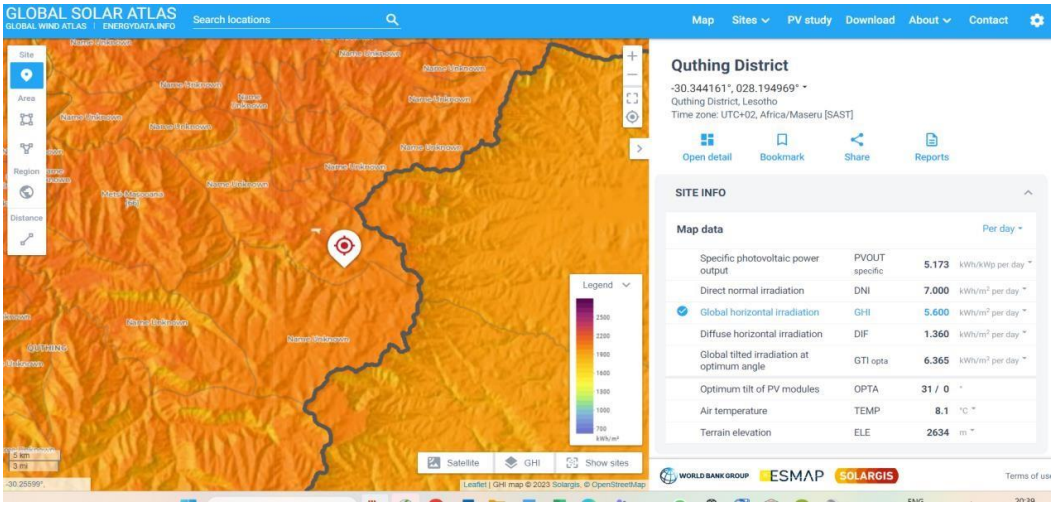

Figure 21: Solar radiation map Lets'a-La-Letsie as extracted from Global Solar Atlas.

3.4 Upper and Lower Reservoir locations

Selecting the ideal site is the first step in the construction and design of pumped storage hydropower plants (PSHP) [84]. Careful planning is needed to guarantee efficiency, cost-effectiveness, and the least possible negative environmental impact when choosing the location of the lower reservoir. The process of choosing appropriate locations for particular kinds of dams and reservoirs involves combining many factors [85]. The terrain, elevation differential, hydrology, closeness to the best renewable resource sources, ecological effect, accessibility, and building costs were all taken into account when choosing the best location for the lower reservoir. Fesalbo et. al. [85] further indicated that the majority of

publications agree on certain criteria for choosing dam locations: the sites must be valleys with maximum flow accumulation for an adequate water volume, higher heights, and a reasonably level slope to support a reservoir that would be least vulnerable to floods. Figure 22 shows the positions of the upper reservoir and lower reservoir along with the river network (red streams).

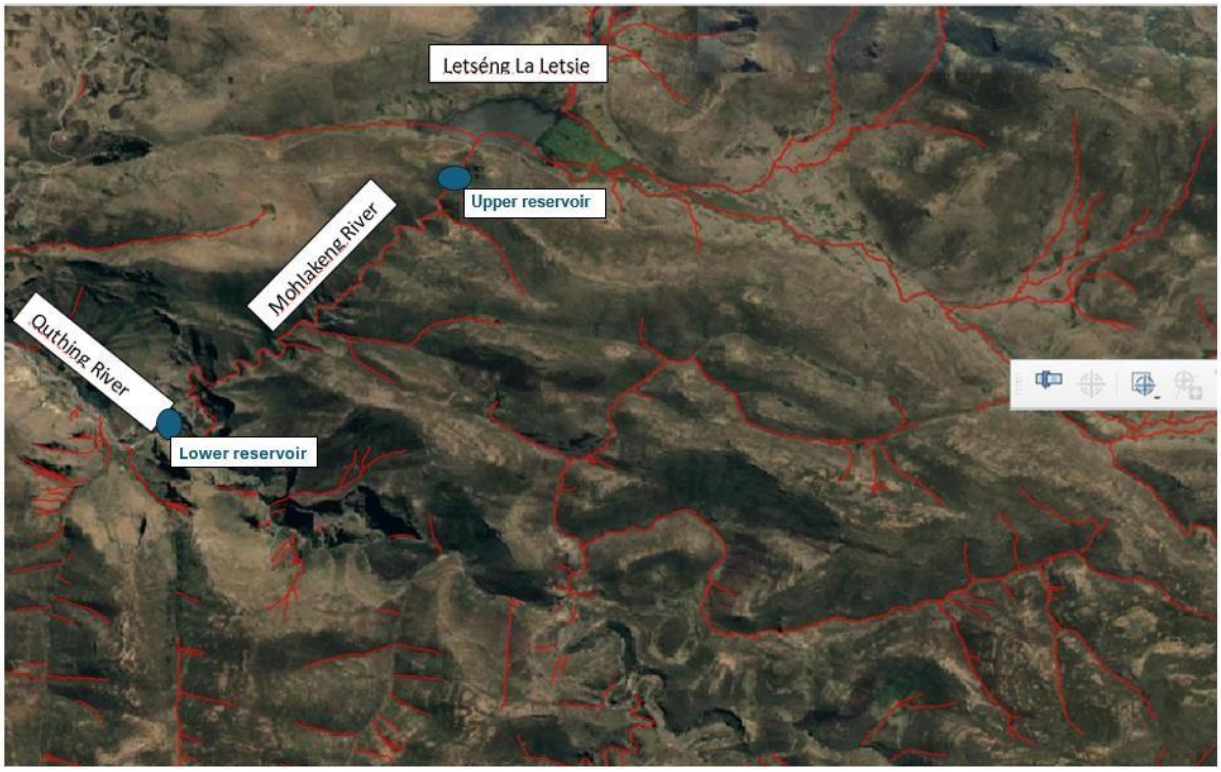

Figure 22: Upper and Lower Reservoir locations

3.5 Turbine selection

Using the turbine selection chart shown in Figure 23, the turbine type was chosen following the computation of the net head, and the design flow rate. After selecting the turbine type from the chart, the turbine was then modelled on TURBN-Pro.

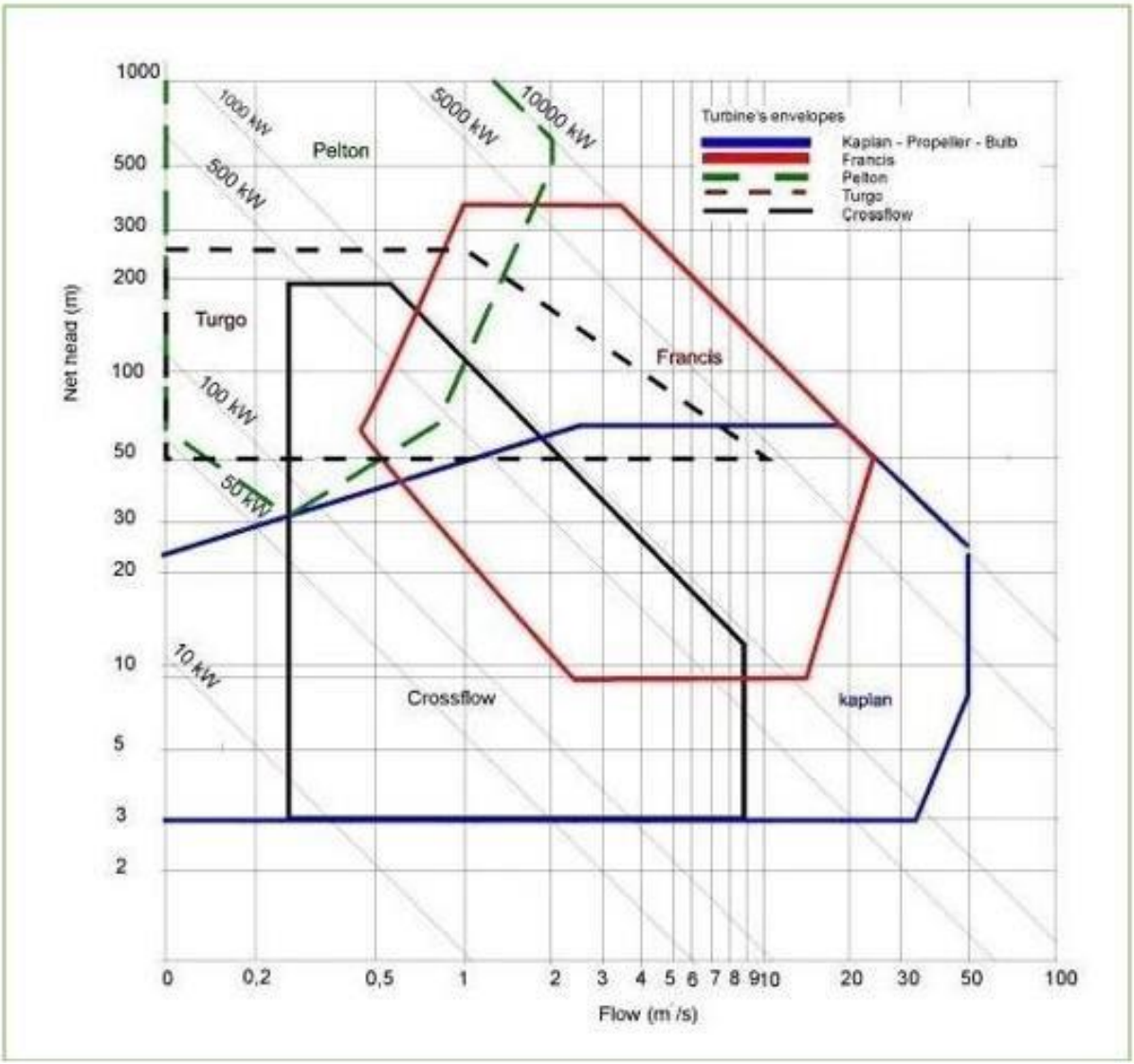

Figure 23: Turbine selection range chart [86]

3.6 Gross head determination and Hydropower generation

The net head is an important parameter to be taken into consideration when designing a hydropower plant. It is defined as the vertical distance travelled by water to convert its potential energy into kinetic energy. Lets'a-la-Letsie digital elevation map with the contour lines, as shown in Figure 24, was used to determine the gross head.

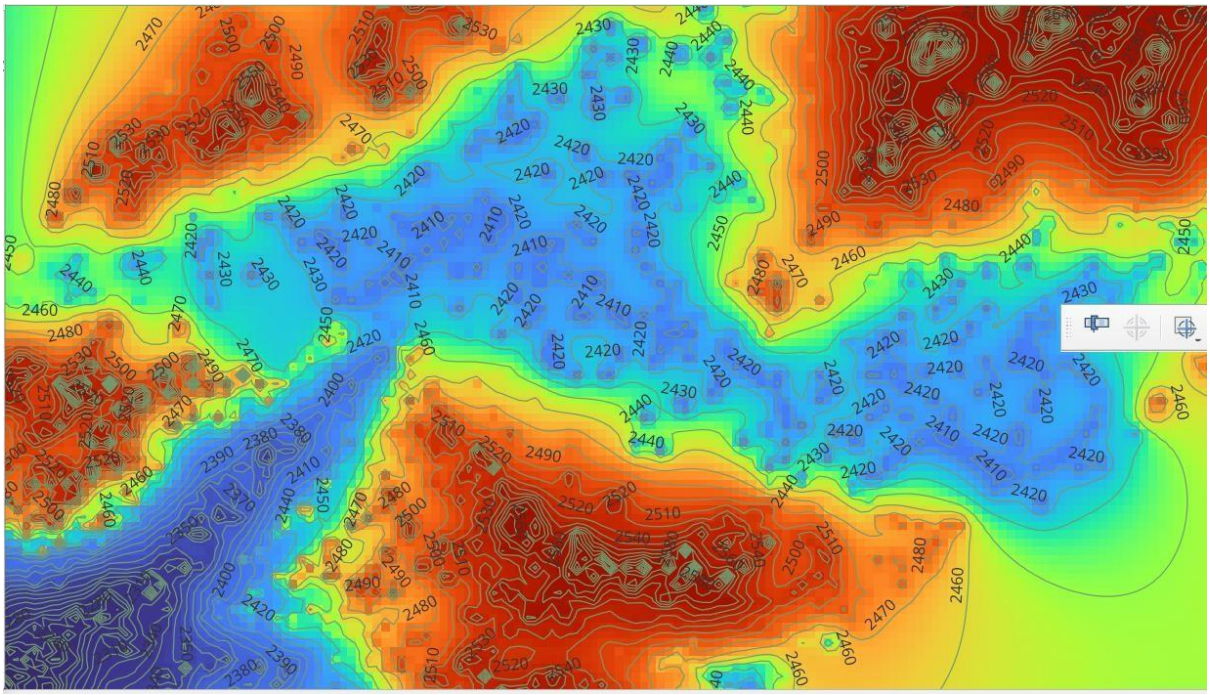

Figure 24: Lets'a-La-Letsie digital elevation map (Self-generated on GIS).

Equation 16 yields the roundtrip efficiency (RTE) which is the product of the power generating efficiency and the pumping efficiency, and represents the efficiency of PHES.

$$\boldsymbol{RTE} = \frac{\boldsymbol{P_{gen}}}{\boldsymbol{P_{pump}}} \qquad \text{Equation 16}$$

Where P_{pump}, is the power input needed to operate the pump; P_{gen} is the produced power from the hydro turbine. Both P_{gen} and P_{pump} were determined from Equation 6.

3.7 Penstock optimum diameter

The Penstock diameter was determined from Google Earth. The determination of the optimum diameter (*D*) of the penstock was done through an iterative method in Microsoft excel using Equation 17 to Equation 19;

$$\mathbf{D} = \sqrt{\frac{\mathbf{4Q}}{\boldsymbol{\pi}\mathbf{V}}} \qquad \text{Equation 17}$$

Where $\boldsymbol{Q}$ = flow rate (m^3/s), $\boldsymbol{V}$= velocity (m/s)

The initial velocity $\boldsymbol{V_1}$ is assumed to be 1 m/s, then knowing $\boldsymbol{D}$, friction factor $\boldsymbol{f}$ was determined using Reynolds number (**Re**) and the relative friction factor.

$$f\left(\frac{\varepsilon}{D} \times \mathbf{Re}\right) = \frac{1.325}{\left[\ln\left(\frac{\varepsilon}{3.7D} + \frac{5.74}{[\mathbf{Re}]_{0.9}}\right)\right]^2}$$ Equation 18

Where μ = kinematic viscosity of water

V is then expressed as:

$$V = \sqrt{\frac{2gDH_f}{fL}}$$ Equation 19

Where **g**= gravitational pull, H_f= head losses, and ***L***= penstock length.

Penstock thick is determined from Equation 20:

$$TH = \left(\frac{D.H}{2\sigma}\right) + \mathcal{E}$$ Equation 20

Where **TH** is penstock thickness, **D** is penstock diameter, **H** design head, $\boldsymbol{\sigma}$ is the allowable stress of the material, and **Ɛ** is the margin of corrosion.

3.8 Stream flow-rates assessments

Below are the specific steps that were followed to determine the flow rates of Lets'a-La-Letsie:

- Group the historical stream flow rates into one year.
- Draw the hydrographs and flow duration curves for all of the previously gauged stream sites at HOKO.
- Develop techniques based on the average stream flow for transferring the flow duration curve information available at the gauged locations to ungauged sites at Lets'a-La-Letsie.
- Provide an Excel application that will compute the flow duration curve.

The catchment area for the gauged station, HOKO, was determined from QGIS and used as a reference to estimate the flow-rates at Lets'a-La-Letsie (ungauged). The following steps were followed on QGIS to estimate the catchment area at HOKO;

- The DEM file for the Lets'a-La-Letsie region was imported into QGIS before being reprojected.
- From the processing toolbox, apply Fill Sinks (Wang & Liu) on the reprojected DEM.
- Apply Strahler order using the filled DEM.
- Apply upslope area using the filled Dem and Deterministic 8 method.
- Convert the extracted output from Raster format to vector format.

- Open the field calculator and determine the catchment area.

3.9 Pump selection and arrangement

The design and selection of the appropriate wind and solar water pumping system requires an understanding of the following design parameters: solar resources, wind resources, how much water needs to be pumped every day, and the entire dynamic head. The selection of the type of water pumping system was carried out while taking the overall characteristics of the site into consideration.

After determining the site information as tabulated in Table 3, these parameters were used to select the most suitable pump for the application.

Table 3: Preliminary Site information

Application	Water pumping.
Location (coordinates)	Coordinates for optimal solar and wind resources.
Pump type	Surface pump.
Water volume	Determined from how long it's estimated to fill-up and empty the upper reservoir.
Static head	Determined from the contour maps.
Pump voltage and current	Ensure the pumps and the solar panels are compatible in terms of voltage and current requirements.
Pump efficiency	Pumps with higher efficiencies will require less energy and give better performance.

Equation 21 yields the diameter of the pump suction pipe (D_s); where Q is the pump inlet volumetric flow rate and V_s is the mean fluid velocity. V_s is assumed to be 0.3 m/s [87].

$$\mathbf{Ds} = \mathbf{0}. \sqrt{\frac{\mathbf{Q}}{\mathbf{Vs}\ \mathbf{64}}} \qquad \text{Equation 21}$$

Equation 22 estimates the diameter of the pump delivery pipe ($\mathbf{D_d}$); where $\mathbf{Q_d}$ is the volumetric flowrate (0.06 m^3/s).

$$\mathbf{Dd} = \sqrt{\mathbf{0}.\ \mathbf{0744}\boldsymbol{Q}} \qquad \text{Equation 22}$$

Equal-sized fixed-speed pumps will be chosen to achieve the required flow rates. This will help with spares availability for maintenance. The number of chosen pumps needs to offer redundancy in case

one or more pumps malfunction. Figure 25 below depicts the overview of how the pumps will be arranged to achieve the required pumping capacities. The booster station in this case implies the cascading reservoirs.

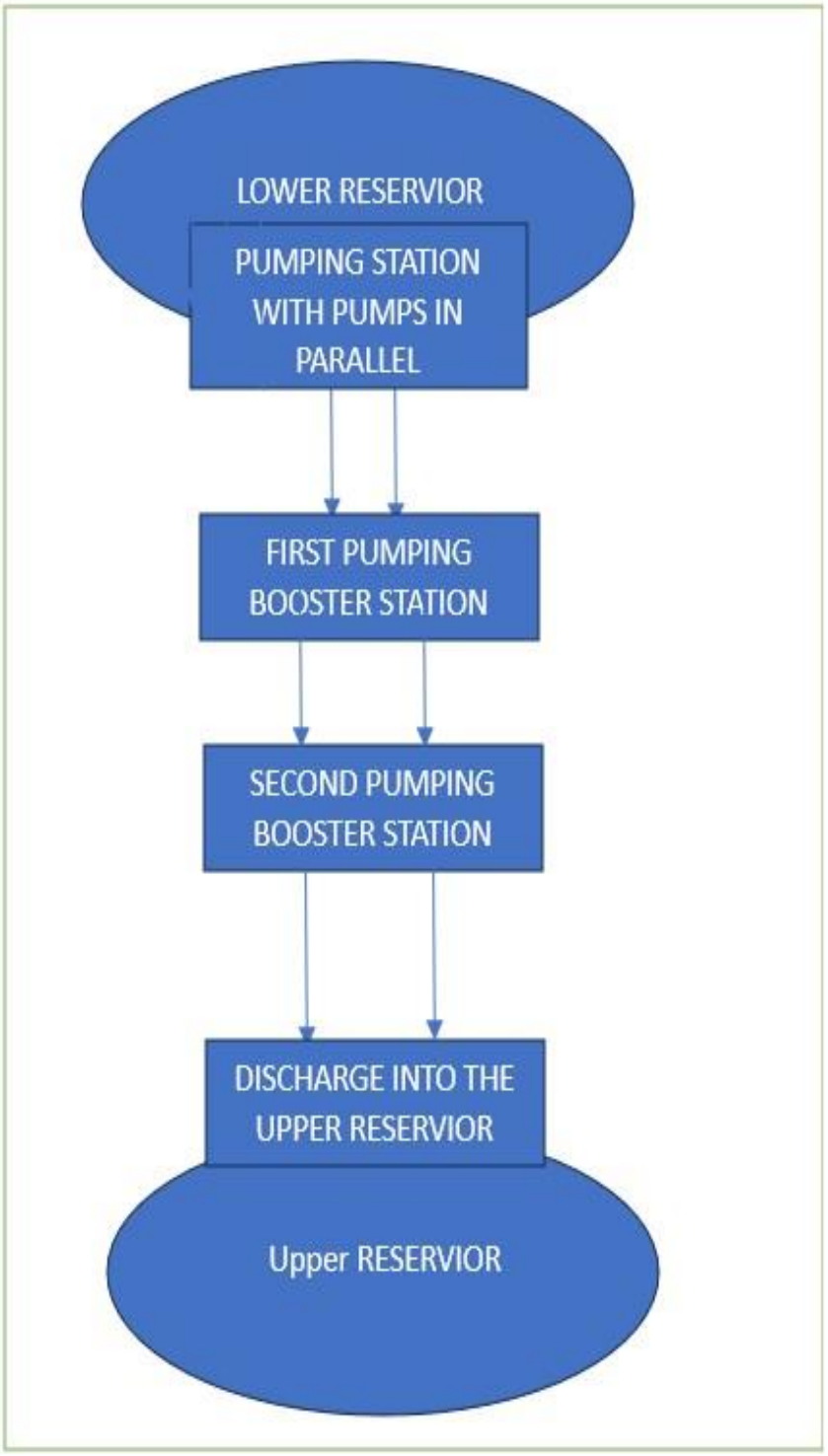

Figure 25: Pumps arrangement schematic diagram

3.10 Modelling hybrid system on HOMER

The pumped hydro was modelled as an electrical storage mechanism with a particular capacity and particular roundtrip efficiency. The procedures and factors taken into account in developing a battery that is comparable to a pumped hydropower plant are covered in this section as per the work done by Canales et al [70]. Canales et al [39] also indicated that in Homer, PSH plants can be represented as a hybrid of a battery bank and a converter.

Firstly, the product of the voltage **V** across the element and the current **I** passing through it, is the amount of electric power **P** produced by an active element or that dissipated or stored by a passive element, thus;

$$\boldsymbol{P = V \times I} \qquad \text{Equation 23}$$

Using Equation 22, multiplying P by the number of hours in period *t* yields the kilowatt-hours (kWh) of energy produced from an average flow rate of **Q**.

$$\boldsymbol{E = P \times t} \qquad \text{Equation 24}$$

The total stored energy (**ES**) (in kW h) of a battery with a fixed voltage **V** and a capacity $\mathbf{C_B}$ (in Ah) that is independent of its discharge current is determined using Equation 25:

$$\boldsymbol{Es = V.\frac{CB}{1000}} \qquad \text{Equation 25}$$

Similarly, the effective volume of the reservoir (in m^3) and the average power **P** (kW) generated over the hours required to empty the reservoir by an average flow rate **Q** (m^3/s) is used to characterize the total stored energy **ES** (in kW h) in a hydroelectric plant, therefore;

$$\boldsymbol{Es = \frac{Volume\ of\ the\ reservior\ .\ P(Q)}{Q\ .\ 3600}} \qquad \text{Equation 26}$$

Combining Equation 25 and Equation 26,

$$\boldsymbol{Es = 9.81\ .\ \eta.\ \frac{H}{}\ .\ Volume\ of\ the\ reservior\ 3600} \qquad \text{Equation 27}$$

Table 4 shows the relationship between pumped hydro storage and its equivalent battery. First, the voltage of the battery was determined. Then the round trip efficiency was assumed to be 100%, while the minimum state of charge was assumed to be 100% [70], [39].

Table 4: Relationship between pumped hydro and its equivalent battery

Pumped Hydro				Equivalent battery	
Reservoir capacity (m^3)				Voltage(V)	
Net head (m)				Round trip efficiency (%)	
Turbine Efficiency (%)				Minimum state of charge	
Design flow-rate(m^3/s)	Hours to empty the reservoir (hrs)	Stored energy (kWh)	Power (kW)	Cb (A.h)	I (A)

PV and wind turbine prices were extracted from Oladigbolu et al. [88]. For the PSP input prices, the method adopted by Blakers et al [89] was used in this study. Table 5 shows the summary of the system components costs as used on HOMER.

Table 5: System components costs

Component	**Initial cost**	**Replacement cost**	**Maintenance cost**	**Reference**
PV system	$1500/kW	$1000/kW	$10/kW	[88]
Wind turbine	$4000/kW	$3200/kW	$200/year	[88]
PSP (Includes power components and storage components)	$870/kW	$10/kW	-	[89]

CHAPTER 4: Results and their discussion

This chapter summarises and examines the findings from a hybrid system assessment of solar, wind, and pumped hydropower storage at Lets'a-La-Letsie in Quthing district. First, the hydropower potential for Lets'a-La-Letsie was computed using the available Quthing river flow rates and gross head between the two selected reservoirs. The design flow rate was calculated using the catchment area ratio method. Furthermore, the wind and solar resources were evaluated using the Global Wind Atlas and Global Solar Atlas, respectively. The ideal position for the wind turbines and solar panels was then identified. The chapter goes on to explain the design of the wind and solar pumping system that is required to deliver water to the upper reservoir.

The hybrid system results from the HOMER software, in which the NPC and LCOE were employed as the primary selection criterion for the optimal system, are further described in this chapter. The LCOE is the average cost per kWh of useable electrical energy produced by the system, whereas the net present

value (NPC) is the present value of all installation and operating costs of the energy system during its lifetime subtracting all revenues generated by it.

4.1 Proposed hybrid system arrangement

Firstly, the intake and the powerhouse locations were selected to obtain the optimal gross head taking the Ramser site at Lets'a-la-Letsie into consideration. The hydropower plant schematic layout for Lets'a-La-Letsie is seen in Figure 26. There are 236 meters of elevation difference between the powerhouse and the upper reservoir (gross head), thus the net head is estimated to be 157 m. The distance between the upper reservoir and the powerhouse, that is the penstock length, is 2780 meters. The figure also shows the abstraction point – the location of the lower reservoir. The depicted position of the wind turbines and solar PVs was determined using the Global Solar Atlas and Global Wind Atlas.

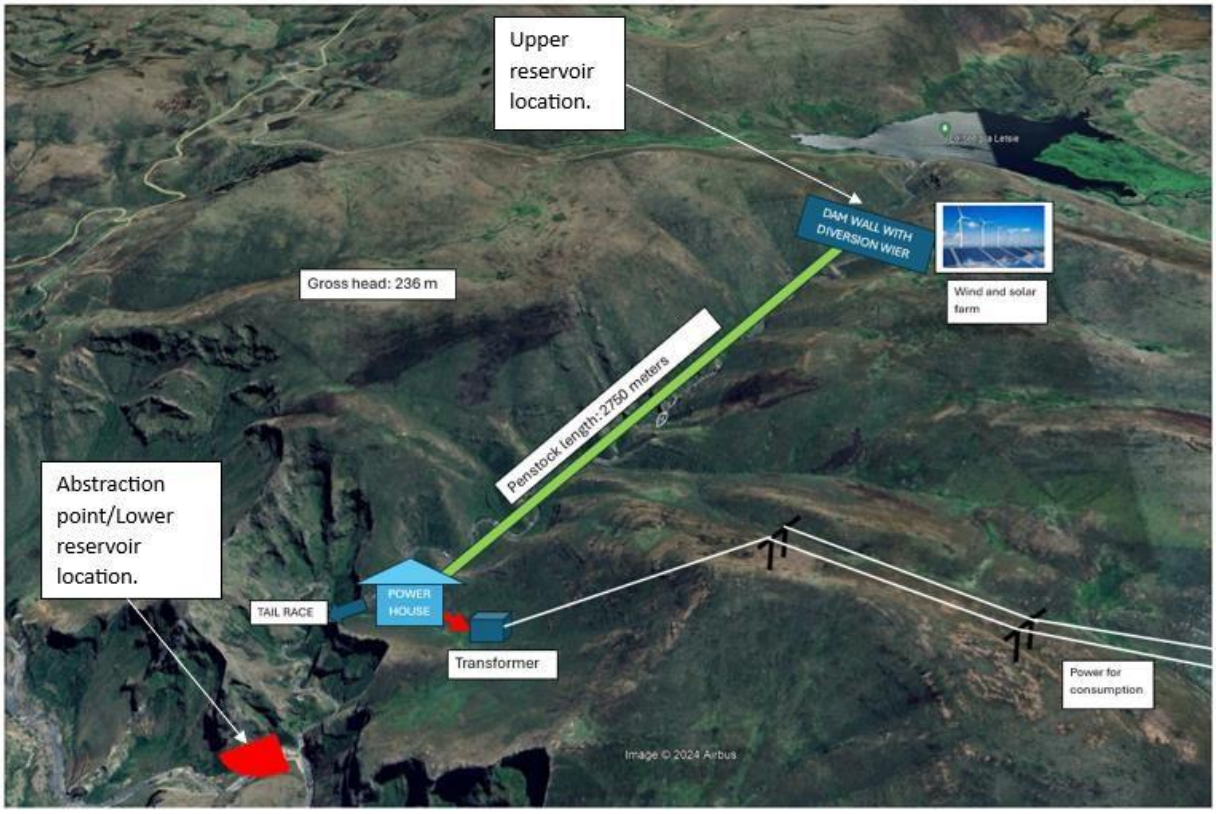

Figure 26: Layout of pumped hydro storage power plant

Figure 27 shows the schematic diagram for the hydro turbine installation - The arrangement is in such a way that the penstock is always full of water during generation mode to avoid cavitation. It can also be seen from Figure 28 that there is a knife gate valve positioned downstream of the penstock, and is used to control the upper reservoir level. When the water level in the upper reservoir is at the minimum level, the valve is closed until there is an adequate level in the upper reservoir.

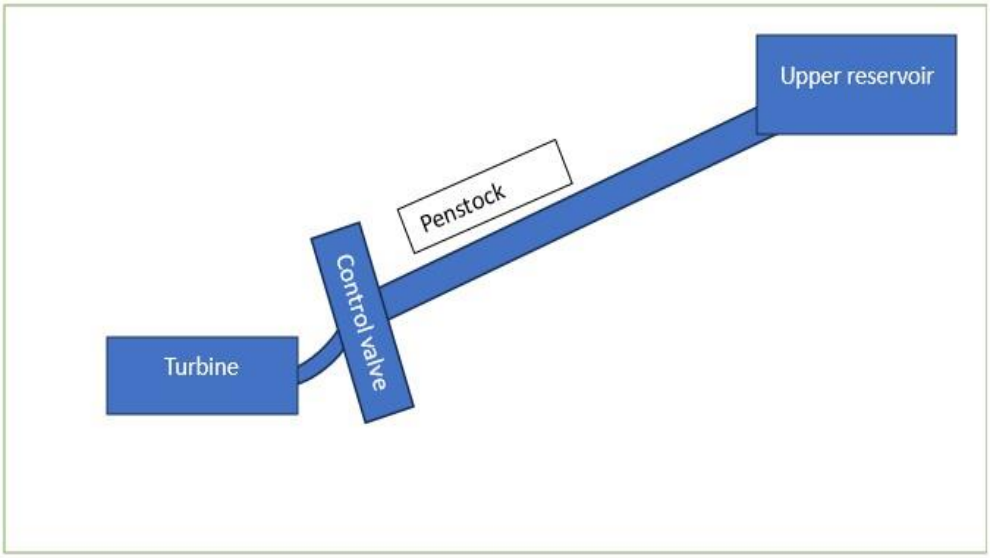

Figure 27: Schematic diagram for turbine installation.

4.2 Upper and lower reservoir catchment areas

Figure 28 shows the digital elevation catchment area map for the upper reservoir in which the darker points indicate higher elevation points. It can be seen from the figure that the upper reservoir gets its supplies directly from Lets'a-La-Letsie; it shares the same catchment area as Lets'a-La-Letsie. The upper reservoir site is located in a valley, hence the maximum flow accumulation for water storage.

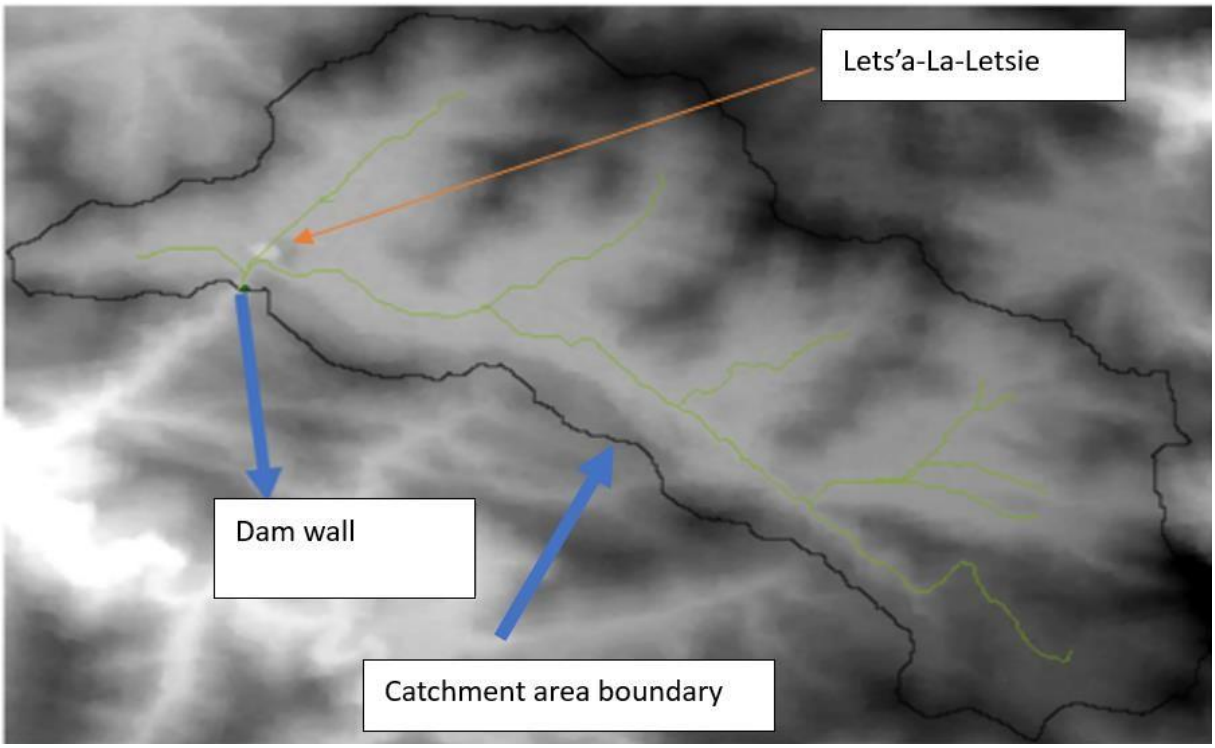

Figure 28: Digital catchment area map for the upper reservoir as extracted from GIS tools

Figure 29 shows GIS results for the upper reservoir volume estimation. Using Figure 30, the capacity of the upper reservoir is estimated as the product of length_1 (24.42 m), length_2 (31.6 m), and the average for the grid _code column (2883 m), which results in the total volume of 2, 066, 535 m^3. In this study, only a small portion of this volume is utilized (based on the available water resources).

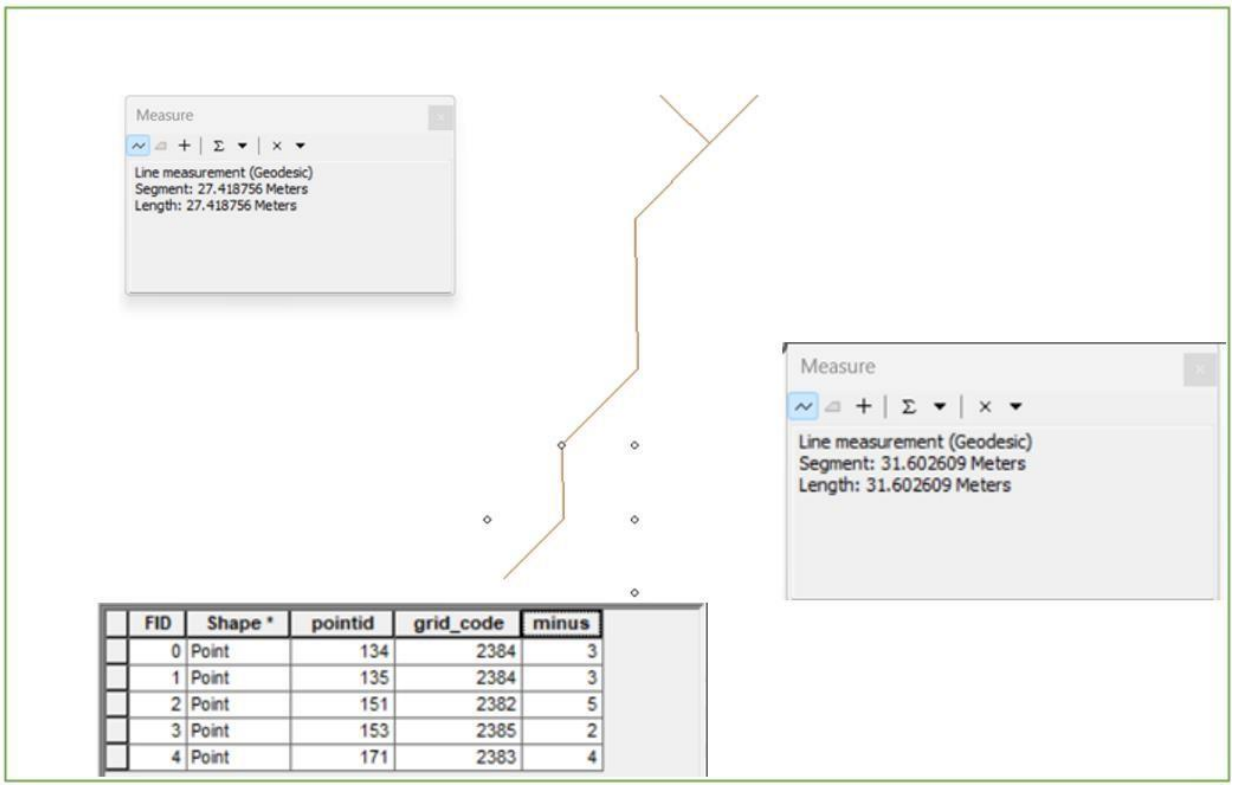

FID	Shape *	pointid	grid_code	minus
0	Point	134	2384	3
1	Point	135	2384	3
2	Point	151	2382	5
3	Point	153	2385	2
4	Point	171	2383	4

Figure 29: Estimation of the upper reservoir volume results using GIS tools.

Figure 30 illustrates the catchment area of the abstraction point as determined by GIS tools. The abstraction point has a catchment area of 46.40 km^2. Meanwhile, the catchment area for HOKO station, downstream of Quthing river, is 600 km^2 as depicted in Appendix 4. This means that the amount of water that can be recirculated from the lower reservoir back to the upper reservoir should be equal to or less than 7.7% of the total water resources at the lower reservoir. This is to avoid interfering with other possible hydropower projects around the study area. In this way, the system is sustainable as there is very minimal top-up water needed to cater for the losses.

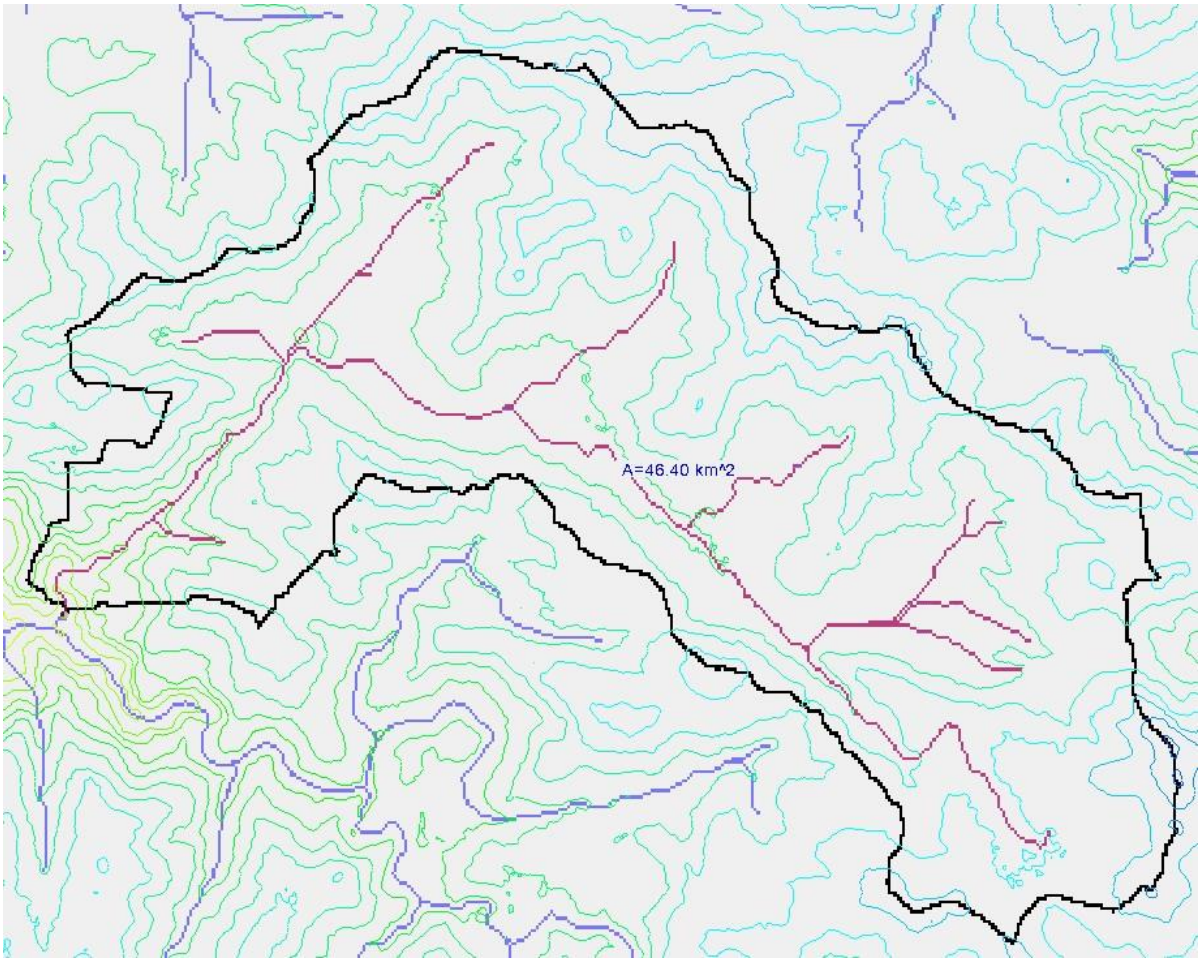

Figure 30: Abstraction point catchment area

4.3 Hydrograph, Flow duration, and power curve results

The data for the derivation of the hydrograph for Lets'a-La-Letsie is from the HOKO hydrometric station at Quthing River from January 2010 to September 2019. Figure 31 shows that the average monthly flow rates are highest from December to March during which the country experiences good rains or even floods in most parts of the country. The highest average monthly flow rates were recorded in January at just above 2.5 m^3/s. Figure 31 also shows that the lowest flow rates are in June and August during winter and autumn which are the dry seasons in Lesotho. The lowest monthly average flow rate was recorded in June at 0.75 m^3/s. The difference between the highest and lowest flow rates along this river is primarily related to seasonal behaviour; the biggest flows occur during the rainy season, while the lowest flow rates occur during Lesotho's dry season, winter.

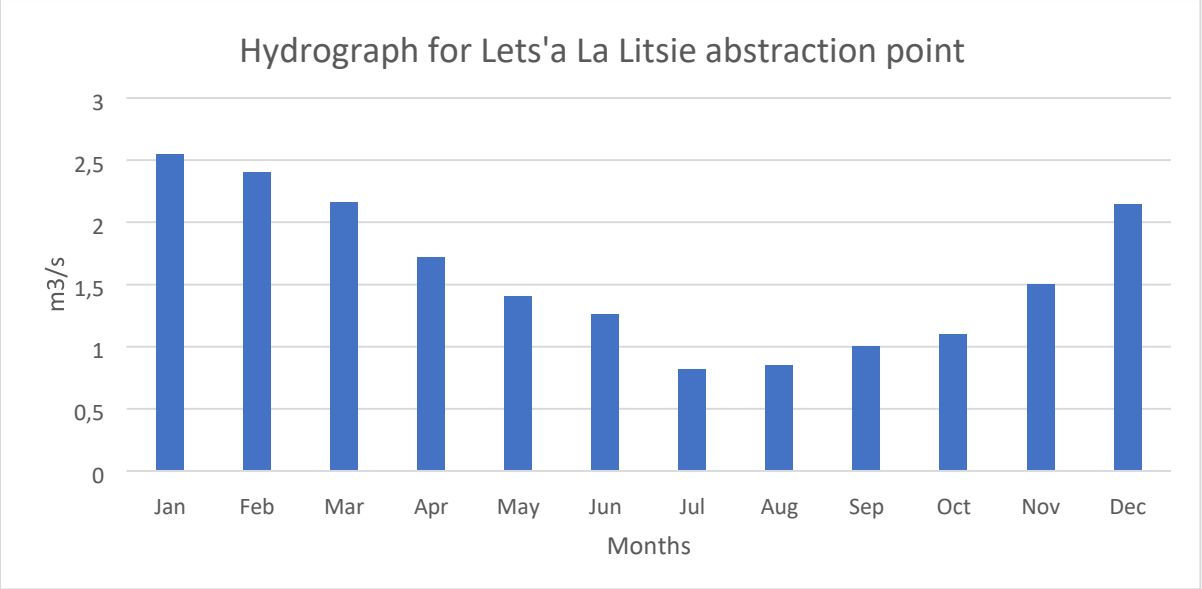

Figure 31: Study area (Mohlakeng River) hydrograph.

The FDC depicts the characteristic distribution of the river flow at a given location, whereas the power curve represents the power produced per-flow rate at various exceedances. Figure 32 demonstrates that the highest flow rate of 1.8 m^3/s happens infrequently, but the flow rate of 0.06 m^3/s occurs regularly. The design flow (Q_d) in this report was set at Q_{60} (0.06 m^3/s). At the stream flow rates equal to or greater than the design flow, the plant will produce rated power with an efficiency of 0.9 as shown by the power curve in Figure 32 below.

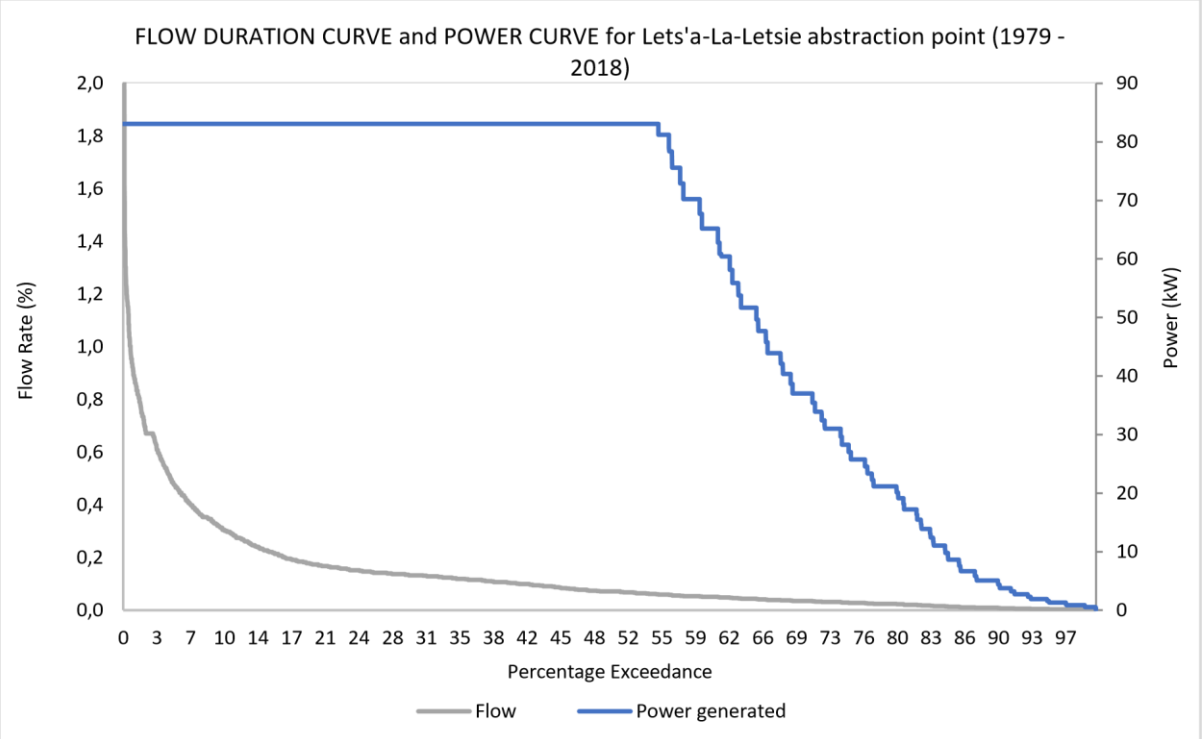

Figure 32: Study area flow duration and power curves.

4.4 Turbine selection results from TurbN pro

Figure 33 depicts the turbine selection chart. The turbine type was chosen following the computation of the net head, design flow rate, and generated power. The selected turbine type at 157 meters net head and 0.06 m^3/s design flow rate is the Pelton turbine. Pelton turbine is normally used in small-scale micro-hydro systems, they generate up to 100 kW and have a net head ranging between 10 m and 200 m [90]. The Pelton turbines are used at higher head sites and lower flow rates than reaction turbines (i.e., Kaplan and Francis turbines), hence they are frequently used in mountainous terrain [91].

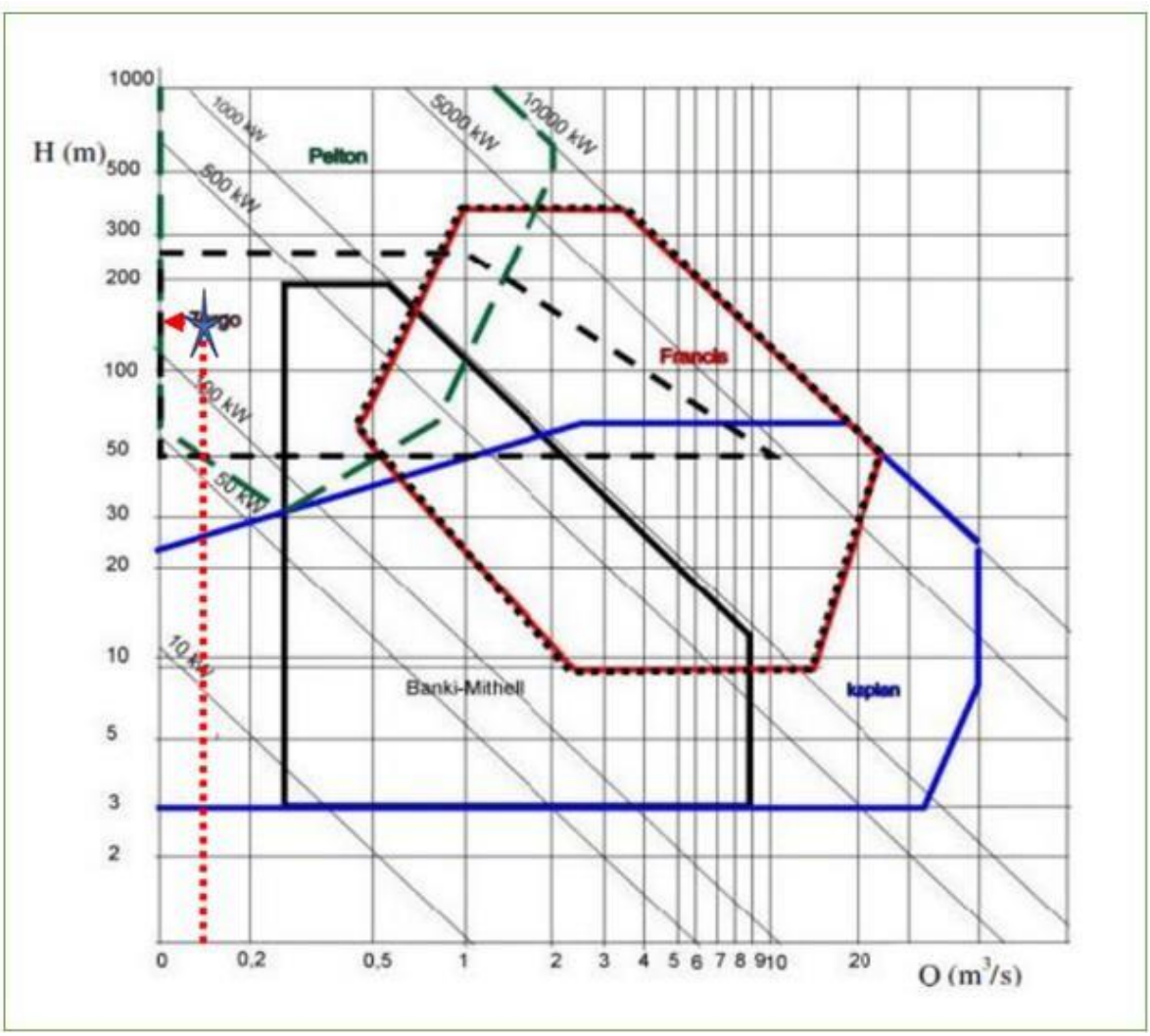

Figure 33: Turbine selection chart [86]

The analysis of the chosen Pelton turbine derived from the TURBNPRO version 3.0 is presented in this chapter. TURBNPRO is the software for hydropower developers, consultants, and students. TURBNPRO allows for easy determination of turbine and hydromechanical components [92].

Figure 34 shows the Pelton turbine design results from the TURBNPRO. The results show that the selected turbine generates 83 kW and 96 kW at the net heads of 143.6 m and 157 m, respectively. The

results further show that the runner pitch diameter is 513 mm, the bucket width is 134 mm, and the maximum runaway speed is 1.74 revolutions per minute (rpm).

Figure 34: TURBNPRO Pelton turbine performance results.

Figure 35 shows the selected turbine dimensional results. Most importantly, the jet orifice diameter is obtained to be 40 mm. Smaller jet diameters of less than 4mm are not favoured due to the difficulty of concentrating the jet and reducing friction losses [91].

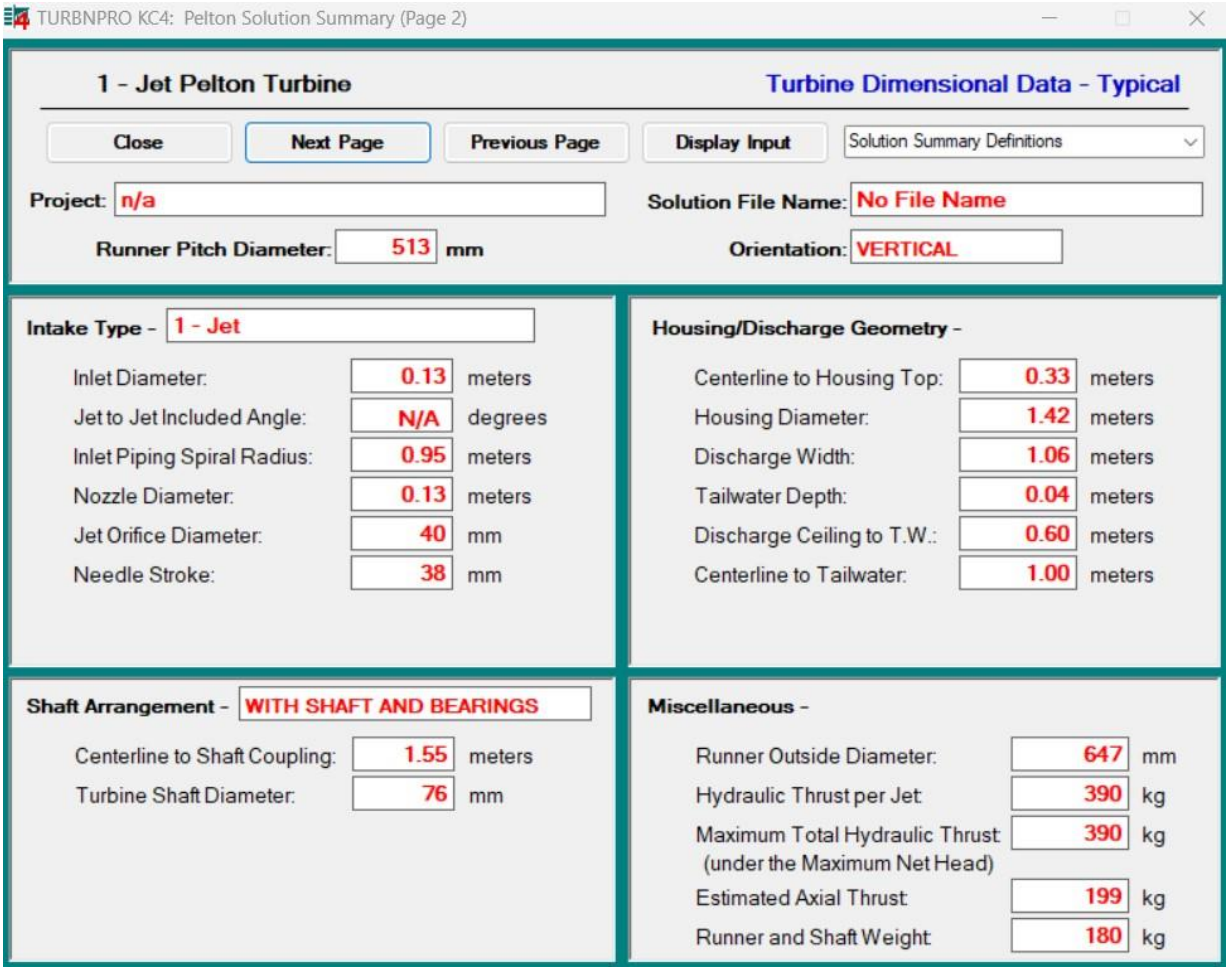

Figure 35: TURBNPRO PELTON turbine size results.

Jet Pelton turbine graphic view, dimensional data and the performance hill curve are shown in Appendix 1 – 2. Table 6 shows the summary of the selected Pelton turbine specifications as obtained from TURBN-pro.

Table 6: Selected Pelton turbine specifications

Runner pitch diameter (mm)	513
Bucket width (mm)	134
Jet orifice diameter (mm)	40
Orientation	Vertical
Turbine shaft diameter (mm)	76
Runner outside diameter (mm)	647
Maximum run away speed (rpm)	1.74

4.5 Optimum Penstock diameter

The optimum penstock diameter was computed as described in Chapter 3 (Methodology). Table 7 displays the output calculations used to find the optimum penstock diameter which is determined to be 0.2989 m.

Table 7: Optimum Penstock diameter determination

Velocity (m/s)	Diameter (m)	Relative Roughness	Reynold's number	Friction Factor	Velocity (m/s)
1	0.2764	0.3618	276395.3196	0.24527	0.79528
0.795278184	0.3099	0.3226	246484.8433	0.22281	0.88358
0.883582706	0.2940	0.3401	259809.0579	0.23273	0.84208
0.84207853	0.3012	0.3320	253633.7143	0.22812	0.86085
0.860846637	0.2979	0.3357	256444.6115	0.23022	0.85221
0.852207055	0.2994	0.3340	255154.5088	0.22925	0.85615
0.85615	0.2987	0.3348	255744.383	0.22969	0.85434
0.854343951	0.2990	0.3344	255474.2065	0.22949	0.85517
0.855171154	0.2989	0.3346	255597.8557	0.22958	0.85479
0.854792388	0.2990	0.3345	255541.2458	0.22954	0.85497
0.854965758	0.2989	0.3345	255567.159	0.22956	0.85489
0.85489	0.2989	0.3345211	255555.2963	0.22955	0.85492
0.85492	0.2989	0.3345282	255560.7267	0.22956	0.85491
0.85491	0.2989	0.3345250	255558.2408	0.22955	0.85491
0.85491	0.2989	0.3345264	255559.3788	0.22955	0.85491
0.85491	0.2989	0.3345258	255558.8578	0.22955	0.85491
0.85491	0.2989	0.3345261	255559.0963	0.22955	0.85491
0.85491	0.2989	0.3345259	255558.9871	0.22955	0.85491

4.6 Selected pumps specifications

Table 8 shows the specifications of the selected solar pump. The pump can achieve a maximum head of 90 meters and a maximum flow rate of 125 m^3/hr. For more details, refer to Appendix 5.

Table 8: Selected pump specifications [93].

Selected pump make	LORENTZ Solar surface pumps
Model	PS40K2-CS-F85-40
Maximum head	90 m
Maximum flow rate	125 m^3/hr

Figure 36 shows the selected pump performance curve. As indicated in Figure 37(red line), at 108 m^3/h, the pump needs 33 kW to achieve 70 meters head. To achieve the required flow rates (design flow rates = 216 m^3/hr) at a given head of 70 meters, the two pumps arranged in parallel will be needed. Appendix 6– 9 show the performance curves of the selected pump at different flowrates and heads.

Figure 36: Selected pump (PS40K2-CS-F85-40) performance curve [93].

Figure 37 shows how the pumps are arranged to deliver water from the abstraction point to the upper reservoir. The orange lines indicate the number of pipelines arranged in parallel, and the blue squares show cascading reservoirs in series. The number of pumps required to achieve a certain flow rate differs depending on the gross head.

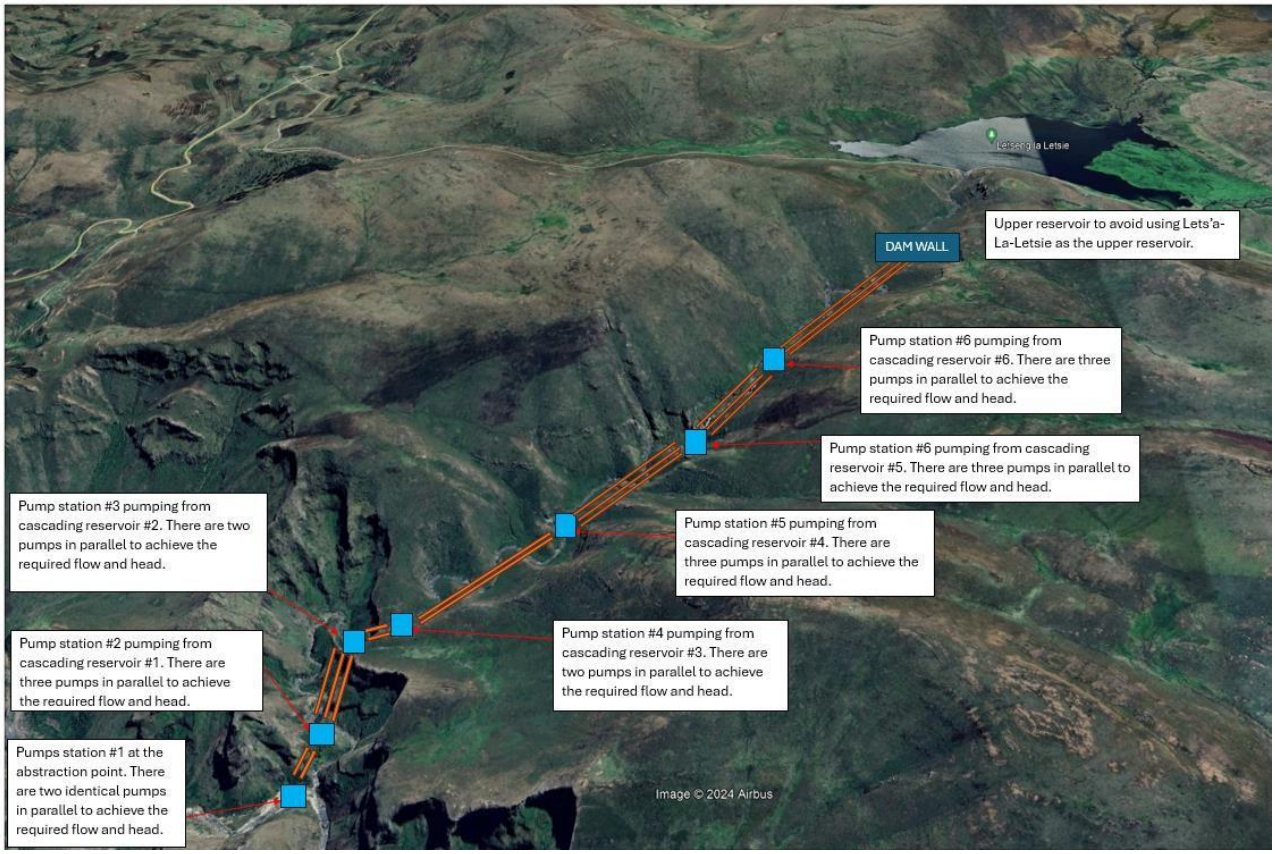

Figure 37: Pumps arrangement layout

Table 9 displays the gross heads between successive reservoirs, the flow rate of each pump against the head, the load, and the number of pumps necessary to convey water to the highest reservoir. To accomplish 216 m^3/h (0.06 m^3/s), a total of 19 pumps is needed. The 19 pumps combined have a total load of 534 kW. The pumping flow rate of 216 m^3/hr, which is equivalent to the design flow rate, is selected to ensure that the upper reservoir is full within 12.5 hours. This will occur during the day when there is adequate solar energy.

Table 9: Pumping performance per reservoir.

Pumping Station Number #	**Elevation between cascading reservoirs (m)**	**Flow rate with the respective head**	**Number of pumps in parallel**	**Power required (kW)/**
1	65	108 m^3/hr at 70m head	2	33
2	72	75 m^3/hr at 80m head	3	25
3	88	75 m^3/hr at 89m head	3	27

4	67	108 m^3/hr at 70m head	2	33
5	89	75 m^3/hr at 90m head	3	27
6	86	75 m^3/hr at 90m head	3	28
7	82	75 m^3/hr at 90m head	3	27

The Net Positive Suction Head available (NPSH-A) for the selected pump is 7.64 meters (which is greater than 7.6 meters) as shown in Table 10. With NPSH-A greater than 7.6 meters, there are no cavitation issues expected from the selected pumps for the given operational parameters.

Table 10: Selected pump cavitation parameters

Parameter	Metric units (m)
Specific gravity	1
Vapor pressure	0.023
hst (Static height in meters - the difference between liquid level and established pump datum.)	1 m
hfs (All suction line losses converted from pressure to meter) including piping entrance losses and friction losses.	0.9 m
Calculate hp (absolute pressure head)	10.33 m
Calculate hvpa (Vapor pressure of the liquid converted to meters)	0.238 m
Calculate NPSHa	8.407 m
Apply S.F. to obtain NPSH(available)	7.64 m

From equations 21 and 22, the diameter of the suction pipe is estimated to be 0.286 m, while the diameter of the discharge pipe is 0.0668 m. In this way, the pump suction is designed to limit frictional head losses to protect the pump from cavitation [68].

4.7 Wind resources assessment results

Figure 38 shows the global wind atlas (GWA) data depicting information on the wind map and mean power densities for Lets'a-La-Letsie. The map shows that the wind speed varies between 4 m/s and 8.3 m/s at 50m height. The location of the wind turbines is therefore selected based on the highest wind speed location as shown in Figure 38. Figure 39 demonstrates the average monthly wind speeds as extracted from HOMER using the coordinates from GWA. It also shows that the average monthly wind

speeds vary from 3.78 m/s and 8.85 m/s at the hub height of 50 meters, with the highest wind speeds experienced in August and September. Variations in wind patterns are typically caused by topographical features, vegetation cover, and other reasons [94]. The results from HOMER further show that the annual average wind speed is 4.77 m/s.

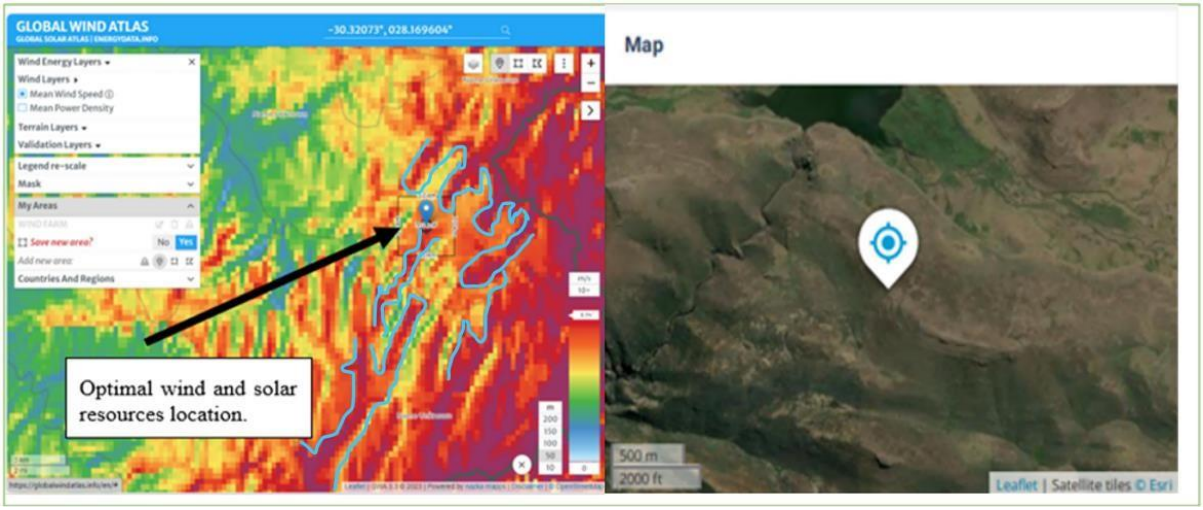

Figure 38: Lets'a-La-Letsie mean wind speed at 50 m height.

Figure 39: Monthly wind speeds average at Lets'a-La-Letsie as extracted from HOMER.

Figure 40 shows the global wind atlas (GWA) data containing information on wind frequency rose, mean power density, and mean wind speeds at 50 meters height. The wind rose's circular shape indicates the direction from which the winds come. In this study, the wind comes from the NWN - NW 40% of the time, and the NWN - WSW 28% of the time. From the mean wind speed graph, it can be seen that 20% of the windiest areas have a mean wind speed ranging from 7.7 m/s to 8.6 m/s. Lastly, the mean power density for the 10% windiest area in the selected region is 631 W/m^2.

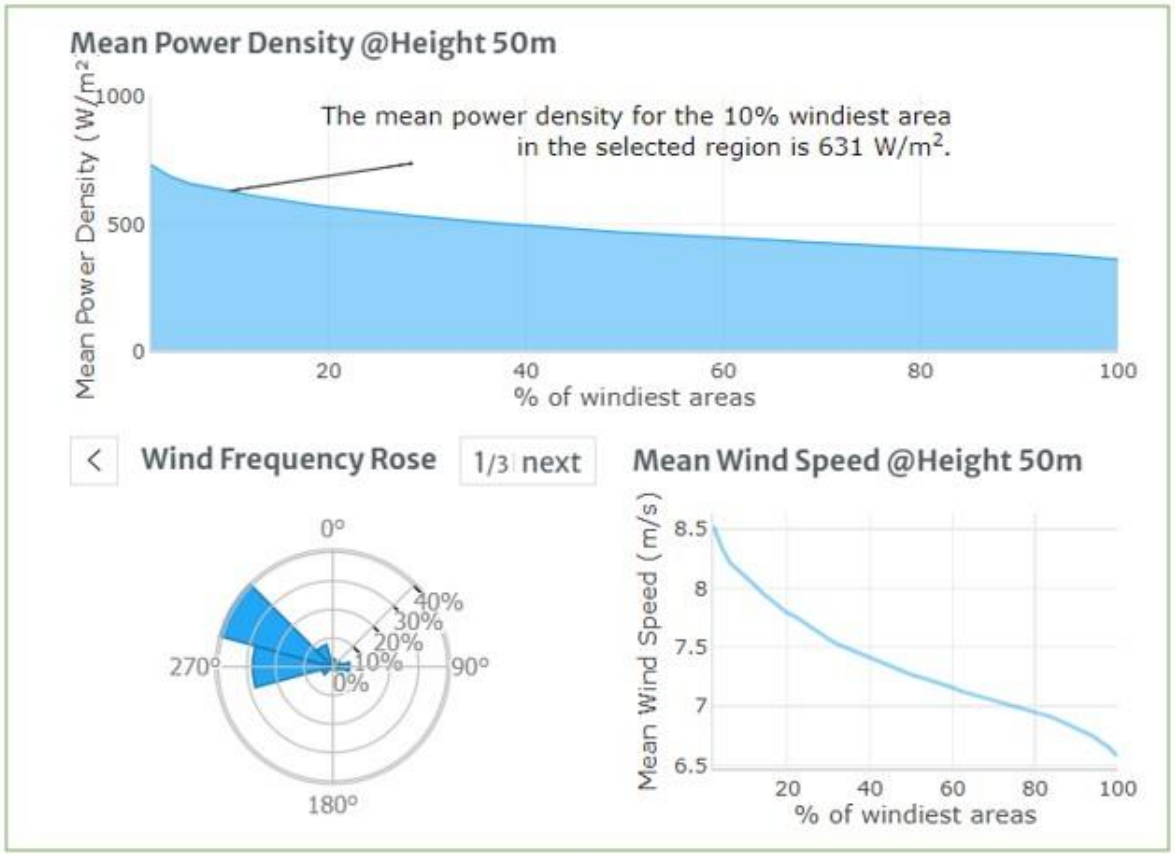

Figure 40: Mean power density, speed, and wind Frequency rose for the study area

4.8 Solar resources assessment results

Figure 41 shows the study area solar map as extracted from the Global Solar Atlas. The Global Solar Atlas map depicts the potential of Photovoltaic (PV) in the area of interest in kWh of the energy produced daily and annually concerning the installed capacity of PV. From Figure 42, the direct normal irradiation amounts to 2468 kWh/m^2/year, while the global horizontal irradiation is 2032.7 kWh/m^2/year for the selected region.

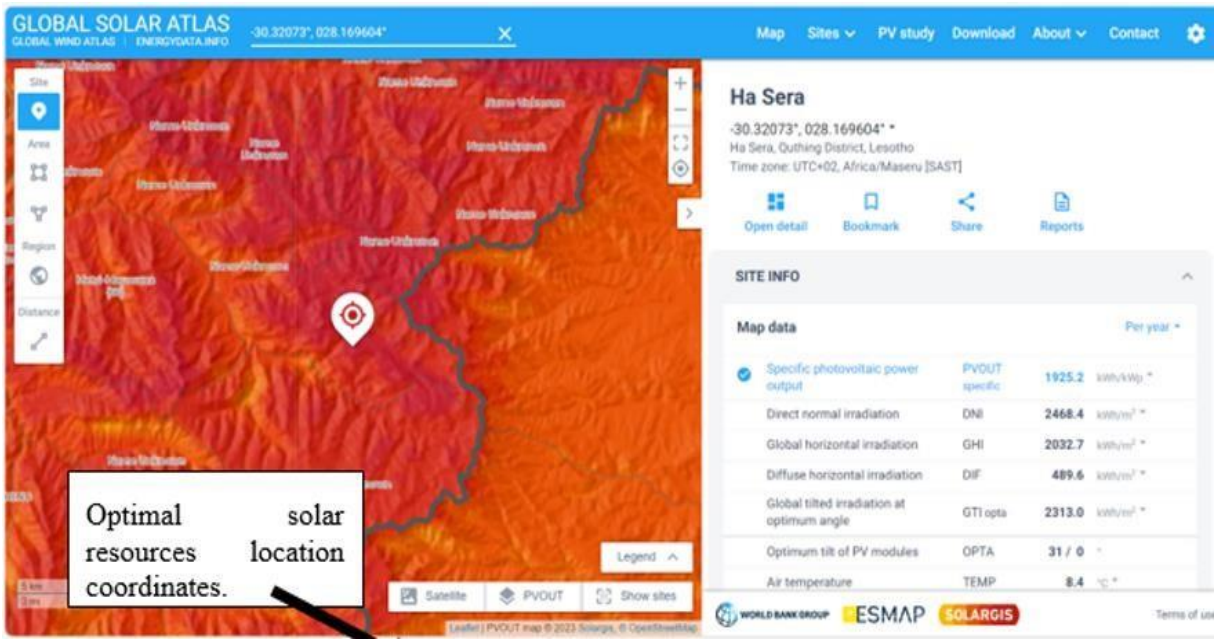

Figure 41: Global solar atlas map for Lets'a-la-Letsie

Figure 42 shows the PVOUT map which summarises the potential for solar photovoltaic (PV) power generation in the research area. The selected position for the solar panels shown in blue in Figure 43 has the average PVOUT of 161 - 162 kW/m2.

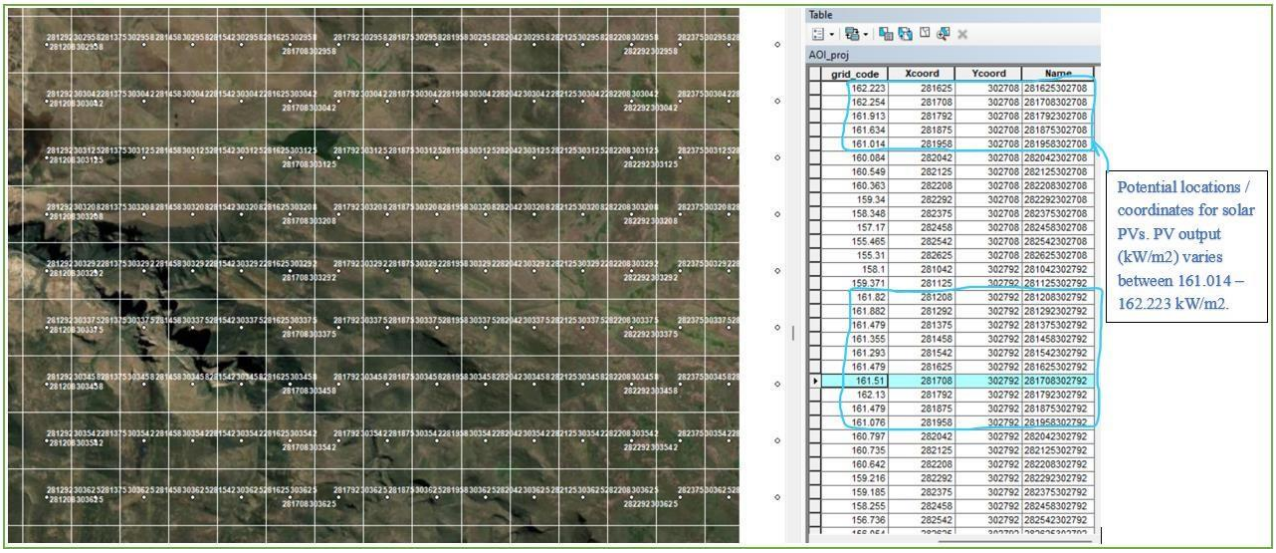

Figure 42: Study area PVOUT (kW/m2) map

Figure 43 shows the monthly average solar global horizontal irradiance and clearness index from HOMER for the selected region. The daily radiation varied between 3.65 kWh/m^2/day in June and 6.90 kWh/m^2/day in December. The annual average global horizontal irradiation is 5.26 kWh/m^2/day; this is also congruent with the 2032.7 kWh/m^2/year obtained from GSA. This indicates that although these resources are currently underutilized, there is a great deal of potential for solar power applications in

this region [88]. The highest daily radiation is observed in November, December, January, and February. The lowest clearness index is recorded in January at 0.565, and the highest in July at 0.668.

Figure 43: Lets'a-La-Letsie monthly average solar global horizontal irradiance

4.9 Load profile results

Using the average consumption per domestic customer (1200 kWh/customer/year) in Lesotho [95] , approximately 1075 households out of 116,633 households in Mphaki and Tsatsane councils [96] will be supplied with power. The average daily load for a typical health centre is 8 kWh/day [97], thus 5 health centres will be powered; namely, Dili Dili health care, Tsatsane health care, Tlatlametsi health care, Makoae health care, and Mphaki health care. The average consumption per school is estimated at 23 kWh/day on average [98]; this means 46 schools can be powered from 1061 kWh/day. The major load in schools is attributed to lighting. The hybrid system is planned to power 35 schools in the Mphaki and Tsatsane councils [99].

Table 11 shows the village load demand classified into five main categories: household load, schools load, clinic load, commercial load and water pumping load. The daily average households load is 3536 kWh/day, the schools' daily average load is 1061 kWh/day, the pumping load amounts to 7020 kWh/day, the clinic load average is 24 kWh/day, and the average daily commercial load is 2400 kWh/day.

Table 11: The system's total load

HOUR	Households Load (kW)	Schools (kW)	Pumping Load (kW)	Clinic Load (kW)	Commercial LOAD (Kw)	TOTAL Load (kW)
0	41.6	2.4	0	0.15	100	144.15
1	41.6	2.4	0	0.15	100	144.15
2	41.6	2.4	0	0.15	100	144.15
3	41.6	2.4	0	0.3	100	144.3
4	41.6	2.4	0	0.3	100	144.3
5	62.4	2.4	0	0.3	100	165.1
6	104	2.4	540	0.9	100	747.3
7	145.6	86	540	1.8	100	873.4
8	166.4	86	540	2.4	100	894.8
9	166.4	86	540	2.7	100	895.1
10	166.4	86	540	3	100	895.4
11	166.4	86	540	2.4	100	894.8
12	166.4	86	540	2.1	100	894.5
13	166.4	86	540	0.9	100	893.3
14	166.4	86	540	0.84	100	893.24
15	166.4	86	540	0.72	100	893.12
16	187.2	86	540	0.6	100	913.8
17	208	86	540	0.6	100	934.6
18	249.6	86	540	0.81	100	976.41
19	249.6	2.4	0	0.81	100	352.81
20	249.6	2.4	0	0.81	100	352.81
21	249.6	2.4	0	0.54	100	352.54
22	187.2	2.4	0	0.3	100	289.9
23	104	2.4	0	0.3	100	206.7

Figure 44 illustrates the scaled hourly loading profile per day of electrical equipment (load) as obtained from Table 11. The average total daily load is 14040 kWh/day, the daily average load is 585 kW, the peak load is 1657 kW, and the load factor is 0.38. The load is relatively higher during the day because of the water pumping requirements.

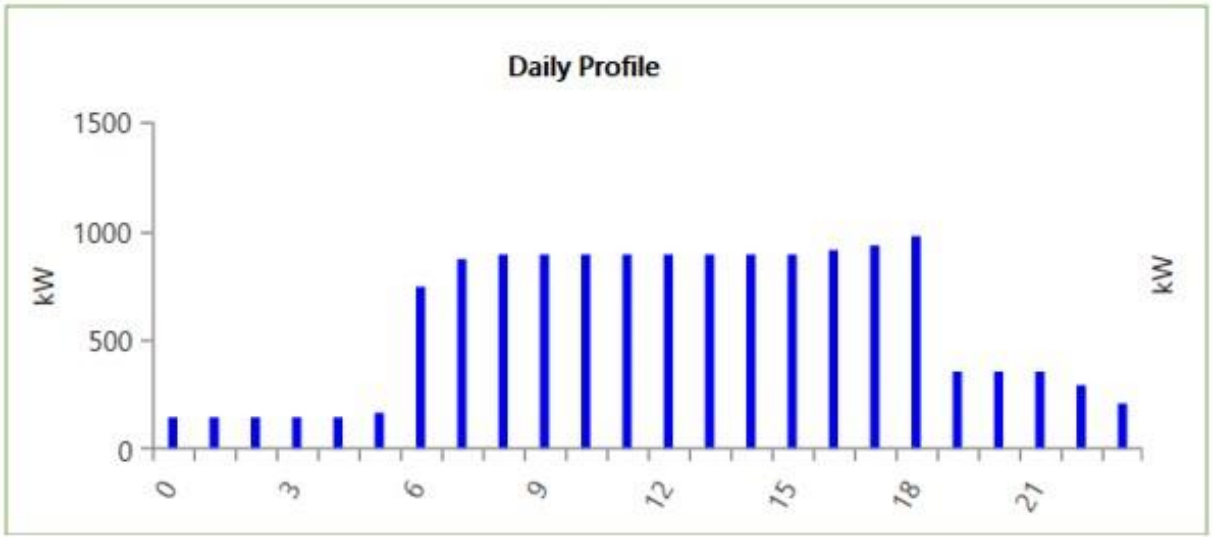

Figure 44: Daily load profile for the selected villages' requirements

4.10 System Architecture from HOMER

Figure 45 shows the schematic diagram of the model adopted to describe the PV-wind and pumped hydropower storage hybrid system proposed in this study. The hybrid system simulated with Homer includes a 1500 kW wind turbine, PV panels, converter, and a battery. The converter is used to turn AC power into DC power. The pumped hydropower storage plant is connected to the DC bus, with the reservoir simulated by a battery following the method proposed by Canales et al. [70]. The photovoltaic panels, electric load, and wind turbines are connected to the AC bus.

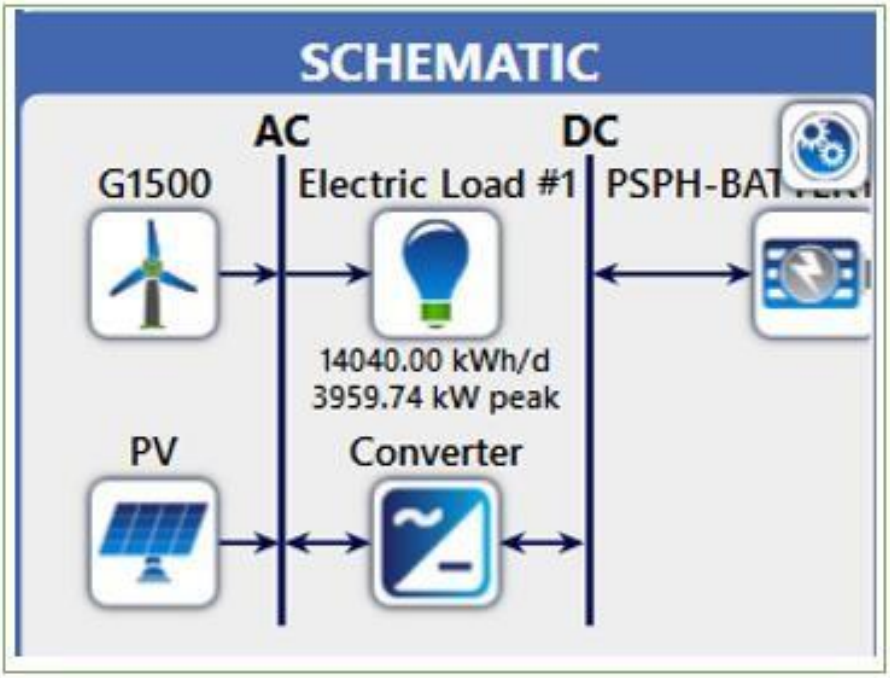

Figure 45: Hybrid system architecture

4.11 Modeling Pumped hydropower storage system as a battery on HOMER

Table 12 shows the data used to reconfigure the model of a prototype battery to describe the performance of the upper reservoir. Unlike a real rechargeable battery, the reservoir will not lose charge for issues related to chemical reactions but water may be lost through evaporation.

A voltage of 240 V is chosen. This voltage is selected because it is widely utilized for home supplies, making it a voltage that most people can easily relate to [70]. The battery has a nominal capacity of 4331.73 Ah and a voltage of 240 V, giving it a total storage capacity of 1039.61 kWh (equivalent to the total energy stored in the reservoir). The total time required to empty the reservoir is 12.5 hours with a discharge rate of 0.06 m^3/s. The reservoir capacity is estimated to be 2700 m^3. As per the work done by Nikolaos et al.[40], this plant can be classified as the daily pumped hydro storage (DPHS) system. However, the 2700 m^3 storage capacity is not in the range prescribed by Nikolaos et al. [40] for daily pumped hydro storage plants (10^6 m^3 – 10^9 m^3). Daily pumped hydro storage plants are mostly appropriate for mitigating the daily load fluctuations, and they are the most common application today [40].

Table 12: Relationship between pumped hydro and its equivalent battery

Pumped Hydro			Equivalent battery	
Reservoir capacity (m3)	2700		Voltage(V)	240

Net Head (m)		157	Round trip efficiency (%)		100%
Turbine efficiency (%)		90%	Minimum state of charge (%)		0
Design flowrate(m3/s)	Hours to empty reservoir(hrs)	Stored energy (kWh)	Power (kW)	Cb (A.h)	I (A)
0.02 0.03 0.04	37.50	1039.61	27.72	4331.73	115.51
	25.00	1039.61	41.58	4331.73	173.27
	18.75	1039.61	55.45	4331.73	231.03
0.05	15.00	1039.61	69.31	4331.73	288.78
0.06	12.50	1039.61	83.17	4331.73	346.54
0.07	10.71	1039.61	97.03	4331.73	404.29

Figure 46 shows the battery model for the pumped hydropower storage system. The parameters of the model are; a maximum capacity of 1894.25 Ah, a capacity ratio of 0.999, and a rate constant of 8.94 per hour.

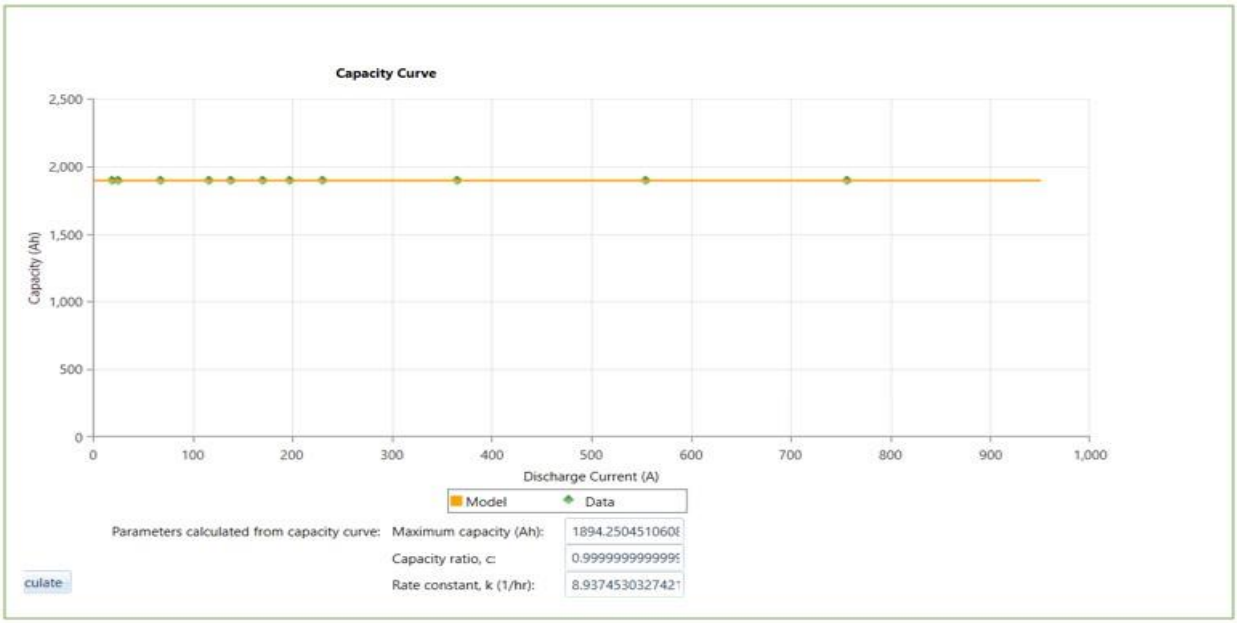

Figure 46: Battery model capacity curve.

4.12 Selected wind turbine power curve

Figure 47 depicts the performance of the selected wind turbine at varying wind speeds but constant hub height (50 meters). The rated power of the selected wind turbine is 1500 kW and its cut-in speed is 4 m/s. The average annual wind speed at Lets'a-La-Letsie is 4.77 m/s, and the wind turbine power output at that speed is approximately 160 kW.

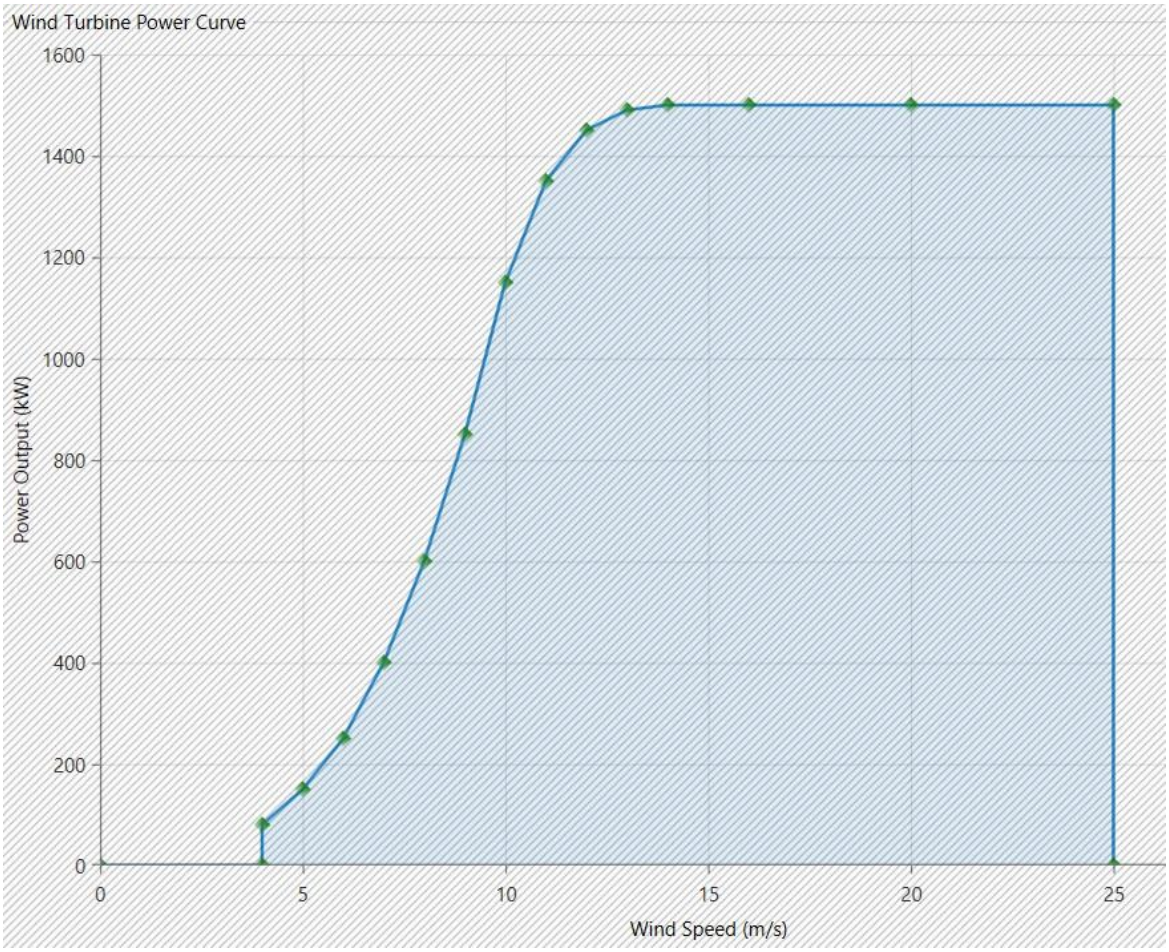

Figure 47: Selected wind turbine power curve.

4.13 HOMER Optimisation results

As shown in Figure 49, the HOMER simulation generates a list of possible design options or system configurations prioritized by their lowest total net present cost (NPC). Examining each viable system configuration allows for an economic and technical merits assessment, including the LCOE and renewable energy fraction. Other system operational variables that can be assessed include annual power generation, annual electric load provided, fuel consumption, excess electricity, capacity shortage, unmet electric load, and pollutants [8].

Based on the simulation results from Figure 48, the arrangement with 5379 kW from PV, one wind turbine with a rated capacity of 1.5 MW, and 60 battery strings in parallel is the best configuration of the hybrid system. This hybrid system's cost of energy (COE) is $0.417 per kWh (M7.86/kWh). This is more than the utility's existing power purchases from 'Muela Hydro at a subsidized M0.15/kWh (US$0.011/kWh), imports from South Africa's Eskom at an average of M0.97/kWh (US$0.069/kWh), and Mozambique's EDM at roughly M1.50/kWh (US$0.107/kWh) [8]. The COE determined by HOMER is significantly greater than the average rate of the Lesotho electricity bill. The high calculated COE rates may be attributed to increased operating and maintenance costs [94].

The Total Net Present Cost (NPC) is $39.6 Million and the operating cost is $907, 074 /year. In addition, the initial capital for the system is $27.9 Million.

The second best hybrid system compromises of 7775 kW PV output and 74 battery strings in parallel. The COE for this system is $0.433, the NPC is $41.1 Million, the operating cost is $1.1 Million and the initial capital is $26.9 Million. This hybrid system does not have wind turbines; hence it has a lower initial capital than the first system.

The third-best hybrid system consists of wind turbines and a pumped hydroelectric plant. This system has a COE of $0.792, an NPC of $75.3 million, an operating cost of $1.48 million, and an initial capital of $56.2 million. This hybrid system has higher initial capital, higher net present value, and higher running costs because it consists of six 1.5 MW wind turbines which are more expensive than PVs, with a total rated capacity of 9 MW and 157 parallel battery strings.

Architecture									Cost			
				PV (kW)	G1500	PSPH-BATTERY MODEL	Converter (kW)	Dispatch	NPC ($)	COE ($)	Operating cost ($/yr)	Initial capital ($)
				5,379	1	60	1,985	CC	$39.6M	$0.417	$907,074	$27.9M
				7,775		74	2,082	CC	$41.1M	$0.433	$1.10M	$26.9M
					6	157	1,989	CC	$75.3M	$0.792	$1.48M	$56.2M

Figure 48: Hybrid optimization results from HOMER.

Figure 49 shows the average monthly electric production for design option number one. It can be seen that PV contributes 74% of the total production while the wind turbine contributes the remaining 26%. The total electric production for this system is 12,469,577 kWh/yr while the excess energy for this system is 41.1% (5,125,943 kWh/year).

Figure 49: Option 1 - Monthly average electric production for wind turbines and solar PV

According to HOMER, the energy stored in batteries equals the potential energy in the top reservoir. The upper reservoir's energy storage capacity is proportional to the optimal number of batteries based on HOMER calculations [100].

Figure 50 shows the percentage of the PSP's daily state of charge throughout the year. The variation of the state of charge is attributed to varying renewable resources output, which in turn affects the level of the upper reservoir. For example, around the 90th day of the year, it is observed that the upper reservoir was only 40% - 60% full due to insufficient solar energy. The pumped hydropower storage system is modelled to have 60 battery strings in parallel and an annual throughput of 1,676,254 kWh/year.

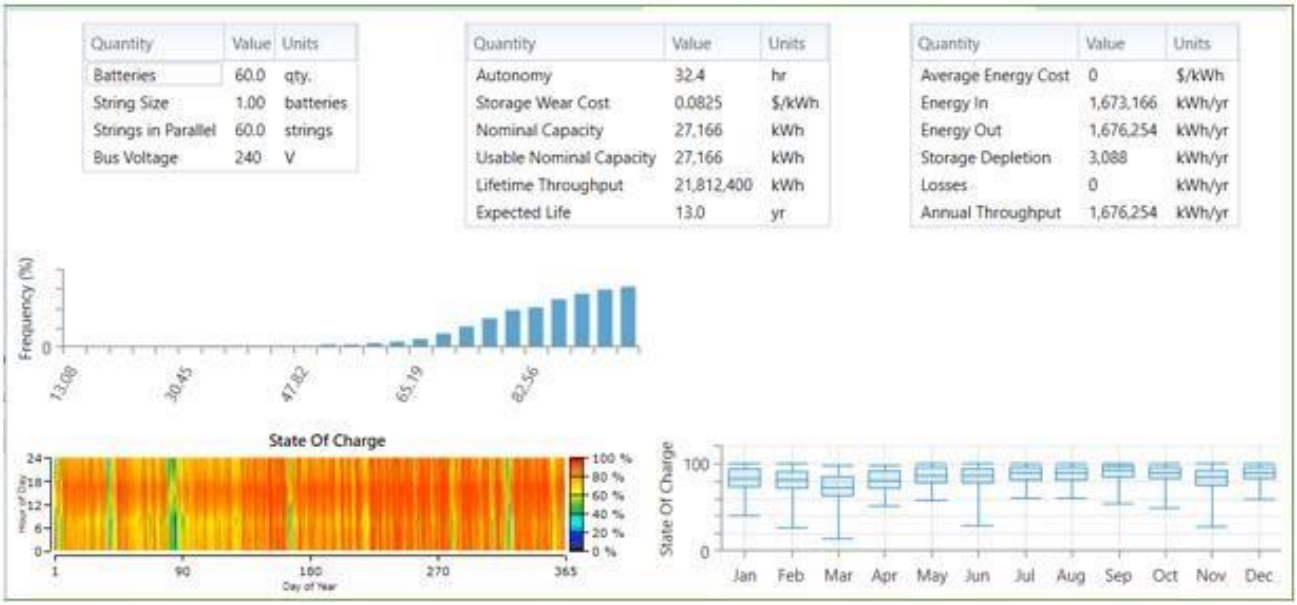

Figure 50: Option 1 – Stored hydropower distribution throughout the year

Figure 51 demonstrates the average monthly electric production for design option number two. This system is made up of only the PVs and PHSP. The excess energy for this system is 45% (6,000,865 kWh/year and the capacity shortage of 0.1% (7,219 kWh/year). The annual electric production from the flat PV is 13,340,628 kWh/year.

Figure 51: Option 2 - Monthly average electric production for solar PV

Figure 52 shows the performance of the pumped hydropower storage system. It can be seen that this system has more PSH power being generated, with an annual throughput of 2,525,622 kWh/year, whereas in option one, the annual throughput is 1,676,254 kWh/yr. The system is modelled to have 74 battery strings in parallel.

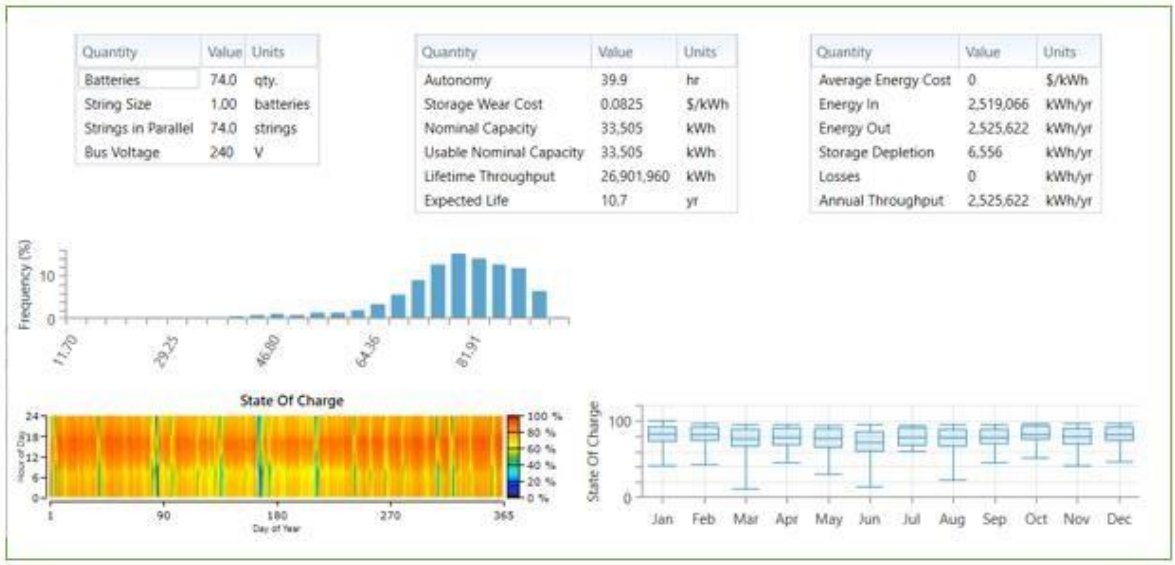

Figure 52: Option 2 - Stored hydropower distribution throughout the year

Figure 53 illustrates the average monthly electric production for design option number three. This system is made up of only the wind turbines and PHSP. The excess energy for this system is 62.2% (12,100,646 kWh/year and the capacity shortage of 0.1% (6,696 kWh/year). The annual electric production from the wind turbines is 19,445,081 kWh/year.

Figure 53: Option 3 – Monthly average electric production from wind turbines

Figure 54 depicts the performance of the pumped hydropower storage system for option 3. The annual throughput of the system is 2,232,633 kWh/year; it is less than the annual PSP throughput for option 2 (solar) but greater than the annual throughput for option 1 (solar and wind). The state of charge for the upper reservoir is relatively low during the first three months of the year. This is attributed to lower wind monthly electric production (pumping power) during that period.

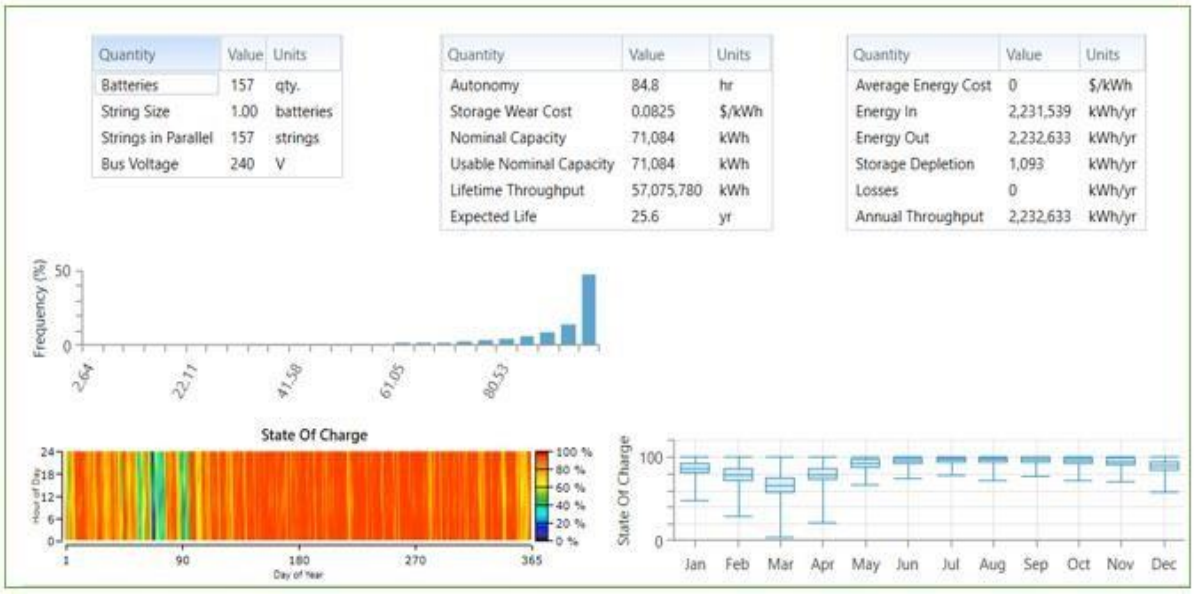

Figure 54: Option 3 – Stored hydropower distribution throughout the year

4.14 Optimal Hybrid system economic indicators

The project's cost-effectiveness is carried out taking all possible scenarios for the solar/wind and PSHP hybrid systems into consideration. As shown in Figure 55, the first consideration is the summary of economic measures for the proposed system. The proposed system has a simple payback period of 7.14 years with a 17.7% internal rate of return (IRR). The 7.14-year payback period which increases to 9.55 years when discounted is an important indicator that shows how long it will take for the project to recoup its initial expenditure. This shorter term represents a faster return on investment which increases the project's economic attractiveness. The IRR of 23.5% demonstrates the project's appeal as it exceeds the normal discount rates in most financial markets, showing great potential for generating positive returns on investment. Lastly, the NPC of $ 1,469,362 indicates the total present value of the project's expenses and revenue over its lifetime. This economic measure is useful in determining the overall financial details of the project, with a positive NPC indicating that the project is financially feasible [101].

Metric	Value
Present worth ($)	$1,469,362
Annual worth ($/yr)	$113,662
Return on investment (%)	14.6
Internal rate of return (%)	17.7
Simple payback (yr)	7.14
Discounted payback (yr)	9.55

Figure 55: Economic measures for the proposed system

4.15 Sensitivity analysis results

In this analysis, it is assumed that the average wind speeds and PV outputs remain constant; hence their sensitivity analysis is not investigated. The sensitivity analysis results for varying wind turbine capital costs and electric load, superimposed with LCOE are illustrated in Figure 56. It can be seen that the PV/wind/pumped hydropower storage hybrid system is only feasible for electric loads greater than 15,00.00 kWh/day. However, when the wind turbine capital costs are increased by a factor of 1.5 and above, HOMER recommends the PV/PSHP hybrid system as the optimal option. It disregards the wind turbine due to the increased costs.

The LCOE for this PV/wind and PSHP hybrid system varies between 0.421 $/kWh and 0.423 $/kWh. Thamae et al. [8] obtained the LCOE of 0.289 $/kWh for the isolated optimized

hydro/wind/PV/diesel/battery hybrid system for Semonkong town in Lesotho. In addition, Amoussou et al. [102] computed the LCOE of 0.21 $/kW for the PV/Wind and PSPP hybrid systems in Cameroon.

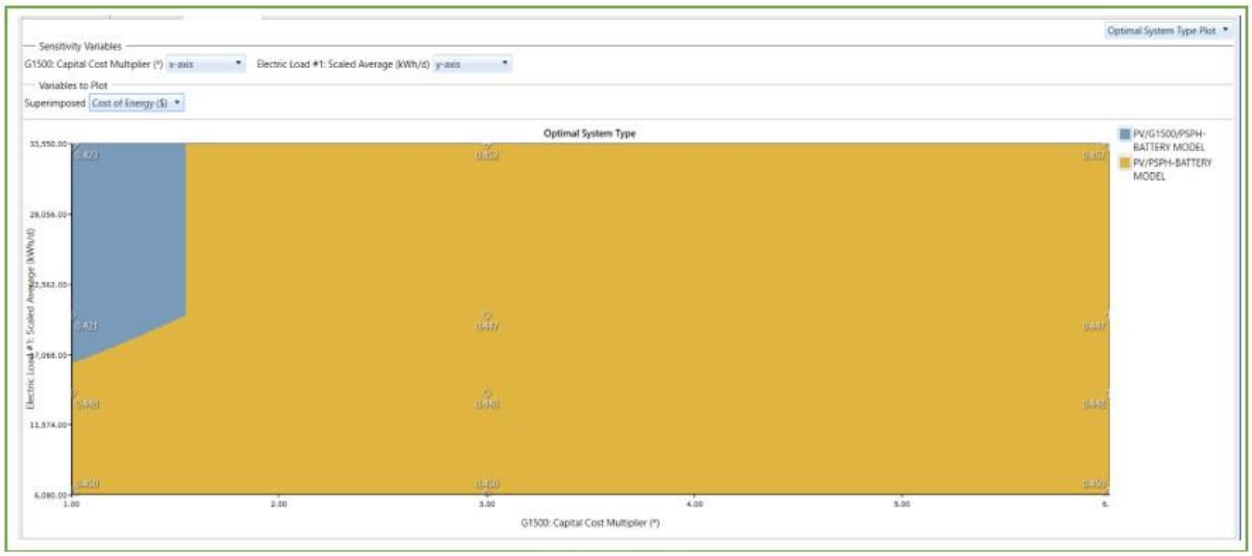

Figure 56: Sensitivity analysis results for the wind turbine capital costs

The sensitivity analysis results for varying PV sizes and the battery strings superimposed with the LCOE at a constant electric load of 14,040 kWh/day is shown in Figure 57. It can be seen that the LCOE ranges between 0.527 and 0.561 for PV sizes less than 13,420.00 kW with the string number varying between 45 and 65. At a constant PV size of 33,551 kW, with the total string number increasing from 27 to 75, the LCOE also increases from 1.136 to 1.231.

The results also show that increasing the PV size at a constant string number results in an increase of the LCOE and the total net present costs. The net present costs for a system with less than 13, 420 kW PV size range between $ 36,000,00 and $ 42,000,000, whilst the total net present costs for a system with at least 26,840 kW PV size range between $ 54,000,000 and $ 78,000,000 million.

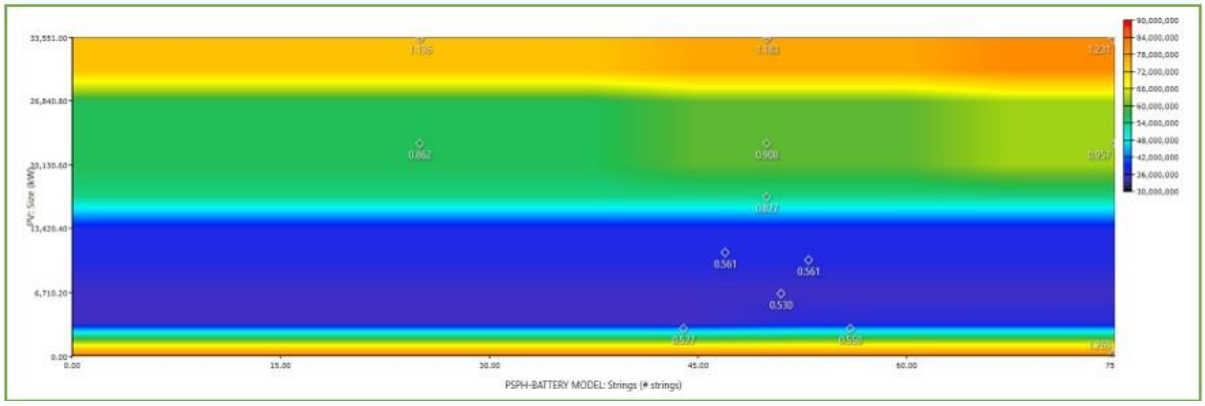

Figure 57: Sensitivity analysis results for varying PV sizes and number of battery strings

In summary, the sensitivity analysis results show that it is important to keep the PV size, number of wind turbines, and the number of battery strings/storage size in check to achieve the optimal/lowest LCOE hybrid system.

CHAPTER 5: Conclusions and Recommendations

5.1 Conclusions

This paper presents the main results of a research study on utilizing cascading wind and solar power pumping systems for recirculating water for pumped hydropower storage systems at Lets'a-La-Letsie in Quthing, Lesotho. The annual average wind speed for the chosen location as determined on HOMER is 4.77 m/s at 50 meters anemometer height. The wind comes from the NWN-NW direction 40% of the time. Additionally, the direct normal irradiation is estimated to be 2468 kWh/m^2/year while the annual average daily irradiation is 5.26 kWh/m^2/day. The load results for the villages near Lets'a La-Letsie show the average total daily load of 14040 kWh/day, with a peak load of 1657 kW. The design flow rate is estimated to be 0.06 m^3/s; the net head is determined to be 157 meters; the penstock length is 2750 meters; and the penstock diameter is 0.2989 meters. The selected turbine is the 100 kW Pelton turbine. The upper reservoir catchment area is 46.4 km^2, and the lower reservoir (abstraction point) catchment area is 600 km^2. The recirculating wind/solar pumping system is made up of 19 identical pumps that can each achieve a maximum head of 90 meters and a maximum flow rate of 125 m^3/hr with the control power of 37 kW.

The HOMER simulation results showed that the most technically and economically viable system configuration is a Solar/wind/pumped hydropower storage hybrid system with an LCOE of $0.417/kWh. Pumped hydropower storage is modelled on HOMER as a battery to take 12.5 hours to empty/fill the upper reservoir with a capacity of 2700 m^3. This system configuration is highly preferred because of its lower net present costs (NPC), operating costs, and lower excess electricity. The pumped hydropower storage annual output for this system is 1, 676, 254 kWh/year, while the PV/pumped hydropower storage hybrid system with the LCOE of $0.433/kWh has the highest pumped hydropower storage annual output of 2, 525, 622 kWh/year. The third best viable system configuration is the wind/pumped hydropower storage hybrid system with the highest LCOE of $ 0.792/kWh. Its pumped hydropower storage plant has an annual output of 2, 232, 633 kWh/year. The selected hybrid system has a return on investment (ROI) of 14.6%, a simple payback period of 7.14 years, and an internal rate of return of 17.7%.

5.2 Recommendations for further studies

The following recommendations will significantly increase the adoption of hybrid microgrids in Lesotho's rural villages. As customer desire and ability to pay are critical, community participation is essential before the construction of any microgrid in these remote settlements. Residents in Lesotho's remote villages should be educated to operate and maintain hybrid microgrids for long-term sustainability.

Secondly, since the catchment area technique for assessing flow rates at Lets'a-La-Letsie is theoretical and requires further validation using real data, the Lesotho government should invest in appropriate equipment and personnel to gather flow rates for all rivers to build hydro microgrids in remote regions. Flow duration curve (FDC) is an important technique in hydrological calculations used to estimate water supplies for hydropower planning. Although the data supplied by the DWA (Department of Water Affairs) are adequate for this investigation, it is suggested that future studies investigate enhancing the reliability of the FDCs by comparing the observed FDC to the recently recorded data.

Further feasibility studies on the possibility of hybridization of solar wind and pumped hydropower storage should be conducted in other areas of the country to inform the planning and development of renewable energy projects, ensuring that the majority of remote rural communities have access to power. Also, in the absence of solar and wind ground data for the Lets'a-La-Letsie site, data extracted from NASA was used for system modeling. Consequently, it is recommended that future studies at the Lets'a-La-Letsie site utilize actual measured ground data instead of satellite-derived data to obtain more accurate results.

Lastly, different storage and dispatch strategies were not investigated in this study. Therefore, further work should be done to investigate the effects of different storage and dispatch strategies on the Cost of Energy (COE) and the Net Present Cost (NPC).

References

[1] A. Gajic, V. Stevanovic, and S. Pejovic, "Pumped-Hydro Storages are Balancing Electric Energy Production of Wind and Solar Reducing Average Costs and Pollution," *Int. J. Fluid Mach. Syst.*, vol. 12, no. 1, pp. 47–55, Mar. 2019, doi: 10.5293/IJFMS.2019.12.1.047.

[2] H. Khorasanizadeh and K. Mohammadi, "Prediction of daily global solar radiation by day of the year in four cities located in the sunny regions of Iran," *Energy Convers. Manag.*, vol. 76, pp. 385–392, Dec. 2013, doi: 10.1016/j.enconman.2013.07.073.

[3] M. Shoaib, I. Siddiqui, S. Rehman, S. Khan, and L. M. Alhems, "Assessment of wind energy potential using wind energy conversion system," *J. Clean. Prod.*, vol. 216, pp. 346–360, Apr. 2019, doi: 10.1016/j.jclepro.2019.01.128.

[4] IRENA "Electricity Storage and Renewables for Island Power: A Guide for Decision Makers", May 2012. Available: https://www.irena.org/publications/2012/May/Electricity-Storage-andRenewables-for-Island-Power-A-Guide-for-Decision-Makers

[5] N. Ghorbani, H. Makian, and C. Breyer, “A GIS-based method to identify potential sites for pumped hydro energy storage - Case of Iran,” *Energy*, vol. 169, pp. 854–867, Feb. 2019, doi: 10.1016/j.energy.2018.12.073.

[6] D. McCollum, L. G. Echeverri, K. Riahi, and S. Parkinson, “ACCESS TO AFFORDABLE, RELIABLE, SUSTAINABLE AND MODERN ENERGY FOR ALL,” no. 2019, 2019.

[7] J. M. Wikman, “A Prototype Model for Pumped Hydro Storage of Off-Grid <10KW Photovoltaic and Wind energy”, Havard University, November 2019, doi: https://nrs.harvard.edu/URN3:HUL.INSTREPOS:37364576”.

[8] M. Mpholo, D. Steuerwald, and T. Kukeera, Eds., *Africa-EU Renewable Energy Research and Innovation Symposium 2018 (RERIS 2018): 23–26 January 2018, National University of Lesotho On occasion of NULISTICE 2018*. in Springer Proceedings in Energy. Cham: Springer International Publishing, 2018. doi: 10.1007/978-3-319-93438-9.

[9] REN21, “REN21,” no. 2018. Available: https://www.ren21.net/wpcontent/uploads/2019/08/Full-Report_2018.pdf.

[10] B. Michoud and M. Hafner, *Financing Clean Energy Access in Sub-Saharan Africa: Risk Mitigation Strategies and Innovative Financing Structures*. in SpringerBriefs in Energy. Cham: Springer International Publishing, 2021. doi: 10.1007/978-3-030-75829-5.

[11] EIA, “Africa faces both major challenges and huge opportunities as it transitions to clean energy,” no. Africa faces both major challenges and huge opportunities as it transitions to clean energy, 2022.

[12] M. Mpholo, M. Taele, and Thamae, “Lesotho Energy Needs Assessment Stakeholders Working in Silos,” National University of Lesotho, Department of Physics & Electronics – National University of Lesotho, SOUTHERN AFRICAN SUSTAINABLE ENERGY INITIATIVE (SASEI) Project, May 2014. [Online]. Available: https://nul-erc.s3.amazonaws.com/public/documents/reports/lesotho-energy-needs-assessmentstakeholders-working-in-silos-1532184404.pdf

[13] S. T. Bahta, “Design and Analyzing of an Off-Grid Hybrid Renewable Energy System to Supply Electricity for Rural Areas,” p. 109.

[14] A. Blakers, M. Stocks, B. Lu, and C. Cheng, “A review of pumped hydro energy storage,” *Prog. Energy*, vol. 3, no. 2, p. 022003, Apr. 2021, doi: 10.1088/2516-1083/abeb5b.

[15] S. Padrón, J. F. Medina, and A. Rodríguez, “Analysis of a pumped storage system to increase the penetration level of renewable energy in isolated power systems. Gran Canaria: A case study,” *Energy*, vol. 36, no. 12, pp. 6753–6762, Dec. 2011, doi: 10.1016/j.energy.2011.10.029.

[16] M. Mpholo *et al.*, “Lesotho electricity demand profile from 2010 to 2030,” *J. Energy South. Afr.*, vol. 32, no. 1, pp. 41–57, Feb. 2021, doi: 10.17159/2413-3051/2021/v32i1a7792.

[17] M. of E. and M. Government of Lesotho, Department of Energy, and Ministry of Energy and Meteorology, “Scaling up Renewable Energy in Low income countries SREP,” Nov. 2027. [Online]. Available: https://documents1.worldbank.org/curated/en/141761542640144240/pdf/132198-WP-srepinvestment-plan-lesotho.pdf

[18] B. M. Taele, L. Mokhutšoane, and I. Hapazari, “An overview of small hydropower development in Lesotho: Challenges and prospects,” *Renew. Energy*, vol. 44, pp. 448–452, Aug. 2012, doi: 10.1016/j.renene.2012.01.086.

[19] M. Simão and H. Ramos, “Hybrid Pumped Hydro Storage Energy Solutions towards Wind and PV Integration: Improvement on Flexibility, Reliability and Energy Costs,” *Water*, vol. 12, no. 9, p. 2457, Sep. 2020, doi: 10.3390/w12092457.

[20] B M Taele, L Mokhutšoane, and Himanshu Narayan, “Solar energy resources potential and sustainable production of biomass energy in Lesotho,” 2010, doi: 10.13140/RG.2.1.2962.0882.

[21] Lekhanya Liteboho, “Analysis of Quthing River and Letseng-laLetsie for Hydropower Potential,” *NUL ERC*, 2020.

[22] “LESOTHO ENERGY POLICY 2015-2025,” Lesotho government, Policy. [Online]. Available: https://nul-erc.s3.amazonaws.com/public/documents/reports/lesotho-energy-policy-2015-20251532182755.pdf

[23] I. Løvvold, “Pumped Hydropower Conversion and Renewable Hybrid Power Plants at Senja”, Available: https://munin.uit.no/handle/10037/20092

[24] USAID, “Powering Health: Photovoltaic (PV) Systems”, doi: https://www.usaid.gov/sites/default/files/2022-05/Powering-Health_Photovoltaic-Systems.pdf.

[25] IEA, “Renewables 2020 - Analysis and forecast to 2025,” 2020. Available: https://iea.blob.core.windows.net/assets/1a24f1fe-c971-4c25-964a-57d0f31eb97b/Renewables_2020-PDF.pdf atus in Africa: Challenges, Progress and Sustainable Pathways,” *Energies*, vol. 16, no. 23, p. 7708, Nov. 2023, doi: 10.3390/en16237708.

[27] N. N. Davis *et al.*, “The Global Wind Atlas: A High-Resolution Dataset of Climatologies and Associated Web-Based Application,” *Bull. Am. Meteorol. Soc.*, vol. 104, no. 8, pp. E1507–E1525, Aug. 2023, doi: 10.1175/BAMS-D-21-0075.1.

[28] M. Mpholo, T. Mathaba, and M. Letuma, “Wind profile assessment at Masitise and Sani in Lesotho for potential off-grid electricity generation,” *Energy Convers. Manag.*, vol. 53, no. 1, pp. 118–127, Jan. 2012, doi: 10.1016/j.enconman.2011.07.015.

[29] Srikanth D, K. Himaja, Ch. Swasthik, P. Uday Kumar, and Vignan Institute of Technology and Science, “Water Pumping System using Solar and Wind Power,” *Int. J. Eng. Res.*, vol. V9, no. 05, p. IJERTV9IS050462, May 2020, doi: 10.17577/IJERTV9IS050462.

[30] Y. Kumar *et al.*, “Wind energy: Trends and enabling technologies,” *Renew. Sustain. Energy Rev.*, vol. 53, pp. 209–224, Jan. 2016, doi: 10.1016/j.rser.2015.07.200.

[31] N. G. Mortensen, “46200 Planning and Development of Wind Farms: Wind resource assessment using the WAsP software”.

[32] T. Aukitino, M. G. M. Khan, and M. R. Ahmed, “Wind energy resource assessment for Kiribati with a comparison of different methods of determining Weibull parameters,” *Energy Convers. Manag.*, vol. 151, pp. 641–660, Nov. 2017, doi: 10.1016/j.enconman.2017.09.027.

[33] D. Hanslian and J. Hošek, “Combining the VAS 3D interpolation method and Wind Atlas methodology to produce a high-resolution wind resource map for the Czech Republic,” *Renew. Energy*, vol. 77, pp. 291–299, May 2015, doi: 10.1016/j.renene.2014.12.013.

[34] T. Mathaba, M. Mpholo, and M. Letuma, “Velocity and power density analysis of the wind at Letšeng-la-terae in Lesotho,” *Renew. Energy*, vol. 46, pp. 210–217, Oct. 2012, doi: 10.1016/j.renene.2012.04.003.

[35] S. Mishra, S. K. Singal, and D. K. Khatod, “Optimal installation of small hydropower plant—A review,” *Renew. Sustain. Energy Rev.*, vol. 15, no. 8, pp. 3862–3869, Oct. 2011, doi: 10.1016/j.rser.2011.07.008.

[36] C. V. Dongen and B. Bekker, “Potential for New Pumped Storage Schemes in South Africa,” in *2020 6th IEEE International Energy Conference (ENERGYCon)*, Gammarth, Tunisia: IEEE, Sep. 2020, pp. 266–271. doi: 10.1109/ENERGYCon48941.2020.9236598.

[37] T. H. Chowdhury, “OVERVIEW OF PUMPED HYDROELECTRICITY STORAGE SYSTEM TO PRODUCE CLEAN ENERGY,” vol. 01, no. 01, 2021.

[38] S. Kucukali, “Finding the most suitable existing hydropower reservoirs for the development of pumped-storage schemes: An integrated approach,” *Renew. Sustain. Energy Rev.*, vol. 37, pp. 502–508, Sep. 2014, doi: 10.1016/j.rser.2014.05.052.

[39] F. A. Canales, A. Beluco, and C. A. B. Mendes, “A comparative study of a wind hydro hybrid system with water storage capacity: Conventional reservoir or pumped storage plant?,” *J. Energy Storage*, vol. 4, pp. 96–105, Dec. 2015, doi: 10.1016/j.est.2015.09.007.

[40] P. C. Nikolaos, F. Marios, and K. Dimitris, “A Review of Pumped Hydro Storage Systems,” *Energies*, vol. 16, no. 11, p. 4516, Jun. 2023, doi: 10.3390/en16114516.

[41] P. Toufani, E. Nadar, and A. S. Kocaman, “Operational benefit of transforming cascade hydropower stations into pumped hydro energy storage systems,” *J. Energy Storage*, vol. 51, p. 104444, Jul. 2022, doi: 10.1016/j.est.2022.104444.

[42] IRENA “Innovative operation of pumped hydropower storage - Innovation Landscape Brief,” no. 2020, Available: https://www.irena.org/-/media/Files/IRENA/Agency/Publication/2020/Jul/IRENA_Innovative_PHS_operation_2020.pdf

[43] M. Petrollese, P. Seche, and D. Cocco, “Analysis and optimization of solar-pumped hydro storage systems integrated in water supply networks,” *Energy*, vol. 189, p. 116176, Dec. 2019, doi: 10.1016/j.energy.2019.116176.

[44] V. Yildiz and J. A. Vrugt, “A toolbox for the optimal design of run-of-river hydropower plants,” *Environ. Model. Softw.*, vol. 111, pp. 134–152, Jan. 2019, doi: 10.1016/j.envsoft.2018.08.018.

[45] O. J. Mdee, “Measurement methods for hydropower resources: a review,” 2018.

[46] E. D. Castronuovo and J. A. P. Lopes, “Optimal operation and hydro storage sizing of a wind–hydro power plant,” *Int. J. Electr. Power Energy Syst.*, vol. 26, no. 10, pp. 771–778, Dec. 2004, doi: 10.1016/j.ijepes.2004.08.002.

[47] J. S. Anagnostopoulos and D. E. Papantonis, “Pumping station design for a pumped-storage windhydro power plant,” *Energy Convers. Manag.*, vol. 48, no. 11, pp. 3009–3017, Nov. 2007, doi: 10.1016/j.enconman.2007.07.015.

[48] A. Zisos, G.-K. Sakki, and A. Efstratiadis, “Mixing Renewable Energy with Pumped Hydropower Storage: Design Optimization under Uncertainty and Other Challenges,” *Sustainability*, vol. 15, no. 18, p. 13313, Sep. 2023, doi: 10.3390/su151813313.

[49] Y. R. Pasalli and A. B. Rehiara, “Design Planning of Micro-hydro Power Plant in Hink River,” *Procedia Environ. Sci.*, vol. 20, pp. 55–63, 2014, doi: 10.1016/j.proenv.2014.03.009.

[50] S. P.C. and K. Sawazaki, “River discharge prediction for ungauged mountainous river basins during heavy rain events based on seismic noise data,” *Prog. Earth Planet. Sci.*, vol. 8, no. 1, p. 58, Dec. 2021, doi: 10.1186/s40645-021-00448-1.

[51] R. Jha and V. Smakhtin, *A review of methods of hydrological estimation at ungauged sites in India*. Colombo, Sri Lanka: International Water Management Institute, 2008.

[52] J. B. Swain, “HYDROLOGICAL MODELING OF A TYPICAL UNGAUGED BASIN OF ODISHA”, DEPARMENT OF CIVIL ENGINEERING NATIONAL INSTITUTE OF TECHNOLOGY ROURKELA 2013. Available:: https://core.ac.uk/download/pdf/53189597.pdf

[53] M. L. Mul and M. Mul, *Understanding hydrological processes in an ungauged catchment in subSaharan Africa*. in A Balkema Book. Leiden: CRC Press/Balkema, 2009.

[54] H.-J. Wagner and J. Mathur, *Introduction to Hydro Energy Systems*. in Green Energy and Technology. Berlin, Heidelberg: Springer Berlin Heidelberg, 2011. doi: 10.1007/978-3-64220709-9.

[55] M. R. Goodarzi and M. Vazirian, “A geostatistical approach to estimate flow duration curve parameters in ungauged basins,” *Appl. Water Sci.*, vol. 13, no. 9, p. 178, Sep. 2023, doi: 10.1007/s13201-023-01993-4.

[56] C. Prieto, N. Le Vine, D. Kavetski, E. García, and R. Medina, “Flow Prediction in Ungauged Catchments Using Probabilistic Random Forests Regionalization and New Statistical Adequacy Tests,” *Water Resour. Res.*, vol. 55, no. 5, pp. 4364–4392, May 2019, doi: 10.1029/2018WR023254.

[57] H. Lee, M. S. Chae, J.-Y. Park, K. J. Lim, and Y. S. Park, “Development and Application of a QGIS-Based Model to Estimate Monthly Streamflow,” *ISPRS Int. J. Geo-Inf.*, vol. 11, no. 1, p. 40, Jan. 2022, doi: 10.3390/ijgi11010040.

[58] M. A. Osei, L. K. Amekudzi, D. D. Wemegah, K. Preko, E. S. Gyawu, and K. Obiri-Danso, “Hydro-Climatic Modelling of an Ungauged Basin in Kumasi, Ghana,” Catchment hydrology/Modelling approaches, preprint, Aug. 2017. doi: 10.5194/hess-2017-421.

[59] B. Z. Abate, T. T. Assefa, T. B. Tigabu, W. B. Abebe, and L. He, “Hydrological Modeling of the Kobo-Golina River in the Data-Scarce Upper Danakil Basin, Ethiopia,” *Sustainability*, vol. 15, no. 4, p. 3337, Feb. 2023, doi: 10.3390/su15043337.

[60] F. Saka and H. T. Babacan, “Discharge Estimation by Drainage Area Ratio Method at Some Specific Discharges for 2251 Stream Gauging Station in East Black Sea Basin, Turkey”.

[61] D. Emerson, “Evaluation of Drainage-Area Ratio Method Used to Estimate Streamflow for the Red River of the North Basin, North Dakota and Minnesota,” Scientific Investigations Report, 2005.

[62] N. W. Kim, Y. Jung, and J. E. Lee, “Spatial propagation of streamflow data in ungauged watersheds using a lumped conceptual model,” *J. Water Clim. Change*, vol. 10, no. 1, pp. 89–101, Mar. 2019, doi: 10.2166/wcc.2018.059.

[63] A. Y. Hatata, M. M. El-Saadawi, and S. Saad, “A feasibility study of small hydro power for selected locations in Egypt,” *Energy Strategy Rev.*, vol. 24, pp. 300–313, Apr. 2019, doi: 10.1016/j.esr.2019.04.013.

[64] B. A. Nasir, “Design Considerations of Micro-hydro-electric Power Plant,” *Energy Procedia*, vol. 50, pp. 19–29, 2014, doi: 10.1016/j.egypro.2014.06.003.

[65] Q. Chen, D. Chen, R. Li, J. Ma, and K. Blanckaert, “Adapting the operation of two cascaded reservoirs for ecological flow requirement of a de-watered river channel due to diversion-type hydropower stations,” *Ecol. Model.*, vol. 252, pp. 266–272, Mar. 2013, doi: 10.1016/j.ecolmodel.2012.03.008.

[66] S. Ahammed, “Optimization Of Hybrid Renewable Energy System (HRSE) Using Homer Pro,” vol. 5, no. 5, 2021.

[67] R. Banik, S. Ray, P. Das, and A. Biswas, “Optimization Of Hybrid Renewable Energy Systems Using Soft Computing Approaches,” vol. 9, no. 03, 2020.

[68] I. C. Hoarcă, N. Bizon, I. S. Șorlei, and P. Thounthong, “Sizing Design for a Hybrid Renewable Power System Using HOMER and iHOGA Simulators,” *Energies*, vol. 16, no. 4, p. 1926, Feb. 2023, doi: 10.3390/en16041926.

[69] A. Beluco *et al.*, “Dataset after Seven Years Simulating Hybrid Energy Systems with Homer Legacy,” *Data Sci. J.*, vol. 19, p. 14, Mar. 2020, doi: 10.5334/dsj-2020-014.

[70] F. A. Canales and A. Beluco, “Modeling pumped hydro storage with the micropower optimization model (HOMER),” *J. Renew. Sustain. Energy*, vol. 6, no. 4, p. 043131, Jul. 2014, doi: 10.1063/1.4893077.

[71] National Institute of Applied Sciences and Technology, Centre Urbain Nord, Tunis Cedex, Tunisia, R. Ouederni, B. Bouaziz, National Institute of Applied Sciences and Technology, Centre Urbain Nord, Tunis Cedex, Tunisia, F. Bacha, and National Institute of Applied Sciences and Technology, Centre Urbain Nord, Tunis Cedex, Tunisia, “Modeling and Cost Optimization of an Islanded Virtual Power Plant: Case Study of Tunisia,” *Turk. J. Electr. Power Energy Syst.*, vol. 2, no. 2, pp. 168–179, Oct. 2022, doi: 10.5152/tepes.2022.22024.

[72] S. Karhinen and H. Huuki, “Private and social benefits of a pumped hydro energy storage with increasing amount of wind power,” *Energy Econ.*, vol. 81, pp. 942–959, Jun. 2019, doi: 10.1016/j.eneco.2019.05.024.

[73] T. M. I. Riayatsyah, T. A. Geumpana, I. M. R. Fattah, S. Rizal, and T. M. I. Mahlia, “TechnoEconomic Analysis and Optimisation of Campus Grid-Connected Hybrid Renewable Energy System Using HOMER Grid,” *Sustainability*, vol. 14, no. 13, p. 7735, Jun. 2022, doi: 10.3390/su14137735.

[74] W. Short, D. J. Packey, and T. Holt, “A manual for the economic evaluation of energy efficiency and renewable energy technologies,” NREL/TP--462-5173, 35391, Mar. 1995. doi: 10.2172/35391.

[75] T. Lambert, P. Gilman, and P. Lilienthal, “Micropower System Modeling with Homer,” in *Integration of Alternative Sources of Energy*, 1st ed., F. A. Farret and M. G. Simões, Eds., Wiley, 2005, pp. 379–418. doi: 10.1002/0471755621.ch15.

[76] S. Asmat and S. Sood, “Techno-Economic Analysis of Integration of Battery Energy Storage System in Grid- Connected PV System,” vol. 45, no. 1, 2024.

[77] Z. Liao *et al.*, “Comprehensive analysis of renewable hybrid energy systems in highway tunnels,” *Front. Energy Res.*, vol. 12, p. 1365532, Jan. 2024, doi: 10.3389/fenrg.2024.1365532.

[78] K. S. M. Lannas and J. K. Turpie, “Valuing the Provisioning Services of Wetlands: Contrasting a Rural Wetland in Lesotho with a Peri-Urban Wetland in South Africa,” *Ecol. Soc.*, vol. 14, no. 2, p. art18, 2009, doi: 10.5751/ES-02919-140218.

[79] N. L. Rose *et al.*, “Natural archives of long-range transported contamination at the remote lake Letšeng-la Letsie, Maloti Mountains, Lesotho,” *Sci. Total Environ.*, vol. 737, p. 139642, Oct. 2020, doi: 10.1016/j.scitotenv.2020.139642.

[80] “Information Sheet on Ramsar Wetlands (RIS) page 18.” [Online]. Available: https://rsis.ramsar.org/RISapp/files/41302939/pictures/LS1388map.pdf

[81] L. E. Petterson, “LESOTHO POWER GENERATION MASTER PLAN PROJECT # LEC/GEN/1-2009 FINAL MILESTONES REPORT”.

[82] a DVH Company, “LESOTHO POWER GENERATION MASTER PLAN PROJECT # LEC/GEN/1-2009 FINAL MILESTONES REPORT VOLUME 1 PART 1.1 HYDRO POWER GENERATION OPTION,” 2009.

[83] J. Thomas, “COMPARATIVE ANALYSIS OF WIND ATLASES: WIND RESOURCE ASSESSMENT OF FORESTED SITES FOR WIND POWER DEVELOPMENT”.

[84] H. Ahmadi and A. Shamsai, “Preliminary Site Selection of Pumped Storage Hydropower Plants - A GIS-based approach,” *Vol .*, 2009.

[85] R. M. A. Fesalbon and A. C. Blanco, “HYDROPOWER DAM SITE SELECTION AND VISUALIZATION USING GIS AND RS TECHNIQUES: A CASE OF MARINDUQUE, PHILIPPINES,” *Int. Arch. Photogramm. Remote Sens. Spat. Inf. Sci.*, vol. XLII-4/W19, pp. 207–214, Dec. 2019, doi: 10.5194/isprs-archives-XLII-4-W19-207-2019.

[86] A. Kumar, “STANDARDS/MANUALS/ GUIDELINES FOR SMALL HYDRO DEVELOPMENT”, June 2013, doi: https://iitr.ac.in/Departments/Hydro%20and%20Renewable%20Energy%20Department/static/standards_pdf/1.2_2.1_Planning_and_Layouts.pdf

[87] BSI Engineering, “Pipe Size Rules of Thumb,” vol. 7, Nov. 2020. [Online]. Available: https://bsiengr.com/wp-content/uploads/2020/11/Pipe-Size-Rules-of-Thumb.pdf

[88] J. O. Oladigbolu, Y. A. Al-Turki, and L. Olatomiwa, “Comparative study and sensitivity analysis of a standalone hybrid energy system for electrification of rural healthcare facility in Nigeria,” *Alex. Eng. J.*, vol. 60, no. 6, pp. 5547–5565, Dec. 2021, doi: 10.1016/j.aej.2021.04.042.

[89] A. Blakers, B. Lu, and M. Stocks, “100% renewable electricity in Australia,” *Energy*, vol. 133, pp. 471–482, Aug. 2017, doi: 10.1016/j.energy.2017.05.168.

[90] W. E. Saturday, “NOVEL DOMESTIC DESIGN AND MANUFACTURING OF PELTON TURBINE BUCKET: A KEY TO MANAGE AND ENHANCE SUB-SAHARAN AFRICA’S HYDRO ENERGY POTENTIAL,” In fulfilment for the requirements for the degree of Doctor of Philosophy in Mechanical Engineering at the College of Agriculture, Engineering and Science, University of KwaZulu-Natal., UKZN.

[91] E. Quaranta, “The state-of-art of design and research for Pelton turbine casing, weight estimation, counterpressure operation and scientific challenges,” 2021.

[92] Department of Water Resources, Faculty of Engineering, University of Brawijaya, Malang, Indonesia., L. M. Limantara*, S. Marsudi, Department of Water Resources, Faculty of Engineering, University of Brawijaya, Malang, Indonesia., A. T. Hakim, and Department of Water Resources, Faculty of Engineering, University of Brawijaya, Malang, Indonesia., “Mini Hydropower Plant for Supporting the Renewable Resources at Madong, Toraja Utara Regency Sulawesi Selatan Province-Indonesia,” *Int. J. Innov. Technol. Explor. Eng.*, vol. 9, no. 2, pp. 2805–2813, Dec. 2019, doi: 10.35940/ijitee.B7182.129219.

[93] “BUNDU POWER,” BUNDU Power. Accessed: Apr. 04, 2024. [Online]. Available: https://www.bundupower.co.za/solarsurface-lorentz-single.php?mod=PS40K2-CS-F85-40

[94] A. Safi, S. Anuar, D. M. Nafiz, F. Basrawi, M. Nazani, and A. Shukrie, “Modelling flood reservoir integrated with pumped hydropower storage for electricity production using HOMER,” *MATEC Web Conf.*, vol. 225, p. 05021, 2018, doi: 10.1051/matecconf/201822505021.

[95] LEWA, “LEWA Annual report 2017/2018", ” Lesotho Electricity and Water Authority, Maseru, 2017. [Online]. Available: http://www.lewa.org.ls/library/annual_report_17-18.pdf.

[96] BUREAU OF STATISTICS (BoS), 2016. Maseru Lesotho.

[97] S. Nababan and A. Natsir, “Planning of Hybrid Power Supply System based on Renewable Energy using HOMER,” vol. 13, no. 16, 2018.

[98] K. A. Glaisa, M. E. Elayeb, and M. A. Shetwan, “Potential of Hybrid System Powering School in Libya,” *Energy Procedia*, vol. 57, pp. 1411–1420, 2014, doi: 10.1016/j.egypro.2014.10.132.

[99] Lesotho Local Government, “Quthing District Council Information Handbook,” Department of Planning, Ministry of Local Government and Chiefainship, Lesotho, LOCAL GOVERNMENT DISTRICT INFORMATION HANDBOOK, 2008. [Online]. Available: https://www.giz.de/en/downloads/en-lesotho-quthing-information-handbook.pdf

[100] S. P. Koko, K. Kusakana, and H. J. Vermaak, “Grid-interactive micro-hydrokinetic with pumpedhydro storage: The case study of three South African demand sectors,” in *2017 International Conference on the Domestic Use of Energy (DUE)*, Cape Town, South Africa: IEEE, Apr. 2017, pp. 83–88. doi: 10.23919/DUE.2017.7931828.

[101] M. S. Nkambule, A. N. Hasan, and T. Shongwe, “Performance and Techno-Economic Analysis of Optimal Hybrid Renewable Energy Systems for the Mining Industry in South Africa,” *Sustainability*, vol. 15, no. 24, p. 16766, Dec. 2023, doi: 10.3390/su152416766.

[102] I. Amoussou *et al.*, “Optimal Modeling and Feasibility Analysis of Grid-Interfaced Solar PV/Wind/Pumped Hydro Energy Storage Based Hybrid System,” *Sustainability*, vol. 15, no. 2, p. 1222, Jan. 2023, doi: 10.3390/su15021222.

Appendices

Appendix 1: Jet Pelton turbine graphic view

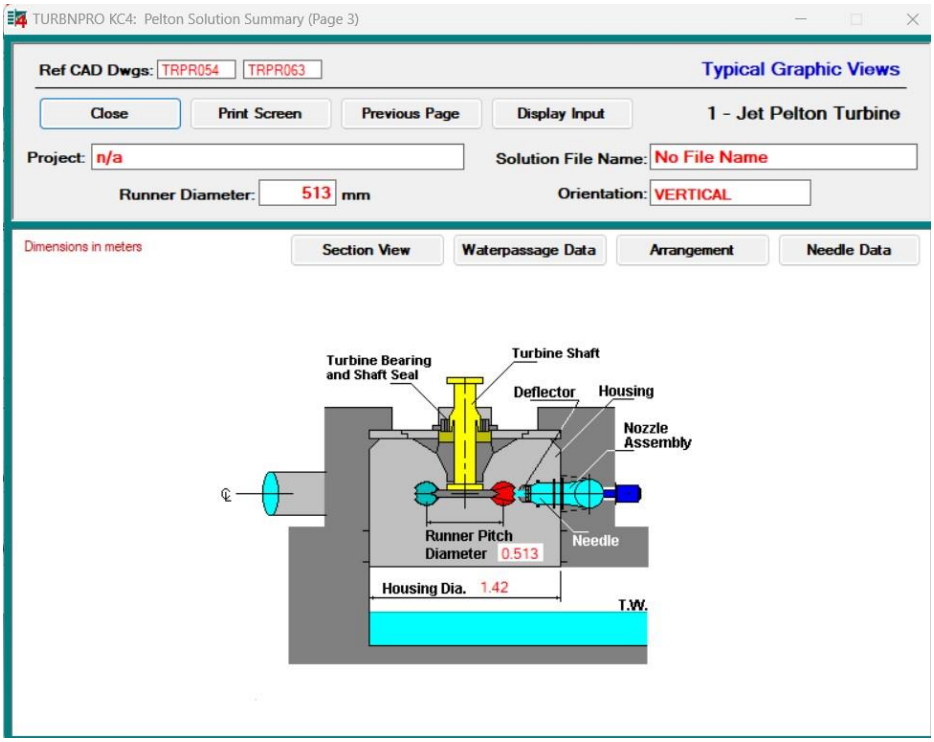

Appendix 2: Typical Jet Pelton turbine dimensionnel data

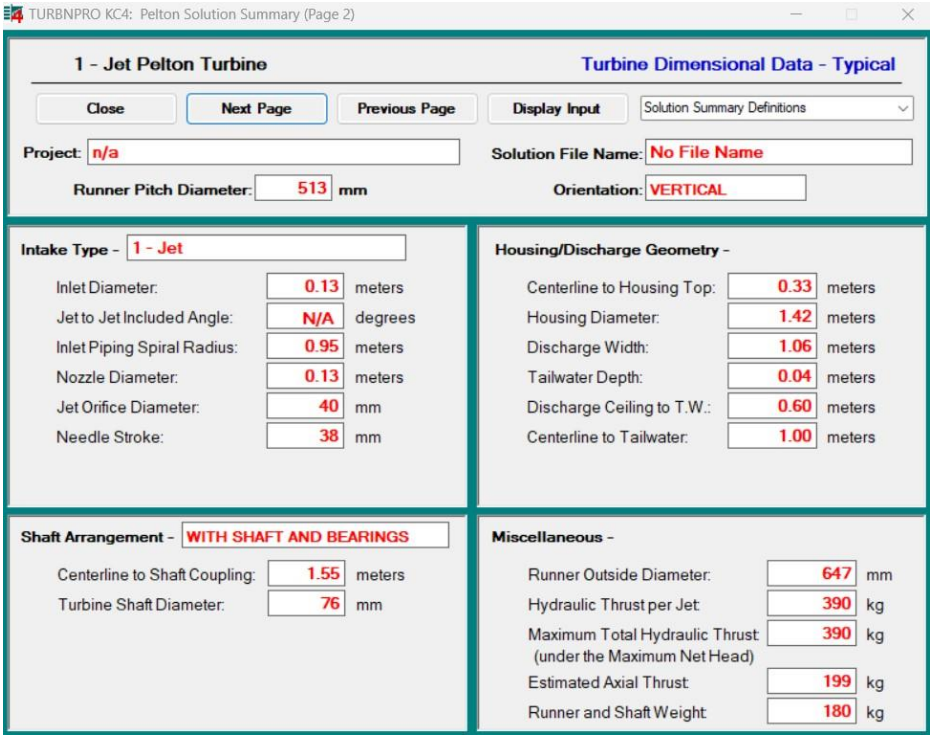

Appendix 3: Lower reservoir catchment area from GIS tools

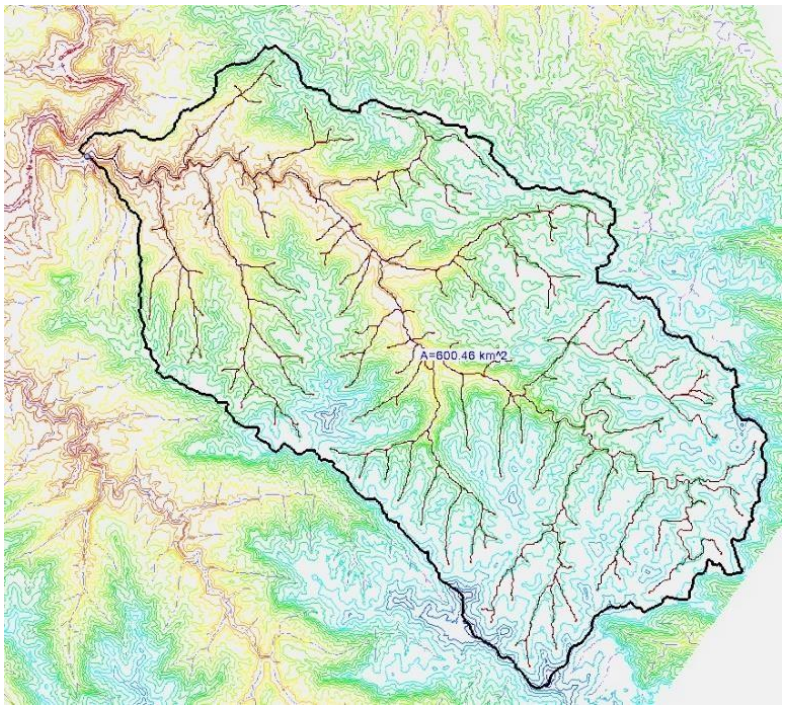

Appendix 4:Selected solar pump specifications

LORENTZ | 90m Solar Surface Pump

SPECIFICATIONS

Model	PS40K2-CS-F85-40
Make	Lorentz
Max Head	90 m
Max Flow Rate	125.00 m^3/h
Controller	PS40K2
Controller Power	37 kW

◂ PS25K2 Series All Pumps ▸

Appendix 5:Pump curve –Two pumps in parallel (each achieves 108 m^3/hr at 70m)

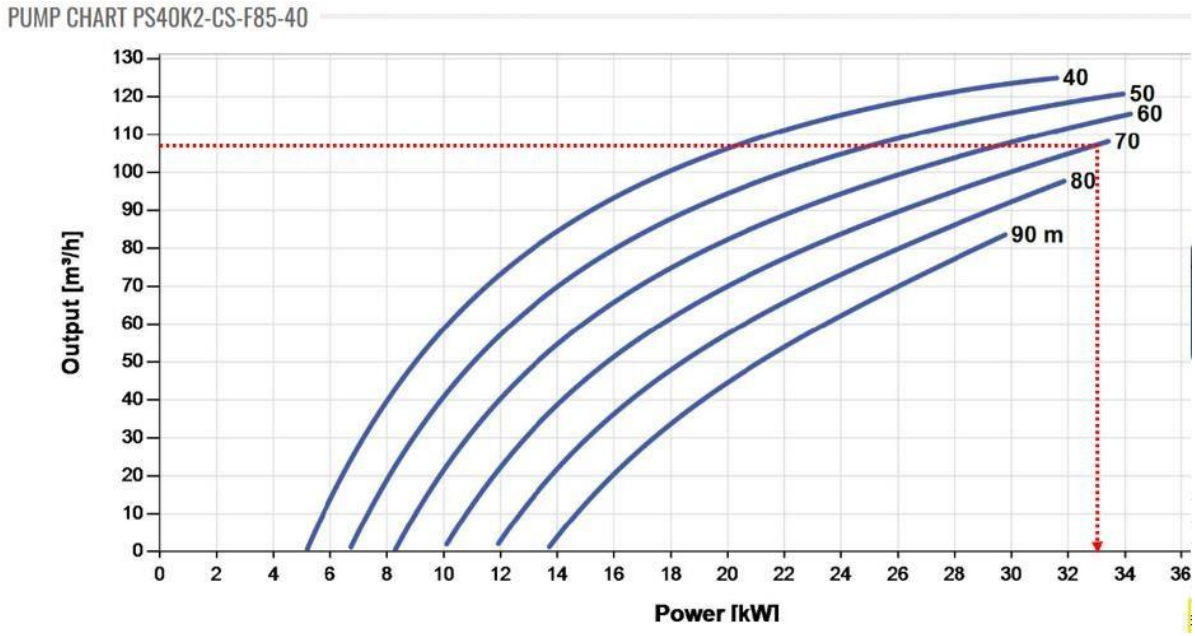

Appendix 6:Pump curve –Two pumps in parallel (each achieves 75 m^3/hr at 80m head)

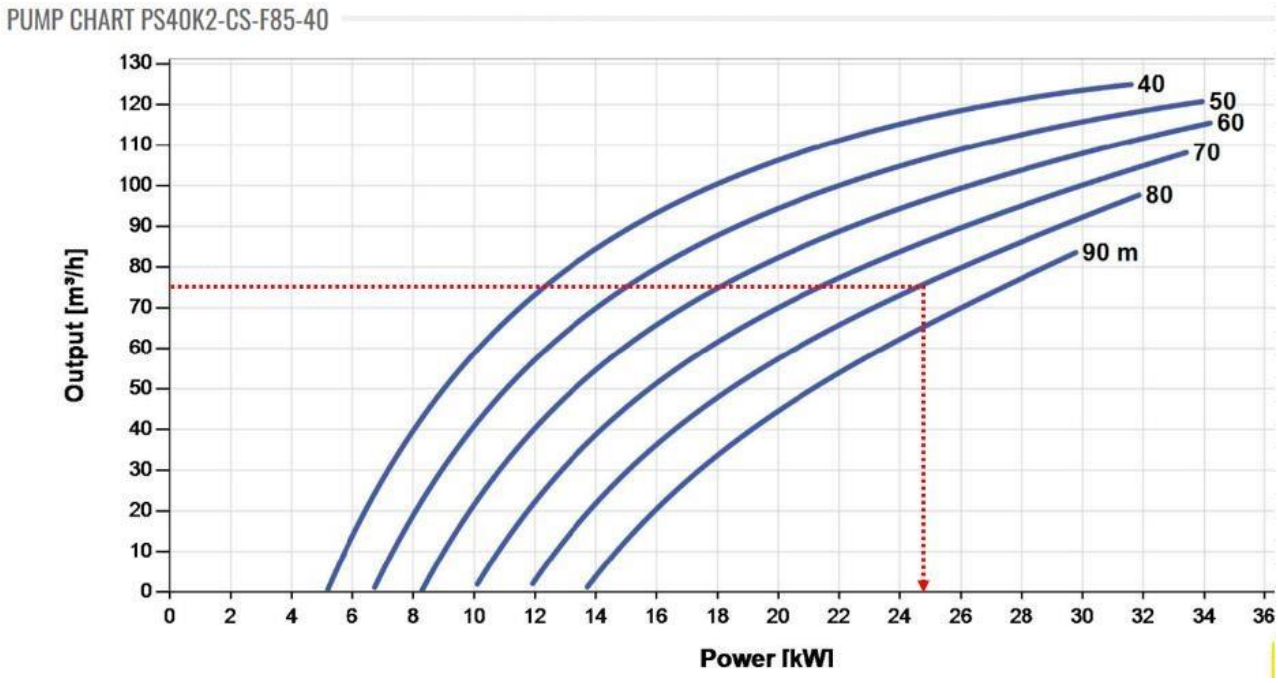

Appendix 7:Pump curve -Two pumps in parallel (each achieves 108 m^3/hr at 90m head)

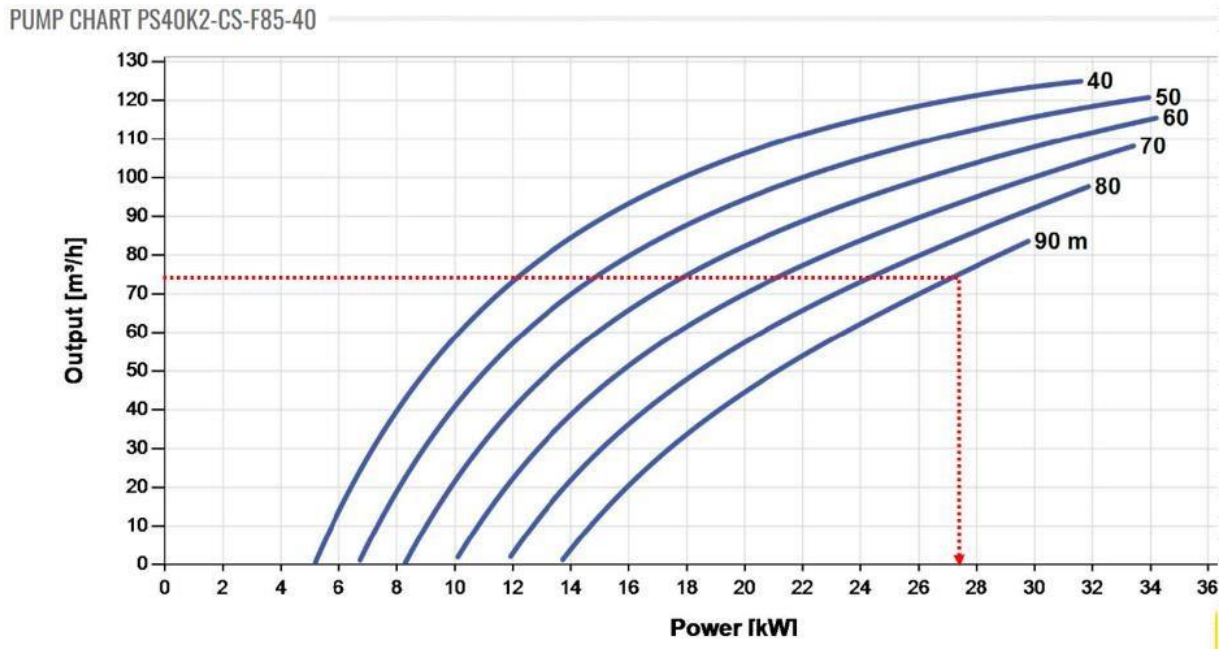

Appendix 8:Pump curve -Two pumps in parallel (each achieves 108 m^3/hr at 70m head)

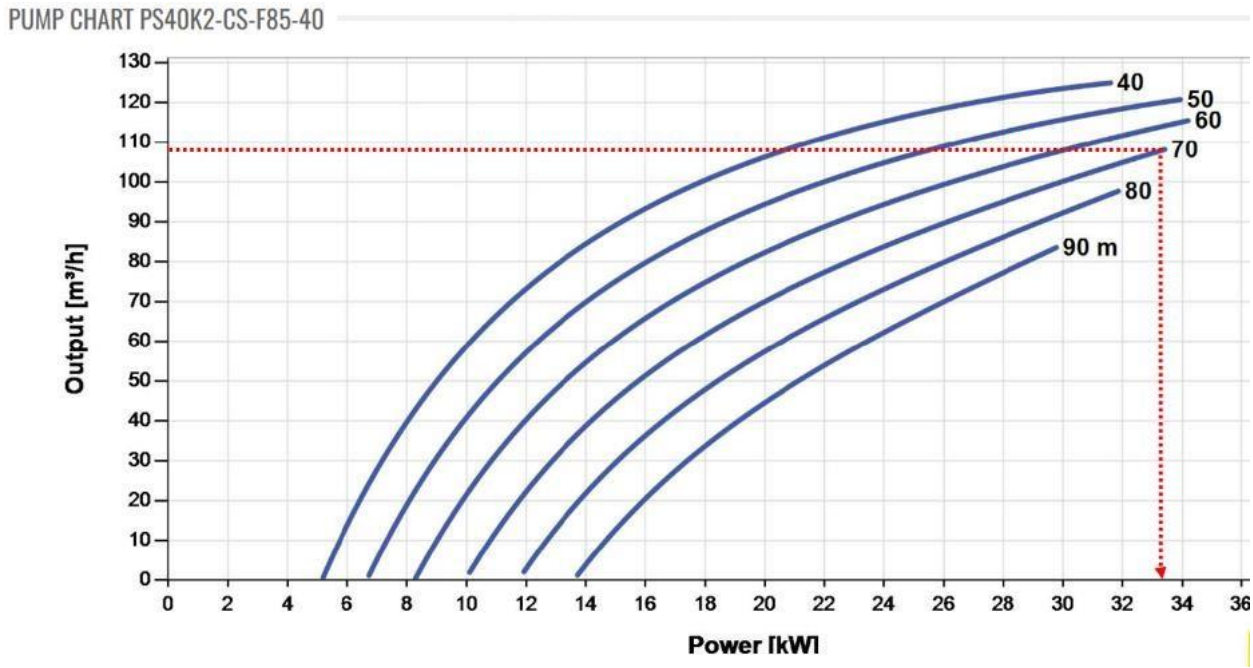

Appendix 9:Pump curve -Three pumps in parallel (each achieves 75 m^3/hr at 90m head)